LA-UR-07-8137

Approved for public release;
distribution is unlimited.

Title:	Monte Carlo (MCNP) Physics Validation for GNEP
Author(s):	Benjamin W. Amiri David D. Dixon Thomas F. Marcille David I. Poston
Submitted to:	United States Department of Energy

Form 836 (7/06)

LA-UR-07-8137

Global Nuclear Energy Partnership

Monte Carlo (MCNP) Physics Validation for GNEP

by
Benjamin W. Amiri
David D. Dixon
Thomas F. Marcille
David I. Poston

December 2007

TABLE OF CONTENTS

1. INVESTIGATION OF MCNP STATISTICAL ERROR

Section Synopsis: A very large number of statistically independent ABR cases were executed, with numerous tallies per case, and in no case was there any indication of computational biases or anomalies. The error "quoted" by MCNP is reasonably consistent with the statistical error obtained via random sampling. The quoted error in k_{eff} is generally found to be 10% to 20% lower than the actual statistical error, while the quoted error for flux and reaction rates appears to match statistical error very well.

A number of numerical case studies were performed to determine:

1. How well does MCNP predict statistical error in ABR calculations?
2. Does MCNP indeed produce stochastic results with no apparent statistical anomalies?

Six different case studies, as listed in Table 1, where performed to provide information regarding the questions above. Within each case study an ABR reactor model was evaluated 40 separate times, each time with a different random seed number within MCNP – which in theory should produce completely independent, stochastic data sets.

Table 1 - List of Case Studies to Investigate Statistical Error

Case Study	Source Neutrons per Cycle	Convergence Cycles	Active Cycles	Run-Time on Stand-Alone 2.4 MHz Opteron Processor
A --- 2M Histories	20000	40	100	~1 hr
B --- 8M Histories	80000	40	100	~4 hr
C ---32M Histories	320000	40	100	~16 hr

1.1 Statistical Error Calculation and Comparison

One of the goals of this study is to determine if the quoted errors from MCNP are indeed valid. MCNP lists a relative error, or fractional error, with nearly every parameter is provides. This relative error is defined as the standard deviation of the parameter divided by the mean of the parameter. To assess the accuracy of the quoted MCNP value, 40 independent results were generated within each case study by changing the random seed number in the MCNP input deck. The relative statistical error of each desired parameter was calculated using these 40 values:

$$\text{Relative error} = \frac{\text{standard deviation}}{\text{mean}} = \frac{\sigma}{\bar{x}} = \frac{\sqrt{\frac{\sum_{1}^{N}(x(n)-\bar{x})^2}{N-1}}}{\bar{x}}$$

The relative error obtained from the N=40 samples within each case study are referred to as the "actual statistical error" throughout the rest of the document.

1.2 ABR Reactor Model Used in this Study

Figure 1 shows a schematic of the ABR model used in this study. All of the reactor assemblies have been homogenized except for one fuel assembly (shown just to the right of the central assembly). In this discrete hex (which shows as a dark blue instead of discrete pins depending on the resolution), all fuel pins are modeled separately (including clad, gap, pellet, hex can, fission gas plena, etc.). The volume fractions of material in this discrete region are identical to all of the other smeared yellow fuel assemblies. For comparison, a smeared fuel assembly is singled out for evaluation in a symmetric location to the discrete assembly, which is indicated by a light pea-green assembly just to the upper left of the central assembly. In addition, several symmetric regions further out in the reactor are evaluated to determine if the fission neutron source within MCNP is uniform and converged.

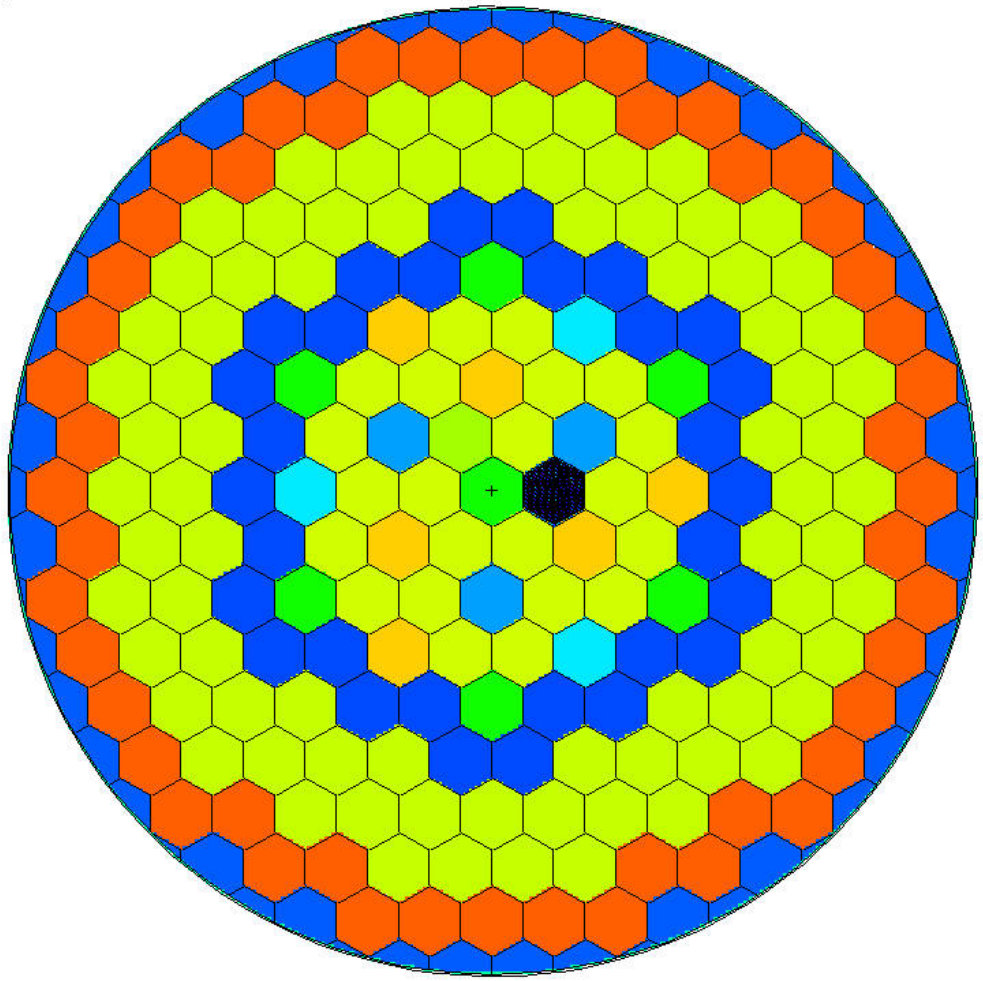

Figure 1 - Schematic of ABR Model

For the fission rate tallies, the assemblies/pins are divided into 20 axial regions of uniform spacing (~4 cm). This ABR model is configured close to critical condition, with the primary control assemblies inserted 50%. This also allows for a study of how discrete and smeared power distributions vary next to the control assemblies. Figure 2 shows the position of the control assembly next to the discrete and smeared fuel assemblies.

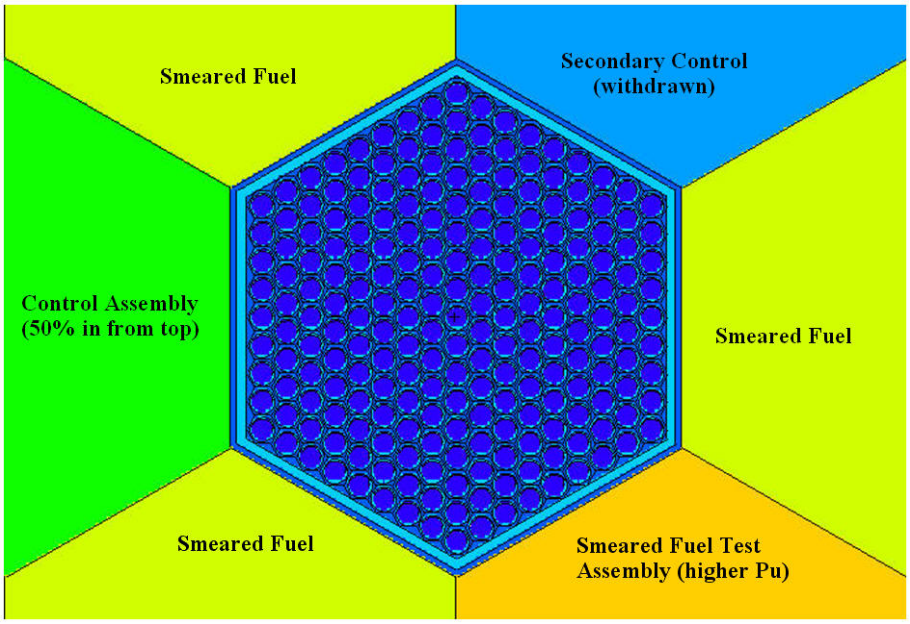

Figure 2(a) - Discrete Bundle and Surrounding Regions (top view)

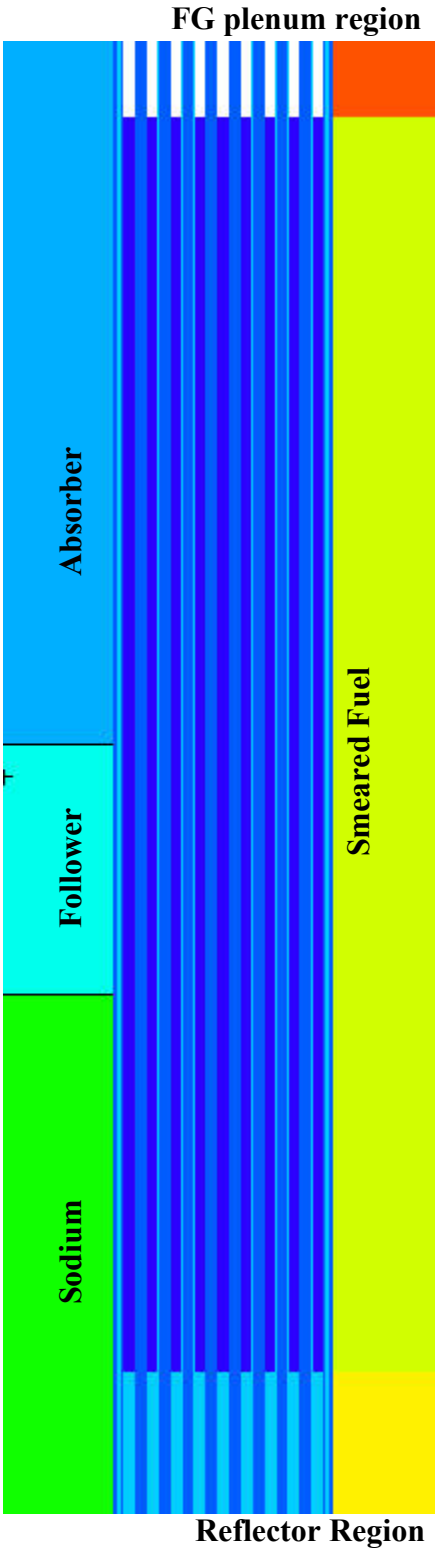

Figure 2(b) - Discrete Bundle and Surrounding Regions (side view)

1.3 System Criticality Results and Errors

The overall system k_{eff} is produced in every MCNP KCODE calculation. The values and errors of k_{eff} for each case study are listed below in Table 2.

Table 2 - k_{eff} Results and Errors for Case Studies A,B,C

	Average Calculated MCNP k_{eff}	Average Quoted Error from MCNP	Actual Statistical Error from 40 Samples
2M Histories	0.99880	0.00037	0.00042
8M Histories	0.99879	0.00018	0.00022
32M Histories	0.99884	0.00009	0.00011

The results in table 2 indicate that a good statistical approximation of k_{eff} can be obtained with MCNP with a relatively short run time. Actually, if k_{eff} is the only parameter of interest, the run times will be shorter than listed in Table A because there would be no additional tallies. The values in Table 2 also indicate that MCNP is producing a true stochastic result, because the error is reduced by the square root of the number of histories.

The other important information in Table 2 shows that the "quoted" error from MCNP is similar to the actual statistical error produced by the 40 trials in each case study. However, it is interesting to note that MCNP appears to consistently under predict the actual error (by ~20%). More case studies would have to be performed to determine if this is indeed a true under prediction, or simply that the 3 case studies each produced a data set that had a larger deviation than an average data set. If it is indeed found that MCNP under predicts error, then in practical terms a case would have to be run longer to achieve an actual user defined error; e.g. if MCNP under predicts error in k_{eff} by 20%, a typical case would have run 44% longer to achieve the error level that MCNP claims.

Figure 3 displays all of the individual calculated k_{eff} values for case studies A, B, and C, along with the average value of each case study. The trends of this figure correspond very well to what would be expected in a stochastic calculation; both in how the points are spaced about the mean and how the spread reduces with additional histories.

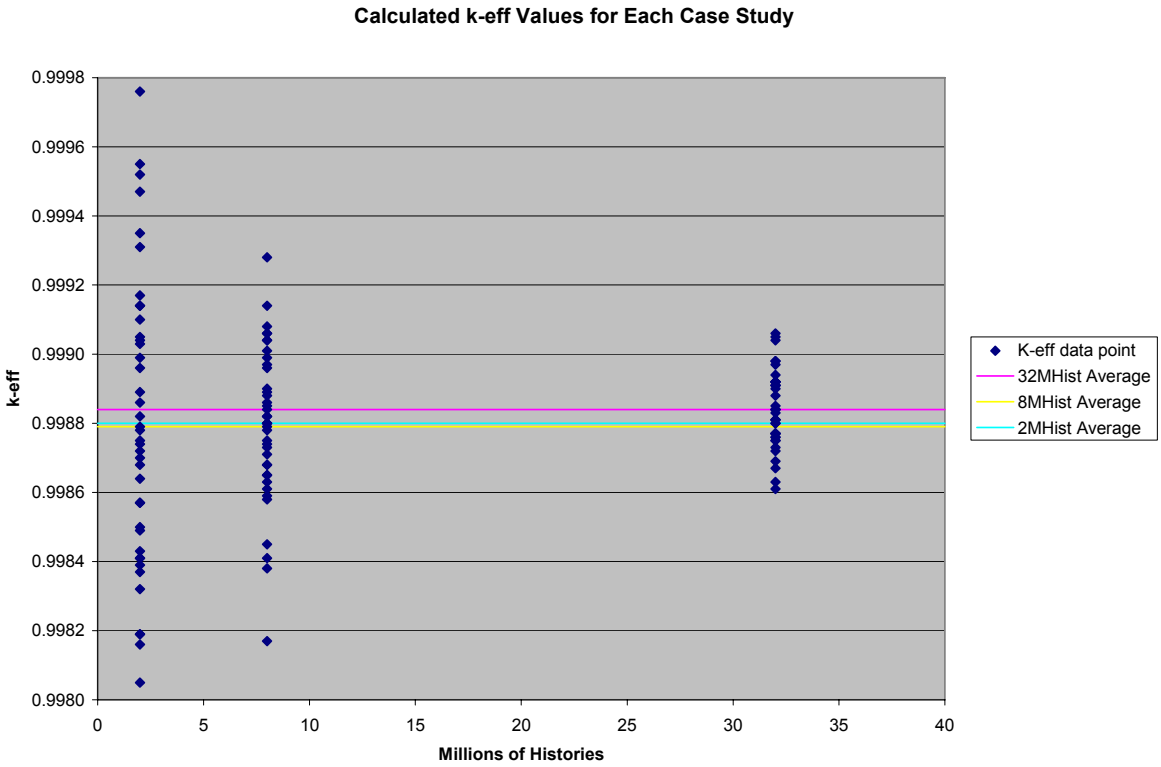

Figure 3 - Calculated k_{eff} for Case Studies A,B,C

1.4 Axial Fission Rate in Smeared Bundle

The comparison of MCNP quoted error and statistical error for the smeared hex axial distribution is in Table 3.

Table 3 - Axial Fission Rate Tallies in Smeared Hex

	Relative Fission Rate in ~4cm Axial Section of Smeared Fuel Hex	Average Quoted Error from MCNP	Actual Statistical Error from 40 Samples
2M Histories	1.000	0.0071	0.0079
8M Histories	1.000	0.0035	0.0040
32M Histories	1.000	0.0018	0.0019

The relative fission rate of each case is the same because they are all normalized to the average of one. These values could easily be normalized to an actual fission rate with an assumed power, MeV/fission and neutrons per fission, but that would not change any of the statistical evaluation. The important aspect of Table 3 is how well the quoted error agrees with the statistical sample, but as was seen in Table 2, the statistical value is slightly higher. The errors in Table 3 also show that a very good statistical approximation of the hex-averaged axial power profile can be obtained with a relatively small number of histories (i.e. short run time).

Table 4 shows the complete results for all of the axial location in the smeared hex.

Table 4 - Comparison of Quoted and Statistical Error in Smeared Hex

Axial Fission Rate and Errors in Smeared Bundle										
	2M Histories			8M Histories			32M Histories			
Axial Position (cm)	Fission Rate / Bundle Average	"Quoted" Error from MCNP	40 Sample Statistical Error	Fission Rate / Bundle Average	"Quoted" Error from MCNP	40 Sample Statistical Error	Fission Rate / Bundle Average	"Quoted" Error from MCNP	40 Sample Statistical Error
82.3	0.449	0.0098	0.0117	0.448	0.0049	0.0060	0.448	0.0025	0.0025
78.1	0.557	0.0090	0.0102	0.556	0.0045	0.0059	0.557	0.0022	0.0024
73.9	0.658	0.0083	0.0081	0.658	0.0042	0.0048	0.659	0.0021	0.0020
69.6	0.755	0.0078	0.0091	0.755	0.0039	0.0044	0.755	0.0019	0.0026
65.4	0.845	0.0073	0.0089	0.845	0.0037	0.0037	0.845	0.0018	0.0021
61.2	0.927	0.0070	0.0077	0.927	0.0035	0.0035	0.928	0.0017	0.0019
57.0	1.002	0.0067	0.0073	1.002	0.0034	0.0035	1.003	0.0017	0.0021
52.8	1.068	0.0065	0.0087	1.069	0.0033	0.0036	1.070	0.0016	0.0019
48.5	1.128	0.0063	0.0064	1.129	0.0032	0.0039	1.129	0.0016	0.0016
44.3	1.182	0.0062	0.0063	1.180	0.0031	0.0032	1.180	0.0015	0.0016
40.1	1.220	0.0061	0.0077	1.219	0.0031	0.0035	1.220	0.0015	0.0016
35.9	1.243	0.0060	0.0074	1.242	0.0030	0.0030	1.243	0.0015	0.0017
31.7	1.247	0.0061	0.0066	1.247	0.0030	0.0030	1.248	0.0015	0.0017
27.4	1.239	0.0061	0.0060	1.236	0.0030	0.0028	1.236	0.0015	0.0018
23.2	1.209	0.0062	0.0060	1.209	0.0031	0.0035	1.207	0.0015	0.0017
19.0	1.167	0.0063	0.0063	1.167	0.0032	0.0041	1.165	0.0016	0.0019
14.8	1.110	0.0066	0.0081	1.112	0.0033	0.0038	1.111	0.0016	0.0021
10.6	1.047	0.0069	0.0089	1.050	0.0035	0.0036	1.048	0.0017	0.0017
6.3	0.987	0.0075	0.0077	0.989	0.0037	0.0044	0.988	0.0019	0.0016
2.1	0.959	0.0089	0.0084	0.959	0.0044	0.0061	0.960	0.0022	0.0022

1.5 Fission Rate Distribution in Individual Pins

The comparison of MCNP quoted error and statistical error for individual pin tally regions that are 4 cm high are in Table 5.

Table 5 - Axial Fission Rate Tallies in Discrete Pins

	Relative Fission Rate in ~4cm Axial Section of Fuel Pellet Region	Average Quoted Error from MCNP	Actual Statistical Error from 40 Samples
2M Histories	1.000	0.045	0.046
8M Histories	1.000	0.023	0.023
32M Histories	1.000	0.011	0.012

The statistical error in the individual pin tallies is much higher than for the smeared hex because of a much smaller volume. The execution time required to obtain the same error in discrete-pin cases versus smeared cases is discussed in a later section of the report. It is also possible to calculate fission rates (and other reaction rates) in every single pin in the core (with 20 axial nodes). This requires long execution time, but it may not be prohibitively long for certain applications.

Tables 6, 7 and 8 show the complete results for all of the axial location in pins within the discretely modeled bundle.

Table 6 - Comparison of Quoted and Statistical Error in Center Pin of Bundle

Axial Fission Rate and Errors in Center Pin of Discrete Bundle									
	2M Histories			8M Histories			32M Histories		
Axial Position (cm)	Fission Rate / Bundle Average	"Quoted" Error from MCNP	40 Sample Statistical Error	Fission Rate / Bundle Average	"Quoted" Error from MCNP	40 Sample Statistical Error	Fission Rate / Bundle Average	"Quoted" Error from MCNP	40 Sample Statistical Error
82.3	0.459	0.064	0.073	0.451	0.031	0.033	0.450	0.016	0.018
78.1	0.567	0.056	0.057	0.561	0.028	0.028	0.568	0.014	0.014
73.9	0.672	0.052	0.055	0.669	0.026	0.026	0.671	0.013	0.016
69.6	0.764	0.048	0.046	0.773	0.024	0.028	0.771	0.012	0.014
65.4	0.858	0.046	0.054	0.859	0.023	0.026	0.865	0.011	0.015
61.2	0.935	0.043	0.046	0.948	0.022	0.023	0.944	0.011	0.011
57.0	1.024	0.042	0.046	1.025	0.021	0.021	1.022	0.011	0.010
52.8	1.085	0.041	0.046	1.093	0.020	0.021	1.094	0.010	0.011
48.5	1.145	0.040	0.046	1.156	0.020	0.018	1.154	0.010	0.011
44.3	1.206	0.039	0.042	1.209	0.019	0.020	1.204	0.010	0.010
40.1	1.242	0.038	0.035	1.240	0.019	0.016	1.243	0.010	0.008
35.9	1.267	0.038	0.040	1.258	0.019	0.021	1.265	0.010	0.011
31.7	1.264	0.038	0.036	1.270	0.019	0.016	1.272	0.010	0.009
27.4	1.272	0.042	0.053	1.255	0.019	0.018	1.257	0.010	0.009
23.2	1.231	0.039	0.041	1.227	0.019	0.022	1.231	0.010	0.011
19.0	1.185	0.039	0.037	1.187	0.020	0.020	1.185	0.010	0.009
14.8	1.143	0.041	0.044	1.128	0.020	0.017	1.126	0.010	0.010
10.6	1.054	0.043	0.043	1.057	0.022	0.020	1.053	0.011	0.013
6.3	0.983	0.047	0.056	0.981	0.024	0.021	0.985	0.012	0.013
2.1	0.940	0.060	0.053	0.932	0.029	0.028	0.927	0.016	0.017

Table 7 - Comparison of Quoted and Statistical Error in Edge Pin Nearest Poison

Axial Fission Rate and Errors in Pin Closest to Control Poison									
	2M Histories			8M Histories			32M Histories		
Axial Position (cm)	Fission Rate / Bundle Average	"Quoted" Error from MCNP	40 Sample Statistical Error	Fission Rate / Bundle Average	"Quoted" Error from MCNP	40 Sample Statistical Error	Fission Rate / Bundle Average	"Quoted" Error from MCNP	40 Sample Statistical Error
82.3	0.420	0.063	0.069	0.417	0.032	0.031	0.417	0.016	0.016
78.1	0.521	0.058	0.059	0.513	0.029	0.024	0.516	0.014	0.014
73.9	0.615	0.053	0.059	0.608	0.026	0.027	0.607	0.013	0.014
69.6	0.700	0.050	0.056	0.696	0.025	0.024	0.702	0.012	0.013
65.4	0.783	0.047	0.054	0.783	0.023	0.024	0.784	0.012	0.011
61.2	0.870	0.045	0.047	0.864	0.023	0.021	0.860	0.011	0.011
57.0	0.935	0.043	0.047	0.932	0.022	0.023	0.933	0.011	0.011
52.8	0.998	0.041	0.051	0.999	0.021	0.026	0.998	0.010	0.011
48.5	1.060	0.040	0.040	1.059	0.020	0.021	1.062	0.010	0.011
44.3	1.133	0.039	0.043	1.129	0.020	0.018	1.130	0.010	0.011
40.1	1.191	0.038	0.042	1.192	0.019	0.021	1.194	0.010	0.012
35.9	1.230	0.038	0.040	1.222	0.019	0.019	1.228	0.010	0.010
31.7	1.244	0.038	0.038	1.235	0.019	0.019	1.242	0.009	0.011
27.4	1.230	0.039	0.040	1.234	0.019	0.019	1.232	0.010	0.010
23.2	1.217	0.039	0.040	1.212	0.019	0.020	1.213	0.010	0.011
19.0	1.177	0.040	0.037	1.178	0.021	0.027	1.174	0.010	0.011
14.8	1.118	0.043	0.045	1.124	0.022	0.023	1.127	0.011	0.012
10.6	1.103	0.050	0.065	1.074	0.023	0.027	1.074	0.012	0.012
6.3	1.028	0.054	0.053	1.027	0.029	0.029	1.027	0.015	0.016
2.1	1.013	0.069	0.072	0.995	0.034	0.037	1.003	0.018	0.018

Table 8 – Comparison of Quoted and Statistical Error in Edge Pin Furthest from Poison

Axial Fission Rate and Errors in Pin Furthest from Control Poison										
	2M Histories			8M Histories			32M Histories			
Axial Position (cm)	Fission Rate / Bundle Average	"Quoted" Error from MCNP	40 Sample Statistical Error	Fission Rate / Bundle Average	"Quoted" Error from MCNP	40 Sample Statistical Error	Fission Rate / Bundle Average	"Quoted" Error from MCNP	40 Sample Statistical Error
82.3	0.444	0.064	0.065	0.455	0.032	0.031	0.449	0.016	0.017
78.1	0.572	0.057	0.065	0.565	0.028	0.028	0.561	0.014	0.013
73.9	0.671	0.052	0.051	0.670	0.026	0.029	0.665	0.013	0.014
69.6	0.758	0.049	0.057	0.768	0.024	0.031	0.764	0.012	0.011
65.4	0.860	0.047	0.052	0.855	0.023	0.025	0.855	0.012	0.011
61.2	0.939	0.044	0.034	0.942	0.022	0.024	0.936	0.011	0.012
57.0	1.008	0.042	0.057	1.012	0.021	0.029	1.012	0.011	0.013
52.8	1.079	0.040	0.038	1.082	0.020	0.022	1.079	0.010	0.009
48.5	1.127	0.040	0.036	1.135	0.020	0.023	1.136	0.010	0.010
44.3	1.175	0.039	0.050	1.179	0.019	0.016	1.185	0.010	0.012
40.1	1.200	0.038	0.039	1.208	0.019	0.017	1.222	0.010	0.010
35.9	1.227	0.038	0.040	1.225	0.019	0.017	1.246	0.010	0.009
31.7	1.224	0.039	0.046	1.229	0.019	0.017	1.247	0.010	0.010
27.4	1.213	0.039	0.034	1.213	0.019	0.018	1.240	0.010	0.010
23.2	1.201	0.039	0.037	1.179	0.020	0.019	1.213	0.010	0.012
19.0	1.146	0.040	0.036	1.136	0.020	0.024	1.166	0.010	0.008
14.8	1.084	0.041	0.044	1.085	0.021	0.019	1.113	0.010	0.011
10.6	1.008	0.043	0.050	1.011	0.022	0.021	1.043	0.011	0.010
6.3	0.949	0.049	0.051	0.946	0.024	0.026	0.975	0.012	0.012
2.1	0.914	0.064	0.064	0.903	0.031	0.031	0.930	0.016	0.015

2. INVESTIGATION OF FISSION SOURCE CONVERGENCE FOR THE ABR

Section Synopsis: Statistically independent ABR cases were executed that verified that MCNP quickly converges to a uniform and stable fission source distribution. There was no statistical difference in k_{eff} calculations in cases with 5, 10, 20, and 40 convergence cycles. A comparison of tallies in remote, symmetric locations in the reactor showed that 10 or more cycles are adequate for a uniform geometric distribution.

An adequately converged fission source is a requirement for accurate and meaningful Monte Carlo calculations. Several statistically independent case studies were executed to determine:

1. Does the MCNP fission source converge to a uniform and stable distribution?
2. How many convergence (inactive) MCNP cycles are required until adequate source convergence is obtained?

An empirical study of fission source convergence was performed by varying the number of convergence (a.k.a. inactive) cycles in MCNP. Theses cases are listed in Table 9. Cases D,E, and F were executed to compare with Case B from the statistical error study, to investigate fission source convergence. In each of these cases, several tallies were tabulated in symmetric core locations to investigate the spatial uniformity and convergence of the fission source. As before, each case was executed 40 times with difference starting random number seeds.

Table 9 - List of Cases Used in Convergence Study

Case Study	Source Neutrons per Cycle	Convergence Cycles	Active Cycles	Run-Time on Standalone 2.4 GHz Opteron Processor
D --- 8M Histories	80000	5	100	~3.4 hr
E --- 8M Histories	80000	10	100	~3.5 hr
F --- 8M Histories	80000	20	100	~3.7 hr
B --- 8M Histories	80000	40	100	~4 hr

The optimum number in inactive cycles will usually depend on who well the initial source guess is. For all of the cases in this study, a very simple approximation was used that distributes the source over 54 discrete points, as shown in Table 10.

There was nothing scientific in choosing the points in Table 10, other than "eye-balling" the core schematic and choosing 18 x,y coordinates that spread reasonably well over the fissile regions of the reactor. Then, at each x,y coordinate, 3 axial source points were places at 20 cm, 40cm , and 60 cm, because the fueled region extends approximately from 0 cm to 80 cm. It is possible to develop a more sophisticated KSRC, or better yet, run MCNP for a typical reactor state and use the resulting KSRC to initiate all future MCNP runs; however, we have typically found that a simple KSRC as shown in Table 10, which only takes a couple of minutes to generate, does very well for all applications.

Table 10 - Initial Neutron Source Points (ksrc) for All MCNP Runs

x	y	z		x	y	z		x	y	z
15	0	20		15	0	40		15	0	60
-8	12	20		-8	12	40		-8	12	60
8	12	20		8	12	40		8	12	60
15	25	20		15	25	40		15	25	60
15	-25	20		15	-25	40		15	-25	60
-15	0	20		-15	0	40		-15	0	60
52	38	20		52	38	40		52	38	60
-52	38	20		-52	38	40		-52	38	60
52	-38	20		52	-38	40		52	-38	60
-52	-38	20		-52	-38	40		-52	-38	60
0	76	20		0	76	40		0	76	60
0	-76	20		0	-76	40		0	-76	60
74	0	20		74	0	40		74	0	60
-74	0	20		-74	0	40		-74	0	60
66	63	20		66	63	40		66	63	60
-66	63	20		-66	63	40		-66	63	60
66	-63	20		66	-63	40		66	-63	60
-66	-63	20		-66	-63	40		-66	-63	60

The first check of fission source convergence is the check a system-wide parameter. The k_{eff} and error in k_{eff} is shown in Table 11 for the 4 different cases. The averaged k_{eff} and average quoted error is based on the 40 independent cases, and the statistical error is the actual standard deviation of the 40 samples.

Table 11 - k_{eff} Results and Errors as a Function of Convergence Cycles

Number of Convergence Cycles	Average Calculated MCNP k_{eff}	Average Quoted Error from MCNP	Actual Statistical Error from 40 Samples
5	0.99878	0.00018	0.00020
10	0.99876	0.00019	0.00022
20	0.99880	0.00018	0.00021
40	0.99878	0.00018	0.00021

It is clear from Table 11 that there is no benefit to added convergence cycles in a k_{eff} calculation. The calculated k_{eff} and the statistical errors are nearly identical for each case. Note that these cases confirm the earlier conclusion that MCNP slightly underestimates error in k_{eff}.

To check the spatial convergence of the fission source, tallies were calculated in three symmetric locations in both the fuel and reflector regions. The fission rate was tallied in hex locations in the outer row of fuel: locations (4,1), (4,9), and (4,17) on Figure 8. The flux was tallied in three symmetric locations in outer row (row 6) of the reflector, because if there were any spatial source convergence issues this is where they would be most apparent. The tallies were also divided into 20 axial locations to complete a 3D picture of source convergence.

A large amount of data was generated to check source convergence (~40,000 tallies and errors). All of the data suggested that a uniform, converged source was achieved very quickly, but it is counterproductive to clutter the text with numerous tables that show essentially the same thing.

Table 12 - Fission-Rate-to-Average in Three Symmetric Outer Fuel Regions

	5 Convergence Cycles			10 Convergence Cycles			20 Convergence Cycles			40 Convergence Cycles		
Axial Loc.	Lattice (4,1)	Lattice (4,9)	Lattice (4,17)	Lattice (4,1)	Lattice (4,9)	Lattice (4,17)	Lattice (4,1)	Lattice (4,9)	Lattice (4,17)	Lattice (4,1)	Lattice (4,9)	Lattice (4,17)
1	0.8903	0.8937	0.8896	0.8914	0.8926	0.8937	0.8917	0.8914	0.8923	0.8914	0.8897	0.8898
2	0.9290	0.9337	0.9299	0.9311	0.9324	0.9327	0.9301	0.9306	0.9332	0.9318	0.9304	0.9302
3	0.9994	1.0037	0.9982	1.0016	1.0019	1.0019	0.9977	1.0010	1.0038	1.0024	0.9996	1.0000
4	1.0686	1.0732	1.0701	1.0709	1.0723	1.0693	1.0694	1.0714	1.0732	1.0715	1.0700	1.0718
5	1.1280	1.1323	1.1289	1.1303	1.1330	1.1306	1.1294	1.1301	1.1331	1.1317	1.1299	1.1322
6	1.1748	1.1799	1.1756	1.1770	1.1799	1.1789	1.1768	1.1769	1.1791	1.1789	1.1766	1.1791
7	1.2065	1.2132	1.2078	1.2087	1.2118	1.2104	1.2089	1.2097	1.2108	1.2112	1.2094	1.2110
8	1.2240	1.2300	1.2239	1.2240	1.2287	1.2277	1.2251	1.2275	1.2262	1.2279	1.2251	1.2269
9	1.2265	1.2326	1.2259	1.2267	1.2299	1.2272	1.2264	1.2279	1.2281	1.2292	1.2260	1.2276
10	1.2125	1.2181	1.2118	1.2121	1.2153	1.2112	1.2118	1.2133	1.2134	1.2140	1.2117	1.2124
11	1.1843	1.1896	1.1841	1.1850	1.1871	1.1837	1.1855	1.1857	1.1853	1.1855	1.1857	1.1853
12	1.1436	1.1490	1.1429	1.1433	1.1450	1.1437	1.1454	1.1444	1.1445	1.1453	1.1443	1.1447
13	1.0920	1.0965	1.0910	1.0908	1.0927	1.0912	1.0930	1.0929	1.0916	1.0943	1.0917	1.0916
14	1.0291	1.0333	1.0287	1.0283	1.0298	1.0291	1.0301	1.0305	1.0288	1.0315	1.0291	1.0290
15	0.9575	0.9610	0.9569	0.9581	0.9587	0.9568	0.9585	0.9588	0.9562	0.9587	0.9569	0.9586
16	0.8793	0.8821	0.8784	0.8786	0.8773	0.8775	0.8798	0.8800	0.8774	0.8780	0.8794	0.8786
17	0.7938	0.7957	0.7931	0.7928	0.7939	0.7933	0.7941	0.7938	0.7923	0.7943	0.7932	0.7939
18	0.7021	0.7048	0.7035	0.7020	0.7045	0.7039	0.7045	0.7035	0.7061	0.7015	0.7056	0.7033
19	0.6094	0.6120	0.6100	0.6103	0.6114	0.6094	0.6115	0.6111	0.6100	0.6096	0.6112	0.6101
20	0.5214	0.5228	0.5207	0.5225	0.5220	0.5212	0.5227	0.5223	0.5231	0.5228	0.5219	0.5221
Tot Pin	**0.9986**	**1.0029**	**0.9986**	**0.9993**	**1.0010**	**0.9997**	**0.9996**	**1.0001**	**1.0004**	**1.0006**	**0.9994**	**0.9999**

Table 13 - Flux-to-Average in Three Symmetric Outer Reflector Regions

	5 Convergence Cycles			10 Convergence Cycles			20 Convergence Cycles			40 Convergence Cycles		
Axial Loc.	Lattice (4,1)	Lattice (4,9)	Lattice (4,17)	Lattice (4,1)	Lattice (4,9)	Lattice (4,17)	Lattice (4,1)	Lattice (4,9)	Lattice (4,17)	Lattice (4,1)	Lattice (4,9)	Lattice (4,17)
2	0.8809	0.8767	0.8805	0.8780	0.8790	0.8774	0.8790	0.8778	0.8787	0.8744	0.8783	0.8774
3	0.9534	0.9471	0.9498	0.9473	0.9507	0.9492	0.9498	0.9501	0.9492	0.9488	0.9495	0.9500
4	1.0160	1.0084	1.0138	1.0114	1.0130	1.0132	1.0121	1.0098	1.0121	1.0114	1.0102	1.0127
5	1.0684	1.0634	1.0672	1.0654	1.0658	1.0662	1.0642	1.0631	1.0658	1.0646	1.0643	1.0674
6	1.1089	1.1061	1.1085	1.1077	1.1069	1.1065	1.1054	1.1062	1.1075	1.1084	1.1061	1.1088
7	1.1390	1.1347	1.1380	1.1384	1.1364	1.1370	1.1375	1.1372	1.1348	1.1381	1.1384	1.1394
8	1.1573	1.1497	1.1543	1.1554	1.1529	1.1559	1.1570	1.1566	1.1526	1.1546	1.1546	1.1542
9	1.1598	1.1536	1.1610	1.1607	1.1557	1.1578	1.1612	1.1593	1.1575	1.1616	1.1587	1.1610
10	1.1505	1.1435	1.1533	1.1513	1.1476	1.1492	1.1504	1.1513	1.1491	1.1526	1.1508	1.1510
11	1.1275	1.1261	1.1339	1.1322	1.1266	1.1297	1.1288	1.1333	1.1301	1.1316	1.1313	1.1280
12	1.0973	1.0946	1.1007	1.0991	1.0949	1.0963	1.0941	1.0997	1.0986	1.0961	1.0995	1.0968
13	1.0586	1.0534	1.0594	1.0583	1.0550	1.0548	1.0551	1.0599	1.0573	1.0553	1.0539	1.0561
14	1.0077	1.0021	1.0079	1.0095	1.0028	1.0055	1.0071	1.0086	1.0059	1.0052	1.0063	1.0058
15	0.9509	0.9453	0.9501	0.9541	0.9461	0.9492	0.9491	0.9493	0.9495	0.9482	0.9496	0.9489
16	0.8878	0.8846	0.8879	0.8909	0.8841	0.8884	0.8853	0.8872	0.8868	0.8856	0.8863	0.8873
17	0.8220	0.8193	0.8230	0.8225	0.8223	0.8213	0.8201	0.8195	0.8238	0.8192	0.8241	0.8197
18	0.7565	0.7500	0.7543	0.7535	0.7547	0.7538	0.7538	0.7526	0.7555	0.7507	0.7560	0.7538
19	0.6873	0.6823	0.6859	0.6860	0.6869	0.6854	0.6821	0.6836	0.6863	0.6830	0.6876	0.6869
Tot Pin	**1.0017**	**0.9967**	**1.0016**	**1.0012**	**0.9990**	**0.9998**	**0.9996**	**1.0003**	**1.0001**	**0.9994**	**1.0003**	**1.0003**

There is very little difference in a magnitude or deviation of the data in symmetric locations in Tables 12 and 13. It is hard to draw any conclusions by looking at the individual data points at each axial node. However, there is a noticeable difference in the deviation of the bolded total pin values – the cases with more convergence cycles are bunched closer to one. Most of the difference is between the 5 and 10 cycle results, and there is no statistical difference between the 20 and 40 cycle results. This data indicates that the spatial fission source distribution does improve slightly between 5 and 20 convergence cycles.

Table 14 lists the average standard deviation between the three symmetric data points for each batch of runs.

Table 14 - Relative Deviation between Symmetric Locations

Number of Convergence Cycles	Deviation at Outer Fuel Locations	Deviation at Outer Reflector Locations
5	0.0111	0.0158
10	0.0076	0.0110
20	0.0073	0.0098
40	0.0068	0.0099

Table 14 does indeed show a higher deviation between symmetric locations at five convergence cycles. At 10 cycles and greater, the deviation between symmetric samples is identical to the statistical standard deviation of a batch of samples at a single location; therefore, the source is fully symmetric and uniform in three dimensions. The higher

variance when using five convergence cycles indicates that the input SDEF in table 10 is not fully symmetric relative to the tally locations.

Overall, all of the data in the fission source convergence study indicates that MCNP quickly converges to a uniform and stable ABR distribution in a relatively small number of convergence cycles.

3. PRACTICALITY OF USING MCNP FOR VARIOUS ABR CALCULATIONS

Section Synopsis: The MCNP ABR model was executed for various combinations of geometry (smeare vs discrete) and tally information. Reaction rates to <1% accuracy within all fueled regions in a smeared-hex model (at 20 axial locations in each hex) can be obtained in less than one cpu-hour. Reaction rates calculations of the same fidelity within one-discretely modeled bundle require on the order of several cpu-hours. Execution times are tabulated for a wide range of possibilities, including a case that discretely models the entire core. An example of tallies in discrete pins is provided to show how the potential usefulness of discrete calculations.

Previous sections have concluded that:

- MCNP appears to provide "clean" stochastic results (not statistical biases or anomalies).
- MCNP provides relatively accurate representations of statistical error.
- MCNP quickly converges to a stable fission source for a typical ABR configuration.

Given these conclusions, the ultimate value of MCNP (or any stochastic approach) will depend on the practicality of using MCNP for various ABR calculations. Practicality is a function of the usefulness of the information, the error of the information, and the time/effort required to obtain the information. "Usefulness" contains the established benefits of MCNP calculations, most importantly the ability to create high-fidelity geometries and the use of continuous energy cross sections. These benefits offer the potential of more accurate reaction rates, reactivity coefficients, etc. in discrete components. Ultimately, the usefulness if defined by the end-user of the data, so this section will concentrate only on the statistical error, and time and effort required to obtain various parameters.

Table 15 - Execution Time of Various MCNP Cases on a Single 2.4 GHz Opteron Processor

	All hexes smeared (cpu-hours)	One hex discrete (cpu-hours)	All hexes discrete (cpu-hours)
No tallies	3.6	3.9	16.9
One hex flux tallies	3.8	4.1	21.4
One hex flux and fission rate	4.1	4.3	25.8
One hex, flux + 4 reaction rates	5.7	5.0	39.8
Four hexes flux talies	3.8	n/a	34.3
Four hexes flux and fission rate.	4.1	n/a	51.4
Four hexes, flux + 4 reaction rates	5.8	n/a	103.6
All (60) hexes flux talies	4.1	n/a	322.1
All (60) hexes flux and fission rate.	4.9	n/a	418.6
All (60) hexes, flux + 4 reaction rates	8.6	n/a	1024.5

All of the CPU-hours listed in Table 15 are for a single-processor MCNP5 job and a 2.4 MHz Opereron. MCNP5 is very efficient at running these jobs in parallel, so the run time can be estimated by the number in Table 15 divided by the number of processors used. Thus, even the longest case in Table 15 (~1000 cpu-hours) would take ~20 hours to

complete on a 50-processor cluster. Note that on our cluster, MCNPX executes from 5% to 25% slower than MCNP5 for single-processor jobs, and in some parallel applications more than 2 times slower. As noted elsewhere, MCNPX and MCNP5 have been observed to produce consistent and similar results, MCNP5 has been chosen because of faster computation time.

Each of the cases in Table 15 produces the same error in k_{eff}, but the error in the tallies is dependent on the volume of the tally region, as well as the flux magnitude and spectra). The most important run-time parameter is how long it takes to get a desired statistical error in a specific calculation. Table 16 lists the time required to achieve a 1% statistical error in various problems.

Table 16 - Execution Time Required for 1% Fission Rate Error

	1 axial node (cpu-hours)	5 axial nodes (cpu-hours)	20 axial nodes (cpu-hours)
One smeared hex	0.03	0.16	0.65
All 60 smeared hexes	0.04	0.20	0.79
All 217 pins in one hex (rest smeared)	1.14	5.72	22.90
All 13020 discrete pins in core	110.73	553.63	2214.51

The substantial increase in run time of individual fuel pins as compared to a smeared hex is caused by the much smaller volume of the pin (actually the fuel pellet, which is where the fission rate is tallied). The run time is almost directly proportional to the axial discretization. One-percent accurate reaction rates at 20 axial locations will take approximately 20 times longer than a 1% accurate reaction rate for the entire pin. However, this approximation becomes less appropriate the higher the level of axial peaking. The higher flux regions within the 20 discrete nodes will have <1% error and vice-versa; so if a 1% error is desired in all nodes, the run time will need be longer to bring the error in the low-flux regions down.

Although the time required calculating fission rate in every pin is large, the application of numerous parallel processors is very effective. On a 50 CPU cluster of 2.4 GHz Opterons, it takes ~12 hours to calculate the fission rate at 5 axial levels within all 13020 fuel pins to a statistical error of ~1%. This may or may not be practical depending on the intended use of the data.

3.1 Some Notable Effects on Execution Time

The use of natural elements versus individual isotopes is an important consideration for MCNP calculations. The number of individual isotopes in an MCNP material has a significant impact on computation time, especially if reaction rates are being tallied. For example, reaction rates in stainless steel might take twice as long to calculate if all isotopes are individually represented as compared to using elemental cross sections. In general, unless in there is significant transmutation expected in the material and/or a very high fidelity calculation is required, it is preferable to use elemental cross sections when available.

The use of repeated structures and multi-leveled universes in MCNP generally makes computation time longer, especially in cases that perform tallies within multiple

lattice/universe structures. However, in most cases, the "simplicity" of using repeated structures is worth the slight increase in computation time caused by this representation.

3.2 Example of Discrete Fission Rate Tallies

Figure 4 plots the axial fission rate distribution within various pins within a discretely modeled assembly. The location of the assembly relative to other assemblies is shown in Figures 1 and 2.

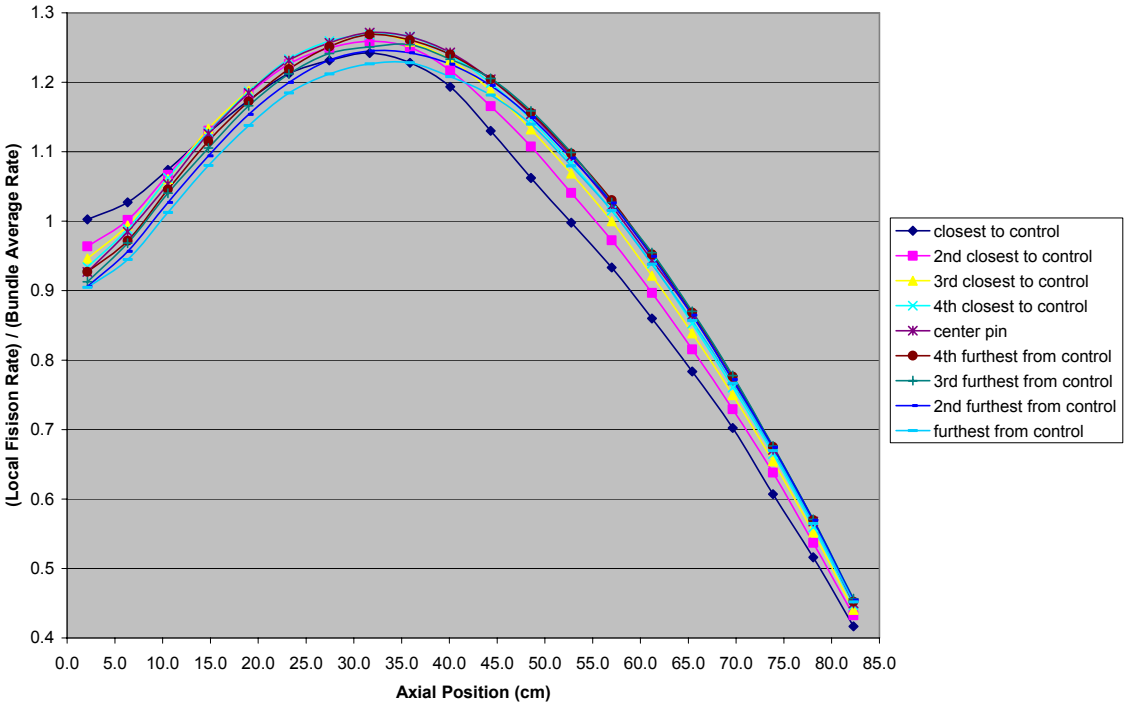

Figure 4 - Axial Fission Rate Distribution in Discrete Bundle Pins (at y=0 horizontal plane)

The effect of the control poison is evident in this plot, especially on the pin closest to the poison. Note that the pin closest to the control assembly has a power peak near the bottom – this may be because the model contains sodium in the region just below the poison, so this fuel may be the first thing that slightly moderated neutrons leaving the sodium encounter.

Figure 5 compares the axial distribution of fissions of a smeared geometry to the average axial distribution of the discrete case. The profile matches very well everywhere except at the bottom of the assembly. This is the same region of interest in Figure 4, and where a more moderated neutron flux may be available. The difference between the smeared and discrete values may be because the smeared bundle is more likely to absorb a thermalized neutron in the fuel.

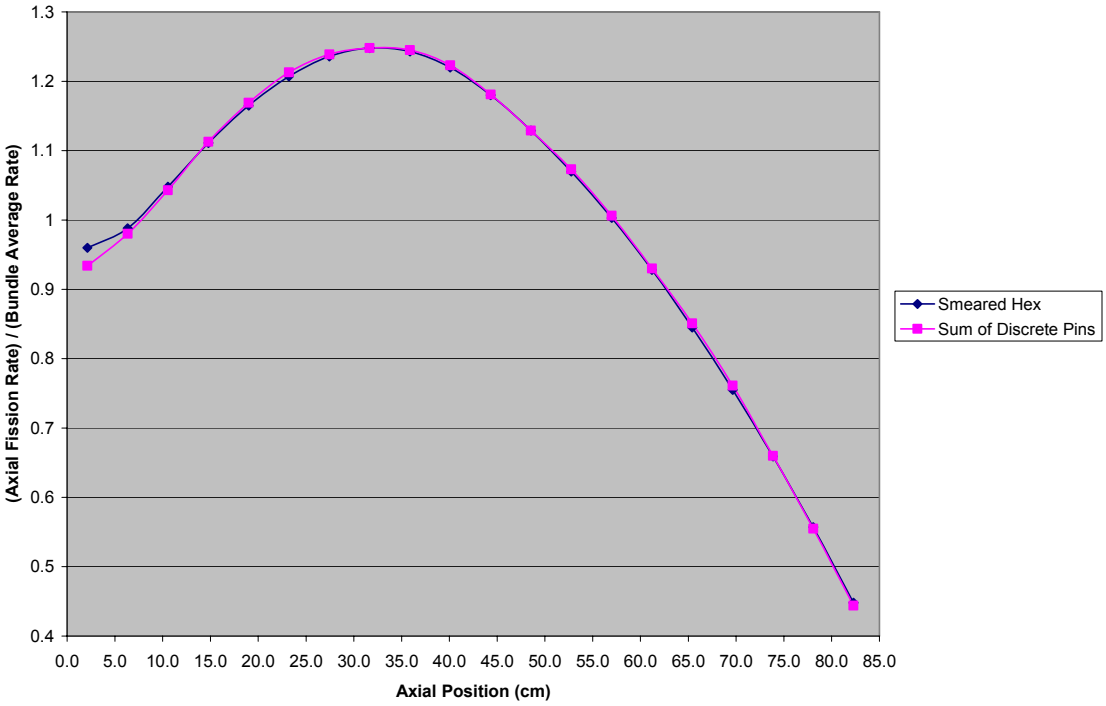

Figure 5 - Bundle Average Fission Rate Distribution

Figures 4 and 5 show the potential importance of performing discrete reaction rate calculations (as opposed to smeared). Several other reasons to use discrete models (e.g. more accurate reactivity calculations) have also been mentioned in this report.

4. PERTURBATION EVALUATION

4.1 MCNP Model Description

The MCNP models for the perturbation and burnup studies were generated using ABRgen. ABRgen is an in-house program that facilitates MCNP model generation by reading an input file containing such core descriptors as number of rows of hexes and pins, component dimensions, material compositions, etc. Any of the hexes can be represented explicitly or homogenized. A radial core plot comparing a case in which all hexes are explicitly modeled can be seen in Figure 6, while Figure 7 shows a core model in which all components except for the control hexes are homogenized.

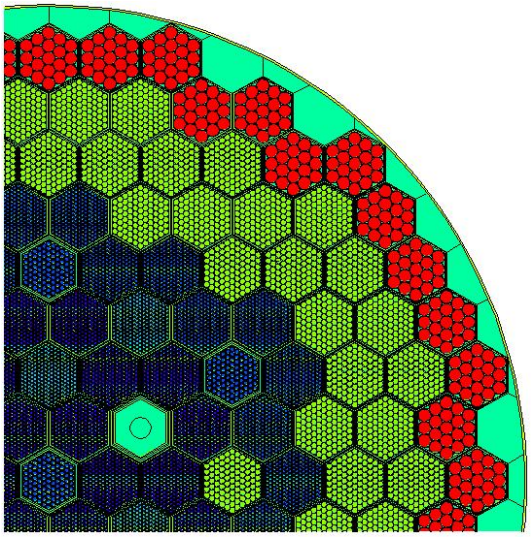

Figure 6 – Detailed Radial Core Plot

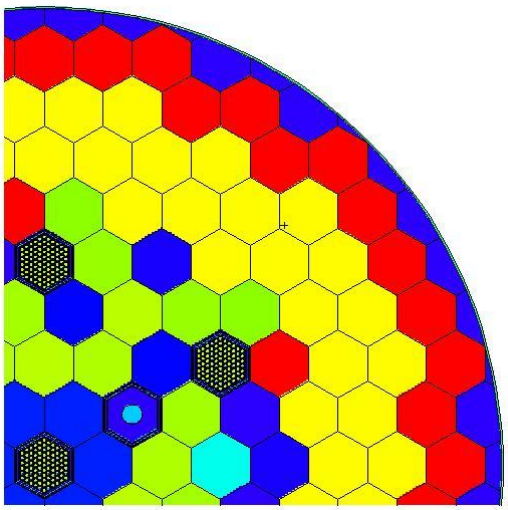

Figure 7 – Homogenized Radial Core Plot

ABRgen hex homogenization is performed by calculating the quantity of each material present in the detailed model, then generating a new MCNP material card containing those isotopes in the appropriate proportions, and filling the hex with that material uniformly. This homogenization is done for radial hex sections, while axial differences in the hex are maintained. For example, the fuel hex contains five distinct axial regions: nosepiece, reflector, fuel, gas plenum, and handling socket. Homogenizing all hex components to produce a single material representing the entire fuel hex would result in a complete loss of axial variation. Maintaining axial variation is essential, so each homogenized hex is split into the requisite number of axial sections. While the fuel hex requires five regions, the control hex requires eight (nosepiece, reflector, empty duct, follower, absorber, gas plenum, upper empty duct, and handling socket), and the reflector or shield hexes require three (nosepiece, reflector/shield, handling socket).

Cross-sections used in this study were from the ENDF/B-V rmccs (recommended Monte Carlo cross-section) files provided in the MCNP5 distribution.

4.1.1 Verification by Using Neutron Balance

One technique used to assess the validity of a Monte Carlo calculation is to perform a neutron balance on a given segment. A neutron balance in this context involves calculating the ratio between the number neutrons produced in and streaming into a segment to the number of neutrons absorbed in and leaking out of the segment. Reaction rates for parasitic capture, (n,2n), and fission were calculated for each fuel hex in the core, segmented in five axial regions. While those three reaction rates account for neutron loss in the segment, ν*fission must be calculated to determine neutron production (where ν is number of neutrons emitted per fission). MCNP reaction rate tallies take the form:

```
f014:n    871
fm014    (-1  11 -2) (-1  11 16) (-1  11 -6 ) (-1  11 -6 -7)
sd014     1
```

In this case, the tally is type 4:n, neutron flux in a cell, and 871 is the fuel cell being considered. There are four multiplier sets on the "fm" card, in each of them -1 indicates that the flux should be multiplied by the number density of the region, while 11 indicates the material number filling the cell. The -2 multiplier gives parasitic absorption, 16 gives (n,2n), while -6 gives fission, and -6 -7 gives ν*fission. The segment divisor "sd" card sets the segment volume equal to 1. Though the true segment volume is not 1, by setting it as such one can simplify the conversion between the normalized reaction rates produced by MCNP and physical reaction rates. For example, total fission rate in a given fuel segment is given by the following:

$$\text{Total fission rate} = N\sigma_f\phi V$$

Where N is the material number density, σ_f is the microscopic fission cross-section, ϕ is the neutron flux, and V is the segment volume. Note that the number density and microscopic cross-section are accounted for in the "fm" card. If the true segment volume is provided on the "sd" card, the resultant quantity from the tally will be $N\sigma\phi$, which will then need to be multiplied by segment volume. However, if the segment volume is artificially set to be 1, the resultant tally quantity will be $N\sigma\phi V$, the quantity of interest. This quantity is normalized per source neutron, so one further conversion is necessary to yield physical quantities. The normalization factor for an MCNP criticality calculation is

$$\text{Normalization} = \nu P/Q_{fiss}k_{eff}$$

where ν is the number of neutrons emitted per fission, P is thermal power, Q_{fiss} is recoverable energy per fission, and k_{eff} is the system k_{eff} of the calculation. In this neutron balance calculation, ν is 2.9305 (a value determined from the MCNP calculation), P is 250 MW (desired thermal power), Q_{fiss} is 202 MeV (an assumed value), and k_{eff} is 1.03321 (calculated by MCNP).

In addition to reaction rates, one must also determine leakage into and out of the region to perform a neutron balance. This quantity is calculated using the following MCNP tally cards:

```
f111:n    (26 < 20 [   2  -1 0] < 10)
```

```
          (9905 < 20 [   2  -1 0] < 10)
          (9909 < 20 [   2  -1 0] < 10)
          (9913 < 20 [   2  -1 0] < 10)
          (9917 < 20 [   2  -1 0] < 10)
          (28   < 20 [   2  -1 0] < 10)
fs111      -850
c111      0 1

f121:n     (  850 < 20 [   2  -1 0 ] < 10)
fs121      -26 -9905 -9909 -9913 -9917 -28
c121      0 1
```

These tallies are type 1, or "surface current" tallies. The first tally, "f111", indicates that neutrons crossing surface 26, within cell 20 and having a lattice index of (2,-1,0), and within cell 10 should be counted. In this case, surface 26 is the lower bounding surface of a fuel cell that is repeated within a lattice cell 20, which is then filled into cell 10. Surface 9905 is the axial surface dividing the lowest fuel segment (axial level 1) from axial level 2. The top segment (axial level 5) is bounded axially by surfaces 9917 on the bottom and surface 28 on the top. The tally segment card "fs111", indicates that these axial tallies should only include neutrons that cross the axial surfaces within surface 850, the radial bounding cylinder. The cosine divisor card, "c111" separates neutrons crossing the surface in the positive direction (moving up through the axial surface) from those neutrons crossing in the negative direction (moving down through the axial surface). The second tally, "f121", tracks neutrons crossing the cylinder bounding the fuel pin radially. The tally segment card, "fs121", splits the cylinder into five axial regions, in which the first/bottom region is axially bounded by surfaces 26 and 9905, and the last/top region is axially bounded by surfaces 9917 and 28. (In practice, a sixth tally segment is also produced tracking neutrons crossing cylinder 850 above axial surface 28, but since surface 28 is the upper bound of the fuel segment being considered these neutrons are not relevant to the neutron balance.) The cosine divisor card, "c121", differentiates neutrons crossing the radial bounding cylinder in the positive direction (leaking out from the fuel) from those crossing in the negative direction (streaming into the fuel). All values are then multiplied by the normalization factor calculated above.

A sample neutron balance for a fuel test hex is given in Table 17. The hex analyzed in Table 17 has the (row, hex) index (2,4). Figure 8 shows the overall core layout, with the (row, hex) index and hex type. Figures 9-13 provide neutron balance results for each fuel segment. Figure 9 provides the neutron balance for the lowest axial region (nearest the reflector and nosepiece), and the axial levels increase to Figure 13, nearest the fission gas plenum. All neutron balance calculations were performed using detailed (non-homogenized) MCNP models.

Table 17 – Sample Neutron Balance for hex (2,4)

Reaction Rates (rxn/sec)	Absorption	2.43552E+16	0.37%		Reaction Rates (rxn/sec)	2*(n,2n)	3.09464E+14	4.43%
	(n,2n)	1.54732E+14	4.43%			Nu*Fission	7.31555E+16	0.30%
	Fission	2.49042E+16	0.30%					
Leakage Out (neuts/sec)	Bottom	5.14004E+16	0.68%		Streaming In (neuts/sec)	Bottom	3.87156E+16	0.78%
	Top	6.35896E+16	0.60%			Top	7.13085E+16	0.57%
	Radial	5.49600E+18	0.27%			Radial	5.47911E+18	0.27%
Loss Total:		5.66041E+18	0.262%		Production Total:		5.66260E+18	0.261%
Production/Loss Ratio:		1.00039	0.37035%					

The loss quantity, [*l*], and its associated statistical variance are expressed below. In this formulation, [*capture*] refers to total parasitic capture events in a segment, [*n,2n*] is total (n,2n) events and [*fission*] is total fission. The [*leakb*] term refers to leakage out the bottom of the segment, [*leakt*] is leakage out the top, and [*leakr*] is radial leakage. The associated standard deviation of each quantity is σ:

$$[l] = [capture] + [n,2n] + [fission] + [leakb] + [leakt] + [leakr]$$

$$\sigma_{[l]}^{\ 2} = \sigma_{[capture]}^{\ 2} + \sigma_{[n,2n]}^{\ 2} + \sigma_{[fission]}^{\ 2} + \sigma_{[leakb]}^{\ 2} + \sigma_{[leakt]}^{\ 2} + \sigma_{[leakr]}^{\ 2}$$

The gain, [g], and its associated statistical variance are given by:

$$[g] = 2 \cdot [n,2n] + [nu \cdot fission] + [streamb] + [streamt] + [streamr]$$

$$\sigma_{[g]}^{\ 2} = 4 \cdot \sigma_{[n,2n]}^{\ 2} + \sigma_{[nu \cdot fission]}^{\ 2} + \sigma_{[streamb]}^{\ 2} + \sigma_{[streamt]}^{\ 2} + \sigma_{[streamr]}^{\ 2}$$

The variance of the gain/loss ratio, or balance is then given by:

$$[b] = \frac{[g]}{[l]}$$

$$\sigma_{[b]}^{\ 2} = \sigma_{[g]}^{\ 2} \cdot \left(\frac{\partial [b]}{\partial [g]}\right)^2 + \sigma_{[l]}^{\ 2} \cdot \left(\frac{\partial [b]}{\partial [l]}\right)^2 + \sigma_{[g][l]}^{\ 2} \cdot \left(\frac{\partial [b]}{\partial [g]}\right)\left(\frac{\partial [b]}{\partial [l]}\right)$$

The covariance term, $\sigma_{[p][l]}^{\ 2}$, is ignored in these uncertainty calculations. If more accurate assessments of the statistical uncertainty on derived quantities such as balance are required, then further study will be needed in order to accurately determine the covariance terms. The standard deviations presented in Table 17 and Figures 9-13 are determined by:

$$\sigma_{[b]} = \sqrt{\sigma_{[p]}^{\ 2} \cdot \left(\frac{1}{[l]}\right)^2 + \sigma_{[l]}^{\ 2} \cdot \left(\frac{[p]}{[l]^2}\right)^2}$$

This standard deviation is given below the balance ratio of each hex in Figures 9-13.

In Figure 8, PCR indicates primary control rod, SCR indicates secondary control rod, and MT indicates material test. The material test region is modeled as a reflector hex.

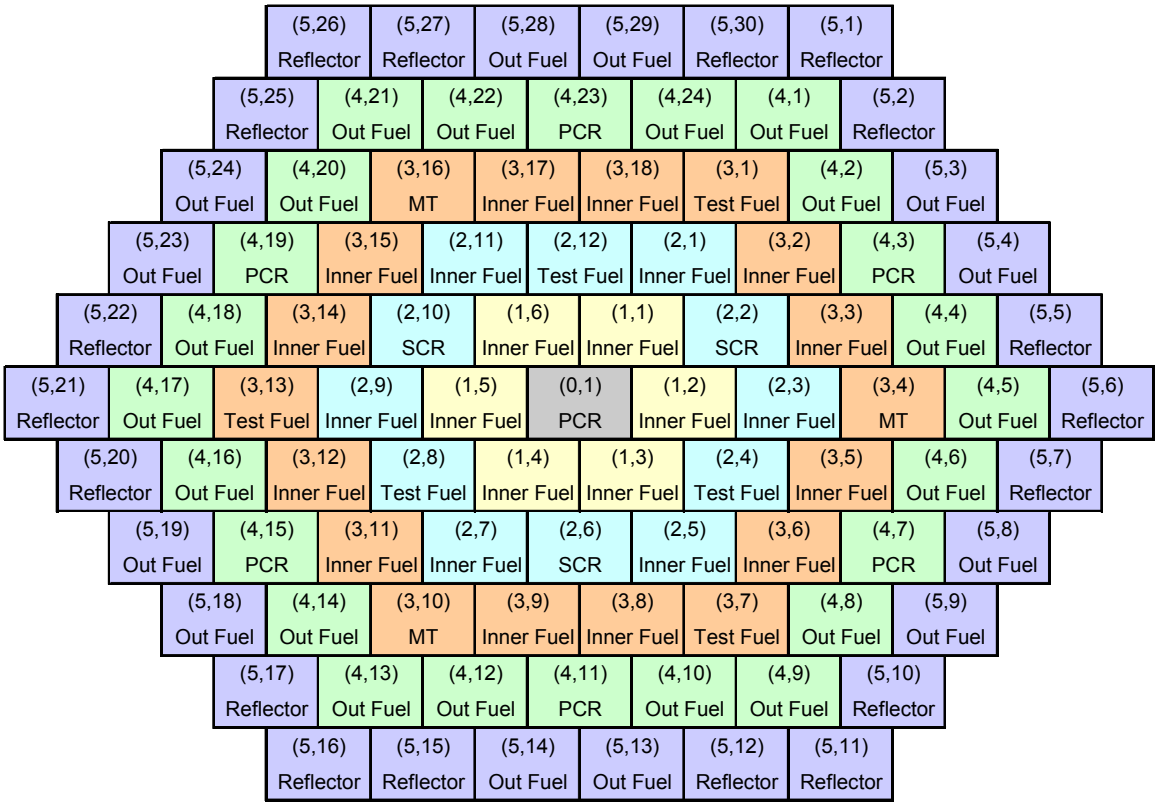

Figure 8 – Overall Core Layout with (row, hex) indices

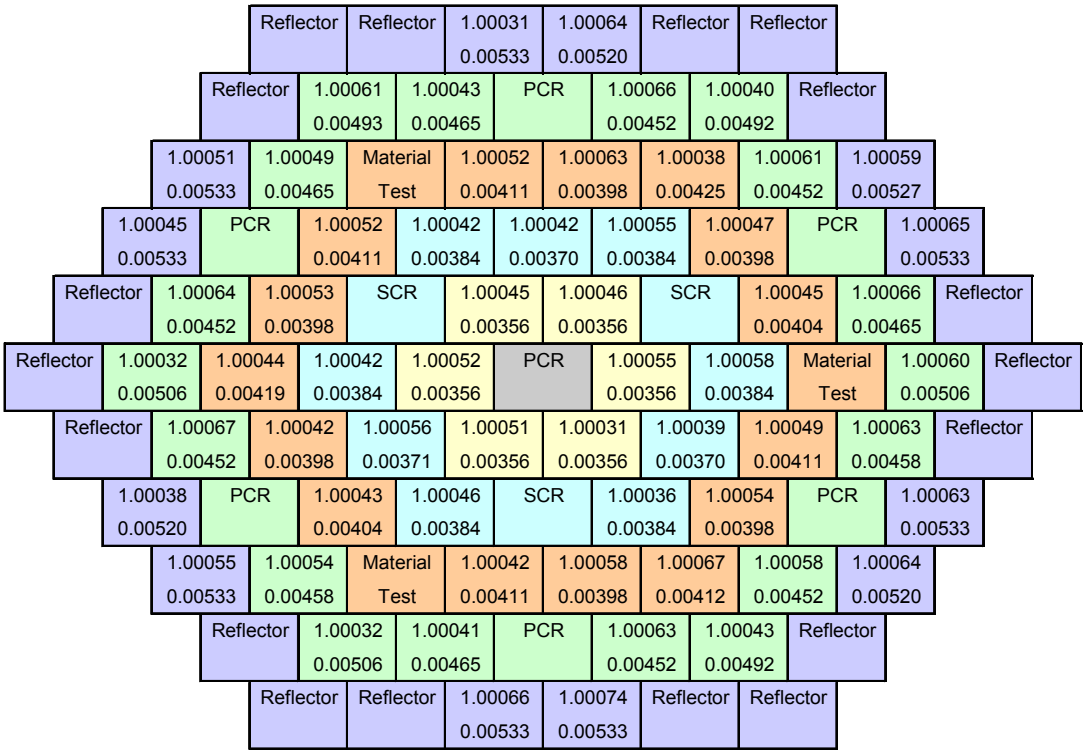

Figure 9 – Neutron Balance at Axial Level 1

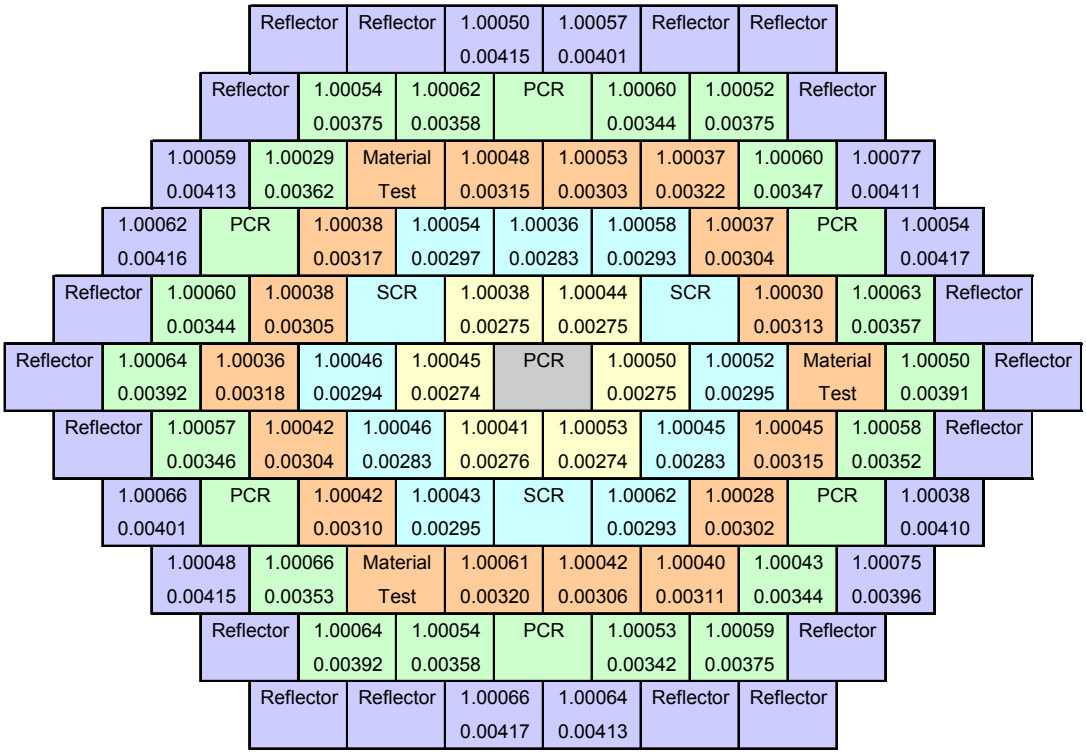

Figure 10 – Neutron Balance at Axial Level 2

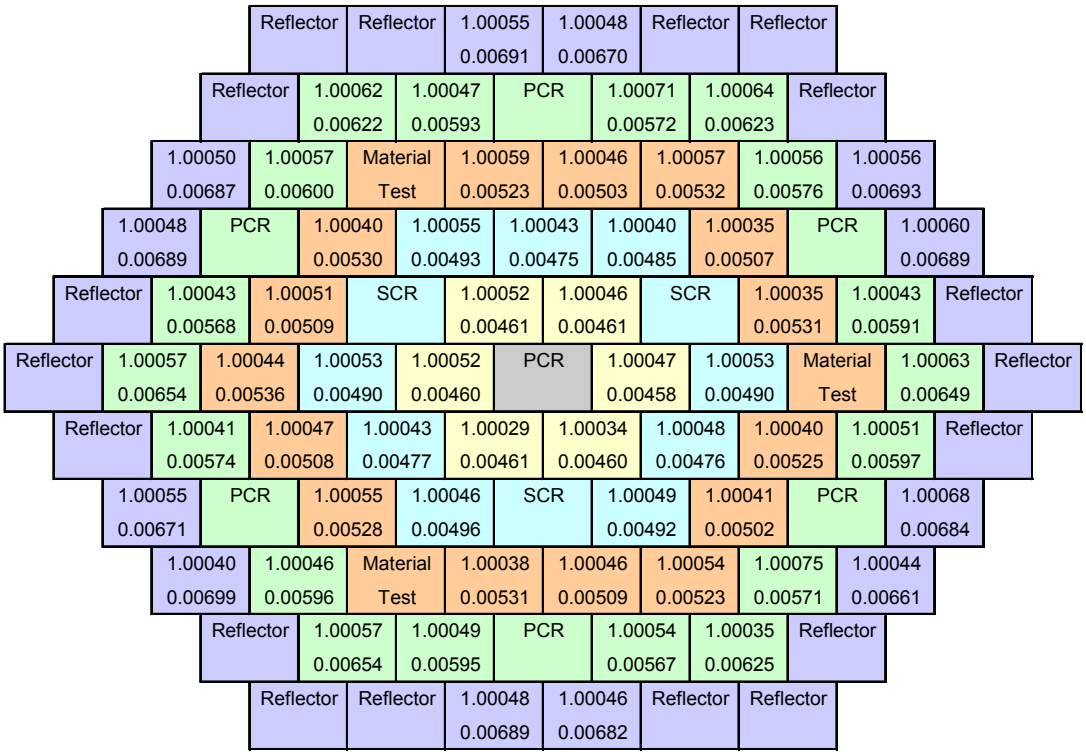

Figure 11 – Neutron Balance at Axial Level 3

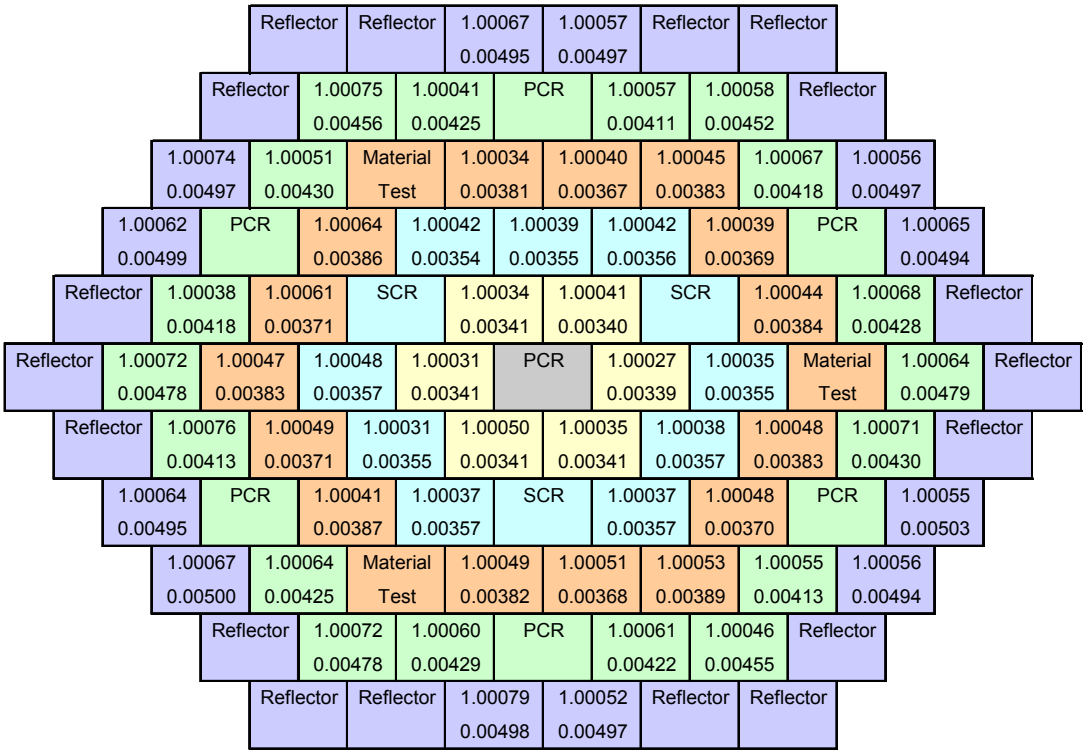

Figure 12 – Neutron Balance at Axial Level 4

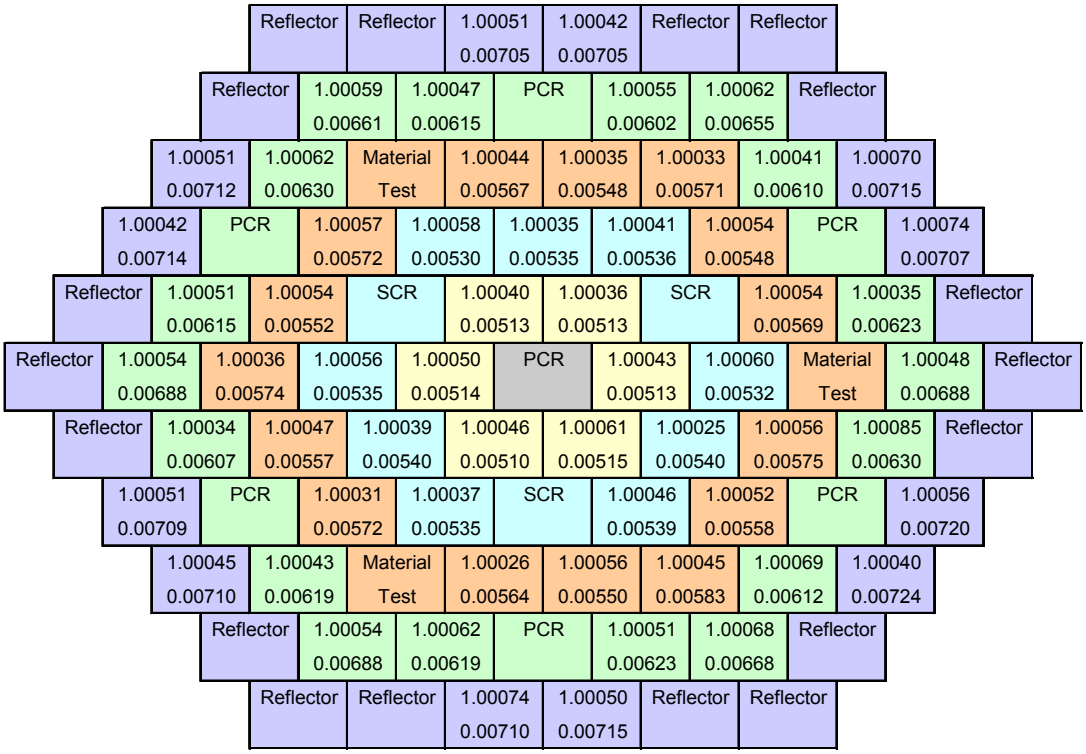

Figure 13 – Neutron Balance at Axial Level 5 (top)

Each of the fuel segments in these axial slices show similar results, which is a balance ratio near unity. MCNP is a steady-state code, and a steady-state operating reactor has a balance ratio of one over any given segment. As such, one would expect a balance ratio near unity in a converged MCNP calculation. Every fuel segment is well within one standard deviation of unity, indicating that the fission source has converged.

4.1.2 Detailed Vs. Homogenized Models

To assess the validity of the homogenized models, system k_{eff} values were compared between a homogenized and an explicitly modeled core as a function of primary control rod bank insertion into the core. Three homogenization schemes were considered: (a) all core components explicitly modeled, (b) all core components homogenized except control hexes, which are explicitly modeled, and (c) all core components homogenized. In Table 18, rod insertion of 0% indicates that the primary control rod bank is fully withdrawn from the core, while 100% indications full insertion. The secondary control rod bank is fully withdrawn in all calculations. Standard deviations are provided in parentheses after the k_{eff} value.

Taking case (a) as the reference, the differences in k_{eff} from the reference case exhibited by the models employing homogenization can be characterized as "bias". The bias in case (b) does not display a clear trend, while the bias in case (c) increases as the control rods are inserted into the core. These trends are plotted in Figure 14. This figure also includes two standard deviations from the reference case as a means of graphically comparing k_{eff} differences (bias) to the statistical uncertainty of the calculations.

Table 18 – Homogenized/Detailed Model Comparison

Rod insertion	(a) Detailed model		(b) Homogenized model, detailed control hexes		(c) Homogenized model	
	k_{eff}	Runtime (min)	k_{eff}	Runtime (min)	k_{eff}	Runtime (min)
0%	1.03273 (0.00022)	858.79	1.03254 (0.00021)	209.86	1.03252 (0.00021)	193.42
20%	1.02616 (0.00019)	850.42	1.02489 (0.00021)	209.76	1.02490 (0.00022)	192.29
40%	1.01078 (0.00020)	841.72	1.01011 (0.00020)	209.92	1.00901 (0.00020)	186.57
60%	0.98998 (0.00018)	833.38	0.98952 (0.00018)	210.55	0.98795 (0.00019)	182.96
80%	0.97258 (0.00021)	824.85	0.97134 (0.00021)	216.01	0.96933 (0.00018)	180.58
100%	0.96411 (0.00019)	824.20	0.96301 (0.00021)	213.20	0.96004 (0.00019)	178.72

Homogenization scheme (b) exhibits smaller biases than case (c), and these biases are not exacerbated by control rod insertion. Homogenization scheme (c) results in the shortest runtime of the three. The runtime is reduced by about 75% in going from (a) to (b), and by about 78% in going from (a) to (c). Since scheme (b) yields results that are less biased

than scheme (c) without incurring a significant runtime penalty, (b) was chosen as the homogenization scheme to be employed for burnup calculations.

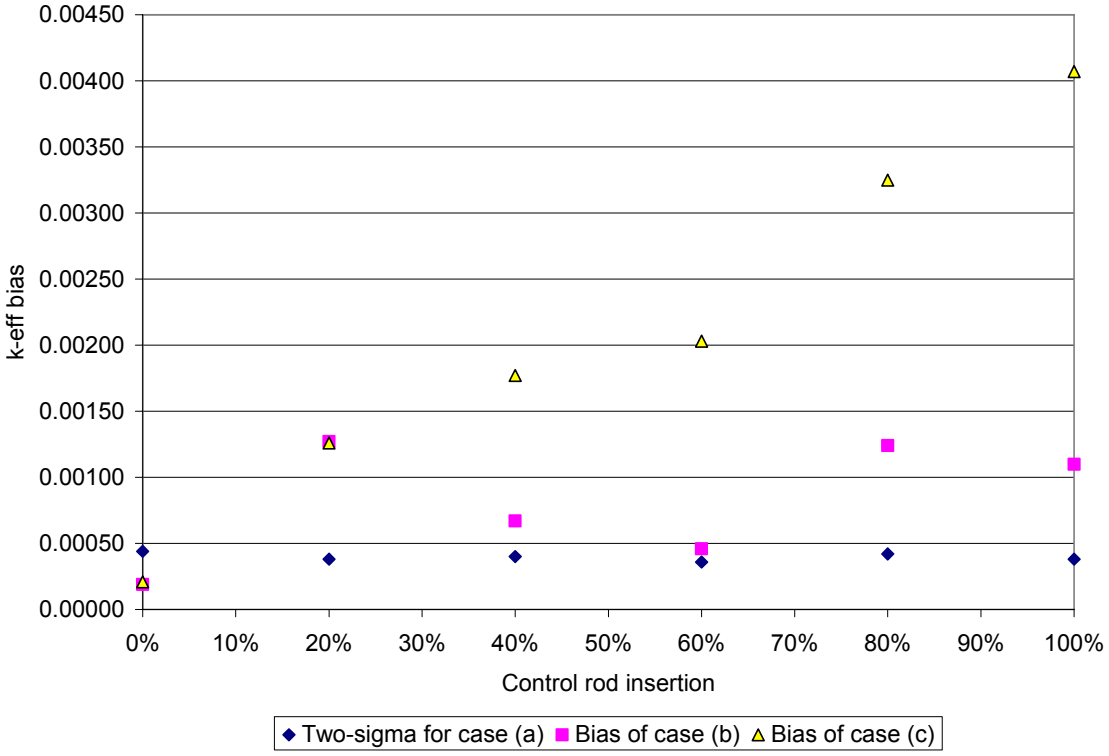

Figure 14 – Homogenization Bias as a Function of Primary Control Rod Insertion

4.2 Perturbation Calculations

The MCNP perturbation option allows one to calculate the effects of small changes to a given problem that might otherwise be obfuscated by the statistical nature of the calculation. The fundamental assumption of perturbation calculations is that the fission source (or eigenfunction) is not reconverged. The perturbation option has been used to determine the difference in net neutron production in every fuel hex as a result of reducing the fuel density by 2%, reducing the clad density by 5%, and reducing the coolant density in the hex by 50%. Detailed MCNP models were used for these calculations. Homogenized models could be used, though the current homogenization scheme homogenizes the fuel, bond, clad, coolant, and hex can into a single material. The fuel hex region being considered in this study is only the inner fuel hex – the fuel, bond (though the bond is neutronically inconsequential), clad, and coolant. To use homogenized models, one could homogenize only the inner fuel hex, or one could consider the entire fuel hex (including the hex can) when calculating net neutron production. In addition, when using a detailed model, as in this study, the primary source of uncertainty is statistical variation, which can be readily quantified. Homogenization introduces another source of error, but one that is more difficult to quantify.

4.2.1 Input Cards

The tally cards required to determine net neutron production in a hex are similar to the reaction rate tallies presented in the neutron balance discussion. The sole difference is that additional tallies are required in order to determine parasitic absorption in the clad and coolant, as net neutron production in the entire fuel hex, not just the fuel itself, is desired. The additional tallies are identical to the fuel tallies, with the appropriate cell number (clad or coolant), and the multipliers for (n,2n), fission, and ν*fission omitted. While (n,2n) reactions can occur in the clad and coolant, preliminary calculations showed that these reaction rates are orders of magnitude below other reaction types, and were ignored for this study.

The MCNP execution strategy entails including six reaction rate tallies in each deck. Generally, these six tallies correspond to six symmetric fuel hexes. The exception is the six "fuel test" hexes, which are treated in a single MCNP run though not all six are symmetric. Within a single run, perturbations are executed for the fuel, clad, and coolant in each of the six hexes, at five axial levels. Thus within a single MCNP deck 90 perturbations must be considered (3 materials x 6 hexes x 5 levels). A sample perturbation card for each material is given below:

```
pert01:n   cell=00871  rho=-10.6342697
pert06:n   cell=00876  rho= -7.1591401
pert11:n   cell=00881  rho= -0.4251360
```

In this case, cell 871 contains fuel material at a density of 10.8513 g/cc, the density of which should be reduced to 10.6343 g/cc, for a reduction of 2%. Cell 876 contains clad material, with the density being reduced from 7.5359 g/cc to 7.1591 g/cc (a 5% reduction), while cell 881 contains coolant, with a density reduction of 0.850272 g/cc to 0.425136 g/cc (a 50% reduction). As a default, MCNP will use a combined 1st and 2nd order perturbation estimate (the mathematical basis for Monte Carlo perturbations is the "differential operator" method – these orders refer to how many terms are carried in the Taylor series expansion of the differential operator). The practical use of the 1st and 2nd order perturbations is assessing the validity of the initial assumption that the fission source is not reconverged for perturbations. In general, a 2nd order term less than 10% of the 1st order term indicates that fission source reconvergence is not necessary and the perturbations are valid. Preliminary calculations showed that the 2nd order terms for fuel density reductions are less than 1% of 1st order perturbation terms.

MCNP produces completely new tally output for each perturbation. As a result, much of the tally data produced from such a run is inconsequential. For example, as a result of a perturbation in fuel hex 6, axial level 5, tally data in fuel hex 1, axial level 1 will be recalculated and produced. Of course, any change in the tally will be not only extremely small but irrelevant. A filter program has been written to sort through the MCNP tally output and extract only the useful and relevant information. The filter output can then be brought into a spreadsheet for analysis. An Excel spreadsheet has been developed to accept the filter output, analyze the data, and present the results in core maps.

Net neutron production [*nnp*] is defined as neutron production in a given fuel hex minus neutron absorption in the hex, as follows:

$$[nnp] = 2 \cdot [n,2n] + [nu \cdot fission] - [n,2n] - [fission] - [absorp_{fuel}] - [absorp_{clad}] - [absorp_{coolant}]$$

Sample calculations of net neutron production are given in Table 19 for three fuel hexes. This table shows the individual components of production, absorption, and net neutron production for a fuel test hex, an inner fuel hex, and an outer fuel hex at each axial level.

Table 19 – Net Neutron Production for Three Fuel Hexes

		Fuel Hex (2,4)		Fuel Hex (1,1)		Fuel Hex (4,1)	
		Test Fuel		Inner Fuel		Outer Fuel	
	Reaction type	Rxns/sec	std dev	Rxns/sec	std dev	Rxns/sec	std dev
Axial Level 1	2*(n,2n)	3.03309E+14	4.3100%	3.20793E+14	4.2200%	1.87622E+14	5.3800%
	Nu*Fission	7.29848E+16	0.2900%	8.73837E+16	0.2700%	5.94618E+16	0.3700%
	Total Production	7.32881E+16	0.2894%	8.77045E+16	0.2695%	5.96495E+16	0.3692%
	Absorption (fuel)	2.42500E+16	0.3500%	2.50808E+16	0.3500%	1.46284E+16	0.5000%
	(n,2n)	1.51655E+14	4.3100%	1.60397E+14	4.2200%	9.38109E+13	5.3800%
	Fission	2.48472E+16	0.2900%	2.98966E+16	0.2700%	2.02950E+16	0.3700%
	Absorption (clad+coolant)	1.11083E+15	0.7400%	1.26307E+15	0.8200%	6.94052E+14	1.0400%
	Total Absorption	5.03597E+16	0.2221%	5.64008E+16	0.2176%	3.57113E+16	0.3007%
	Net Production	2.29284E+16	1.0456%	3.13036E+16	0.8507%	2.39382E+16	1.0236%
Axial Level 2	2*(n,2n)	4.31492E+14	3.6700%	4.57165E+14	3.6100%	2.55093E+14	4.6800%
	Nu*Fission	9.48566E+16	0.2500%	1.11084E+17	0.2300%	7.65659E+16	0.3100%
	Total Production	9.52881E+16	0.2630%	1.11542E+17	0.2422%	7.68210E+16	0.3265%
	Absorption (fuel)	2.80798E+16	0.2900%	2.87586E+16	0.2900%	1.68902E+16	0.4100%
	(n,2n)	2.15746E+14	3.6700%	2.28583E+14	3.6100%	1.27546E+14	4.6800%
	Fission	3.22494E+16	0.2500%	3.79486E+16	0.2300%	2.60943E+16	0.3100%
	Absorption (clad+coolant)	1.34769E+15	0.5700%	1.48977E+15	0.6000%	8.48099E+14	0.7800%
	Total Absorption	6.18927E+16	0.1379%	6.84255E+16	0.1282%	4.39601E+16	0.1654%
	Net Production	3.33955E+16	0.7927%	4.31160E+16	0.6587%	3.28609E+16	0.7948%
Axial Level 3	2*(n,2n)	4.52560E+14	3.5000%	4.51328E+14	3.5000%	2.74277E+14	4.4700%
	Nu*Fission	1.01058E+17	0.2400%	1.16921E+17	0.2300%	8.11207E+16	0.3100%
	Total Production	1.01511E+17	0.0078%	1.17373E+17	0.0070%	8.13950E+16	0.0073%
	Absorption (fuel)	2.96558E+16	0.2800%	2.97874E+16	0.2800%	1.76225E+16	0.4000%
	(n,2n)	2.26280E+14	3.5000%	2.25664E+14	3.5000%	1.37138E+14	4.4700%
	Fission	3.43508E+16	0.2400%	3.99415E+16	0.2200%	2.76444E+16	0.3000%
	Absorption (clad+coolant)	1.44162E+15	0.5300%	1.55901E+15	0.5400%	8.88166E+14	0.8000%
	Total Absorption	6.56745E+16	0.4029%	7.15137E+16	0.3970%	4.62923E+16	0.5640%
	Net Production	3.58361E+16	0.7387%	4.58590E+16	0.6193%	3.51028E+16	0.7440%
Axial Level 4	2*(n,2n)	3.90007E+14	3.8300%	4.08223E+14	3.7900%	2.46206E+14	4.8100%
	Nu*Fission	8.82401E+16	0.2600%	1.02156E+17	0.2400%	7.12508E+16	0.3300%
	Total Production	8.86301E+16	0.5441%	1.02564E+17	0.5056%	7.14970E+16	0.6720%
	Absorption (fuel)	2.59335E+16	0.3000%	2.61460E+16	0.2900%	1.56627E+16	0.4300%
	(n,2n)	1.95003E+14	3.8300%	2.04112E+14	3.7900%	1.23103E+14	4.8100%
	Fission	2.99993E+16	0.2600%	3.48983E+16	0.2400%	2.42855E+16	0.3300%
	Absorption (clad+coolant)	1.25945E+15	0.5800%	1.35608E+15	0.6000%	7.77813E+14	0.7700%
	Total Absorption	5.73873E+16	0.4365%	6.26046E+16	0.4313%	4.08491E+16	0.6139%
	Net Production	3.12428E+16	1.7394%	3.99593E+16	1.4630%	3.06480E+16	1.7684%
Axial Level 5	2*(n,2n)	2.31549E+14	4.7600%	2.46247E+14	4.7600%	1.55363E+14	5.9800%
	Nu*Fission	5.76580E+16	0.3100%	6.75899E+16	0.2900%	4.96947E+16	0.3900%
	Total Production	5.78896E+16	0.4190%	6.78362E+16	0.3964%	4.98500E+16	0.5045%
	Absorption (fuel)	1.81961E+16	0.3700%	1.82296E+16	0.3600%	1.18649E+16	0.5200%
	(n,2n)	1.15775E+14	4.7600%	1.23124E+14	4.7600%	7.76814E+13	5.9800%
	Fission	1.96186E+16	0.3100%	2.31109E+16	0.2900%	1.69555E+16	0.3900%
	Absorption (clad+coolant)	8.59192E+14	0.7500%	9.36606E+14	0.8300%	5.59230E+14	0.9600%
	Total Absorption	3.87897E+16	0.3098%	4.24002E+16	0.2935%	2.94573E+16	0.3780%
	Net Production	1.90999E+16	1.4172%	2.54360E+16	1.1650%	2.03927E+16	1.3486%

Net neutron production for the three fuel hexes presented in Table 19 as a function of axial location is also plotted in Figure 15.

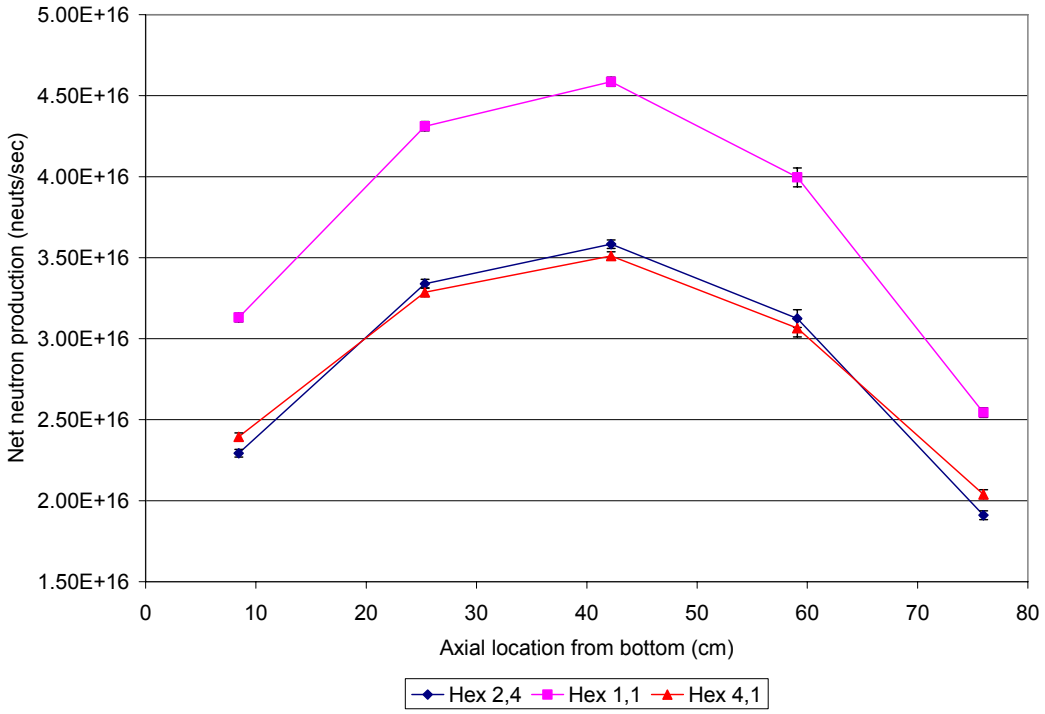

Figure 15 – Net Neutron Production vs. Axial Location for Three Fuel Hexes

Figures 16-20 show a core map at each axial level of number of neutrons produced in the given fuel segment per second. Relative errors are given below the net production rates. In these figures, the test fuel assemblies are indicated with a white background.

		Reflector	Reflector	1.99379E+16 1.163%	2.03378E+16 1.149%	Reflector	Reflector
	Reflector	2.41471E+16 1.019%	2.64311E+16 0.951%	PCR	2.87604E+16 0.883%	2.39382E+16 1.024%	Reflector
1.98908E+16 1.191%	2.62973E+16 0.953%	Material Test	2.52580E+16 0.968%	2.65976E+16 0.907%	1.92013E+16 1.145%	2.84472E+16 0.893%	2.02608E+16 1.153%
2.02372E+16 1.158%	PCR	2.43821E+16 1.008%	2.79656E+16 0.916%	2.26396E+16 1.059%	2.95812E+16 0.876%	2.61061E+16 0.941%	PCR	1.99478E+16 1.165%
Reflector	2.84095E+16 0.896%	2.58215E+16 0.946%	SCR	3.12954E+16 0.853%	3.13036E+16 0.851%	SCR	2.44608E+16 1.013%	2.65445E+16 0.952%	Reflector
Reflector	2.15208E+16 1.106%	1.96348E+16 1.131%	2.94229E+16 0.852%	3.14549E+16 0.853%	PCR	3.12647E+16 0.853%	2.79565E+16 0.924%	Material Test	2.19988E+16 1.124%	Reflector
Reflector	2.87543E+16 0.887%	2.67309E+16 0.899%	2.30337E+16 1.054%	3.11758E+16 0.854%	3.12021E+16 0.853%	2.29284E+16 1.046%	2.53161E+16 0.967%	2.66805E+16 0.947%	Reflector
2.04341E+16 1.150%	PCR	2.51793E+16 0.966%	2.81493E+16 0.910%	SCR	2.95464E+16 0.882%	2.64204E+16 0.903%	PCR	2.02908E+16 1.156%
1.99927E+16 1.161%	2.65199E+16 0.948%	Material Test	2.44705E+16 1.012%	2.56298E+16 0.946%	1.92693E+16 1.142%	2.81907E+16 0.893%	2.03779E+16 1.148%
	Reflector	2.15208E+16 1.106%	2.64750E+16 0.975%	PCR	2.82992E+16 0.890%	2.42112E+16 1.015%	Reflector	
		Reflector	Reflector	1.98029E+16 1.166%	2.02884E+16 1.157%	Reflector	Reflector		

Figure 16 – Net Neutron Production at Axial Level 1

The axial neutron production shape presented in Figure 15 indicates that maximum neutron production occurs near the axial center of the fueled region, while the end

adjacent to the lower reflector exhibits more neutron production than the end near the fission gas plenum. Figures 16-20 show that the (1,1) hex produces more neutrons than the other hexes in largely due to its location in the radial center of the core.

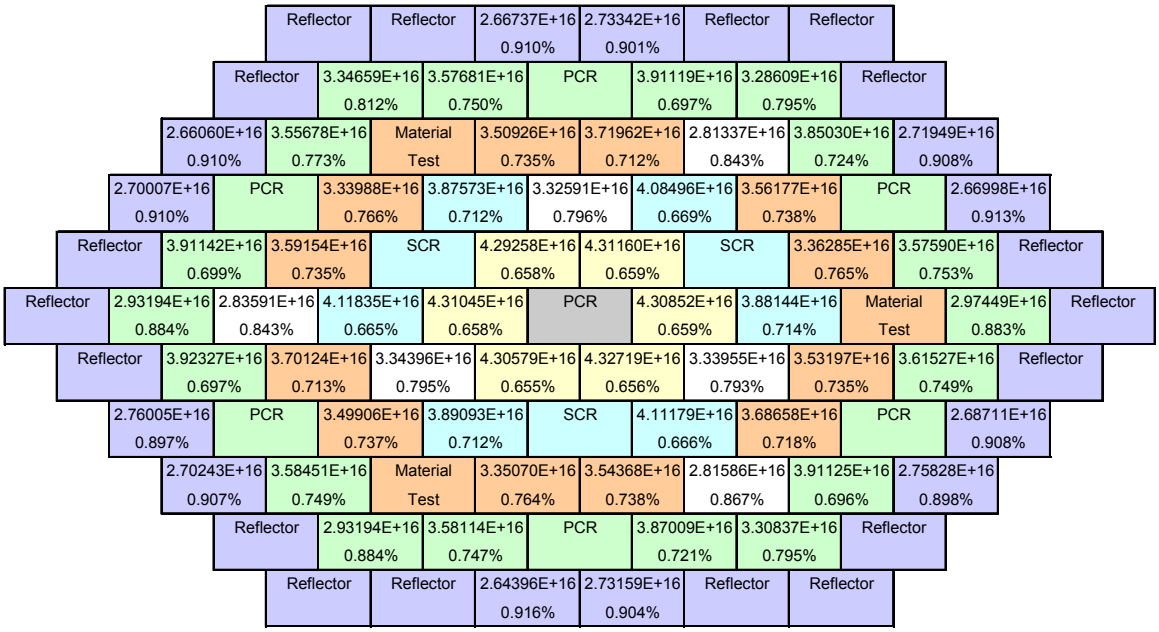

Figure 17 – Net Neutron Production at Axial Level 2

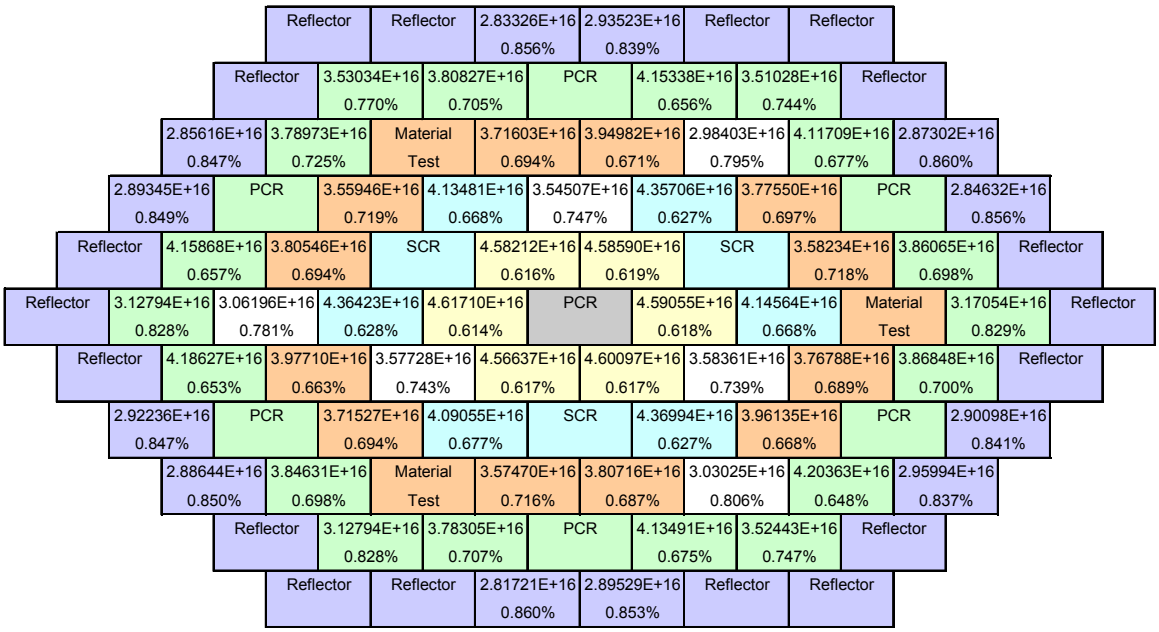

Figure 18 – Net Neutron Production at Axial Level 3

			Reflector	Reflector	2.51804E+16 1.992%	2.55903E+16 1.990%	Reflector	Reflector				
		Reflector	3.08799E+16 1.834%	3.35738E+16 1.657%	PCR	3.66284E+16 1.551%	3.06480E+16 1.768%	Reflector				
	2.48432E+16 2.014%	3.32643E+16 1.721%	Material Test	3.23889E+16 1.645%	3.42373E+16 1.604%	2.60904E+16 1.866%	3.58914E+16 1.620%	2.53797E+16 2.012%				
	2.52765E+16 2.008%	PCR	3.14673E+16 1.669%	3.57728E+16 1.595%	3.06105E+16 1.776%	3.79451E+16 1.487%	3.29771E+16 1.646%	PCR	2.50410E+16 2.011%			
	Reflector	3.63160E+16 1.568%	3.31390E+16 1.645%	SCR	3.98360E+16 1.460%	3.99593E+16 1.463%	SCR	3.11823E+16 1.692%	3.32403E+16 1.680%	Reflector		
Reflector	2.74313E+16 1.954%	2.63937E+16 1.859%	3.79938E+16 1.490%	3.99515E+16 1.461%	PCR	3.99919E+16 1.461%	3.61931E+16 1.581%	Material Test	2.78435E+16 1.951%	Reflector		
	Reflector	3.68058E+16 1.548%	3.46830E+16 1.578%	3.08442E+16 1.769%	3.95184E+16 1.474%	4.01052E+16 1.458%	3.12428E+16 1.739%	3.28243E+16 1.633%	3.39363E+16 1.655%	Reflector		
	2.56759E+16 1.998%	PCR	3.26798E+16 1.628%	3.56971E+16 1.603%	SCR	3.82129E+16 1.481%	3.49277E+16 1.566%	PCR	2.56170E+16 1.970%			
	2.53165E+16 2.003%	3.34795E+16 1.664%	Material Test	3.11341E+16 1.688%	3.28786E+16 1.641%	2.63363E+16 1.913%	3.66447E+16 1.549%	2.59310E+16 1.979%				
		Reflector	2.74313E+16 1.954%	3.32751E+16 1.671%	PCR	3.57923E+16 1.630%	3.04820E+16 1.788%	Reflector				
			Reflector	Reflector	2.51567E+16 1.985%	2.52824E+16 2.020%	Reflector	Reflector				

Figure 19 – Net Neutron Production at Axial Level 4

			Reflector	Reflector	1.70442E+16 1.459%	1.72479E+16 1.475%	Reflector	Reflector				
		Reflector	2.04129E+16 1.317%	2.22719E+16 1.263%	PCR	2.36985E+16 1.209%	2.03927E+16 1.349%	Reflector				
	1.66711E+16 1.498%	2.18783E+16 1.284%	Material Test	2.07829E+16 1.260%	2.18183E+16 1.232%	1.62508E+16 1.528%	2.35015E+16 1.216%	1.70913E+16 1.475%				
	1.69854E+16 1.481%	PCR	2.01686E+16 1.289%	2.29494E+16 1.224%	1.89159E+16 1.424%	2.39251E+16 1.156%	2.13251E+16 1.245%	PCR	1.68343E+16 1.486%			
	Reflector	2.36473E+16 1.218%	2.12393E+16 1.256%	SCR	2.51962E+16 1.176%	2.54360E+16 1.165%	SCR	2.00791E+16 1.295%	2.20432E+16 1.254%	Reflector		
Reflector	1.86248E+16 1.431%	1.64331E+16 1.534%	2.40955E+16 1.189%	2.52963E+16 1.176%	PCR	2.55038E+16 1.160%	2.30283E+16 1.219%	Material Test	1.85105E+16 1.453%	Reflector		
	Reflector	2.38557E+16 1.206%	2.21027E+16 1.220%	1.91049E+16 1.414%	2.54845E+16 1.160%	2.52842E+16 1.174%	1.90999E+16 1.417%	2.09413E+16 1.260%	2.22610E+16 1.244%	Reflector		
	1.72668E+16 1.467%	PCR	2.08332E+16 1.252%	2.30701E+16 1.205%	SCR	2.41175E+16 1.149%	2.20627E+16 1.223%	PCR	1.70727E+16 1.483%			
	1.68904E+16 1.490%	2.22501E+16 1.236%	Material Test	1.99999E+16 1.299%	2.10938E+16 1.266%	1.61157E+16 1.551%	2.40020E+16 1.201%	1.73949E+16 1.471%				
		Reflector	1.86248E+16 1.431%	2.18609E+16 1.280%	PCR	2.34387E+16 1.218%	2.03222E+16 1.362%	Reflector				
			Reflector	Reflector	1.65808E+16 1.496%	1.68682E+16 1.493%	Reflector	Reflector				

Figure 20 – Net Neutron Production at Axial Level 5 (top)

4.2.2 Local Reactivity Effects

Once net neutron production has been calculated for each fuel hex, one can then determine how this quantity changes as a result of various perturbations to assess the effect of the perturbation on local reactivity. In this context, a change in reactivity is defined simply as a change in the net neutron production.

4.2.2.1 Fuel Density Reduction

The change in net neutron production as a result of a 2% reduction in fuel density at each axial level is presented in Figures 21-25. This change is a reduction of 10.8186 g/cc to 10.60223 g/cc for the inner fuel, 10.8171 g/cc to 10.60076 g/cc for the outer fuel, and 10.8513 g/cc to 10.63427 g/cc for the test fuel. Note that the uncertainties presented in Figures 21-25 are absolute errors (not relative errors).

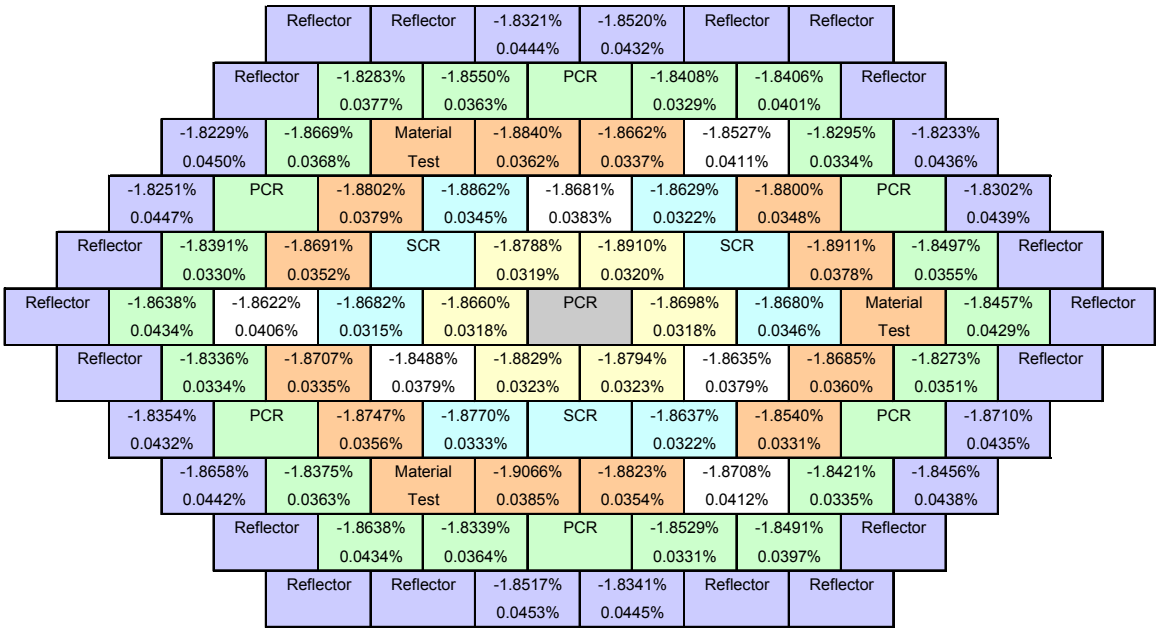

Figure 21 – Reactivity Change Resulting from 2% Fuel Density Reduction in Axial Level 1

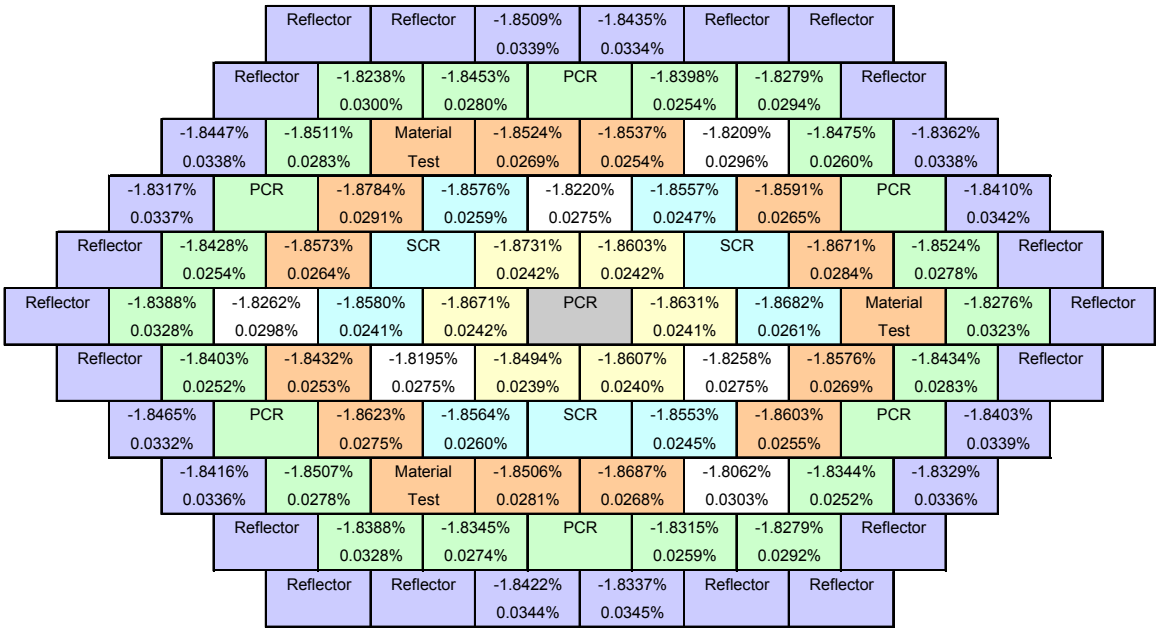

Figure 22 - Reactivity Change Resulting from 2% Fuel Density Reduction in Axial Level 2

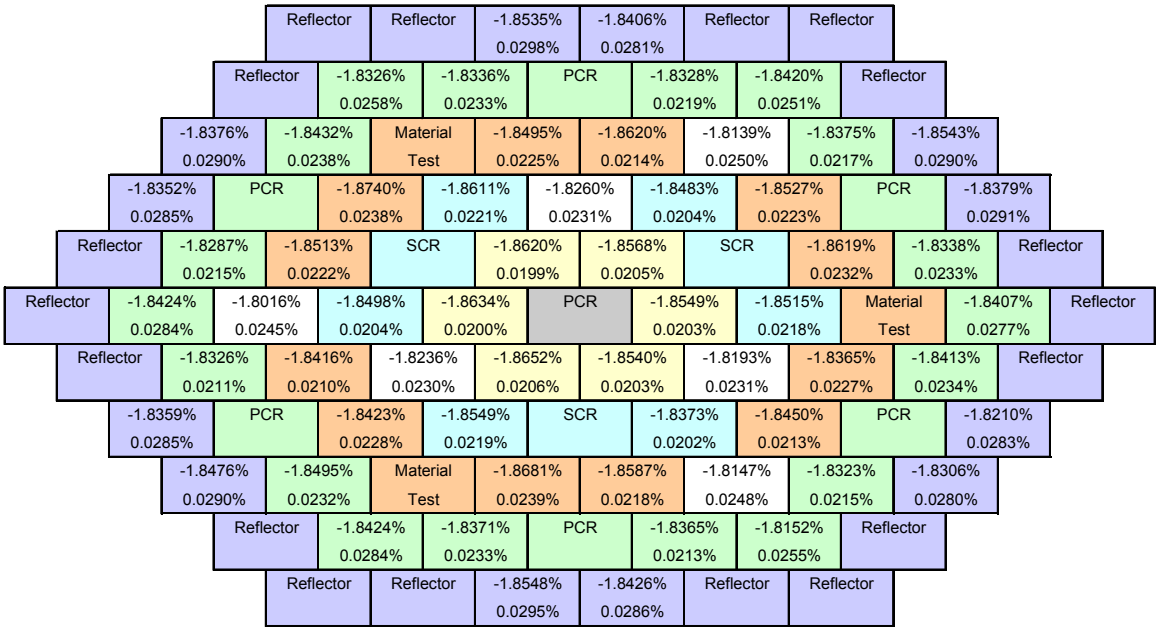

Figure 23 – Reactivity Change Resulting from 2% Fuel Density Reduction in Axial Level 3

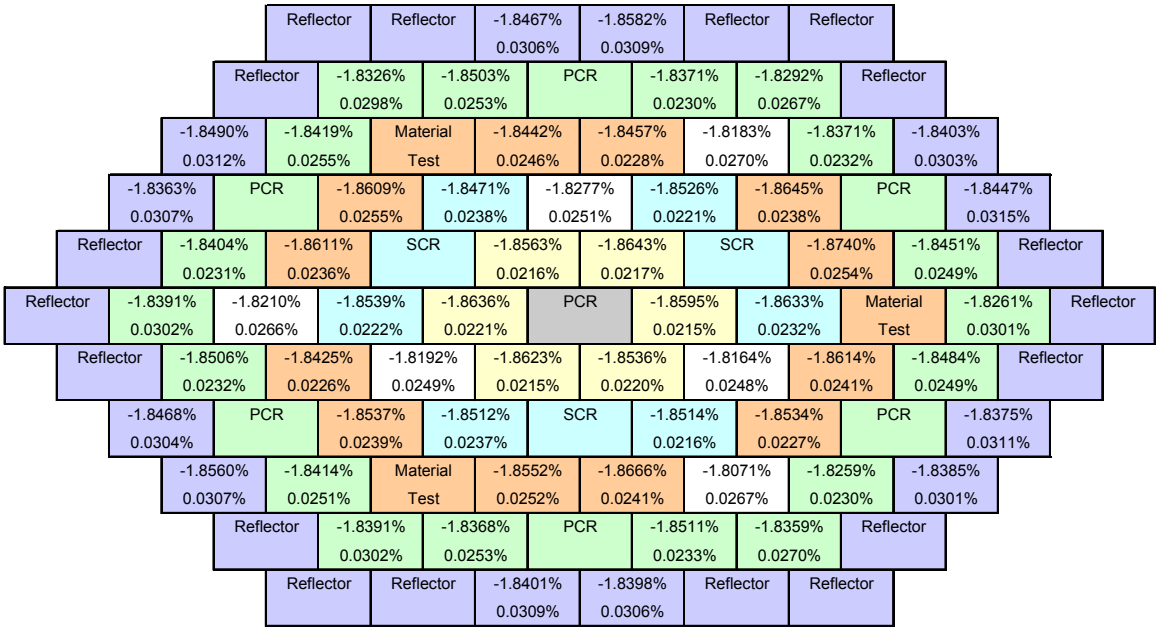

Figure 24 – Reactivity Change Resulting from 2% Fuel Density Reduction in Axial Level 4

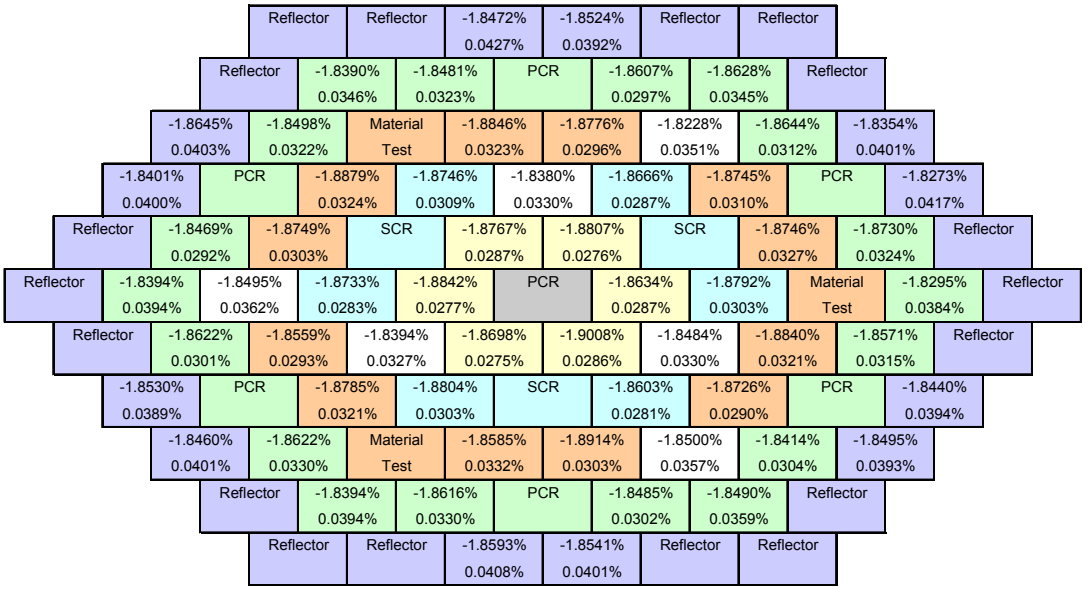

Figure 25 - Reactivity Change Resulting from 2% Fuel Density Reduction in Axial Level 5

Perturbation theory seems to handle fuel density reduction readily. A 2% fuel density reduction reduces the net neutron production of the fuel-clad-coolant region by between 1.84% and 1.90%. Statistical errors of the perturbations are less than 2% than the perturbation itself. For example, hex (1,1) exhibits a perturbation of -1.8807% with an absolute statistical uncertainty of 0.0276%. The relative error of the perturbation is thus (0.0276/1.8807) 1.47%

4.2.2.2 Clad Density Reduction

The change in net neutron production as a result of a 5% reduction in clad density is presented in Figures 26-30. The clad density in this case is reduced from 7.53594 g/cc to 7.15914 g/cc.

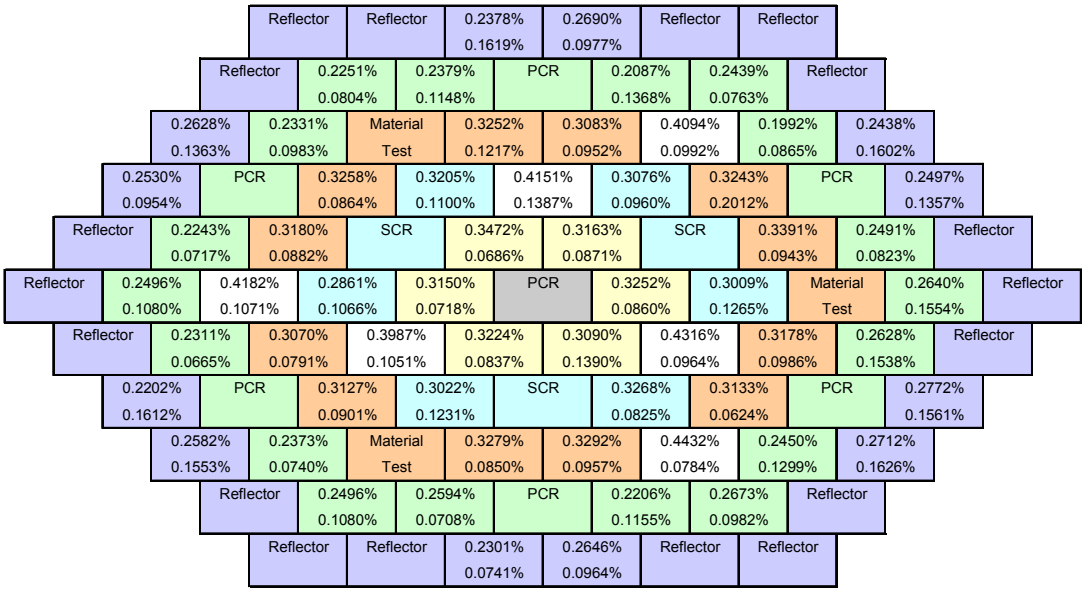

Figure 26 - Reactivity Change Resulting from 5% Clad Density Reduction in Axial Level 1

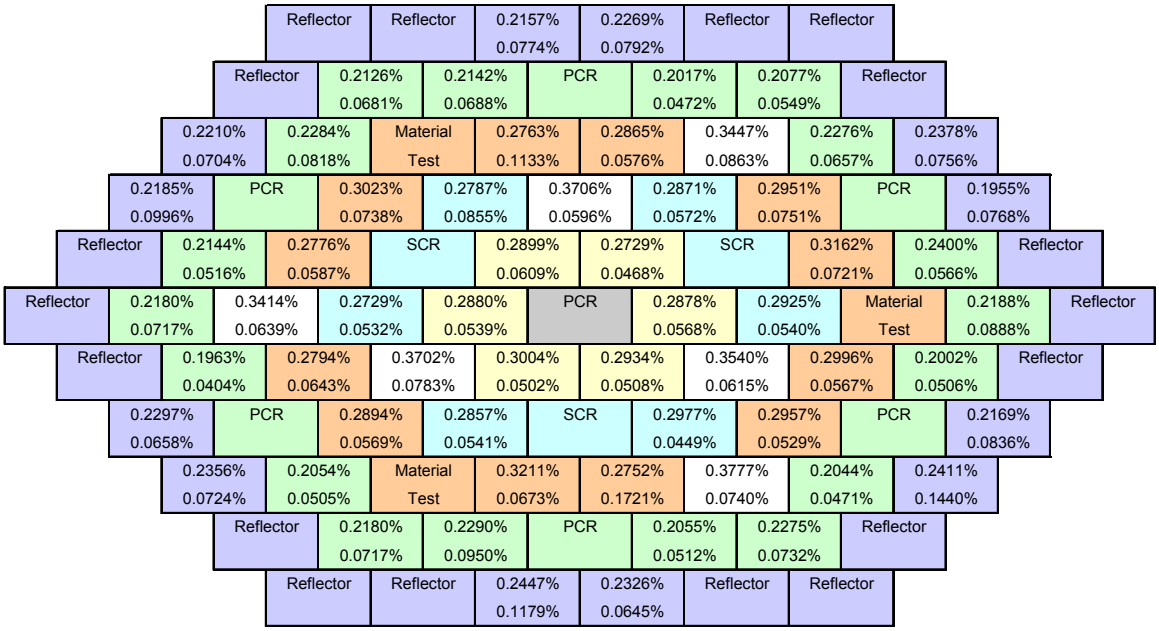

Figure 27 - Reactivity Change Resulting from 5% Clad Density Reduction in Axial Level 2

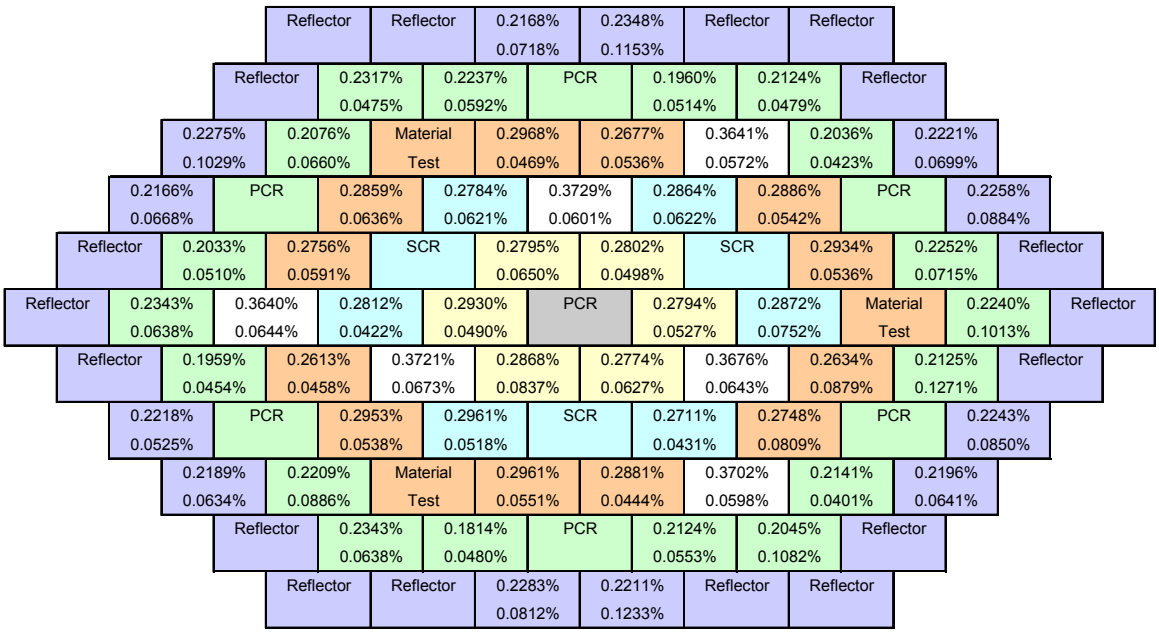

Figure 28 - Reactivity Change Resulting from 5% Clad Density Reduction in Axial Level 3

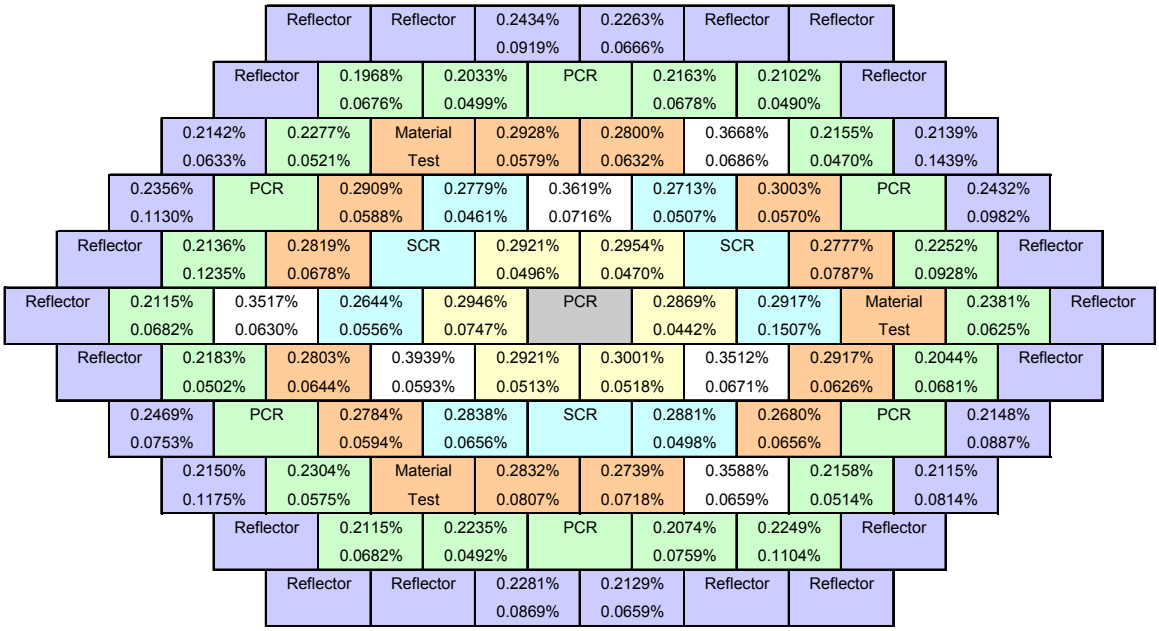

Figure 29 - Reactivity Change Resulting from 5% Clad Density Reduction in Axial Level 4

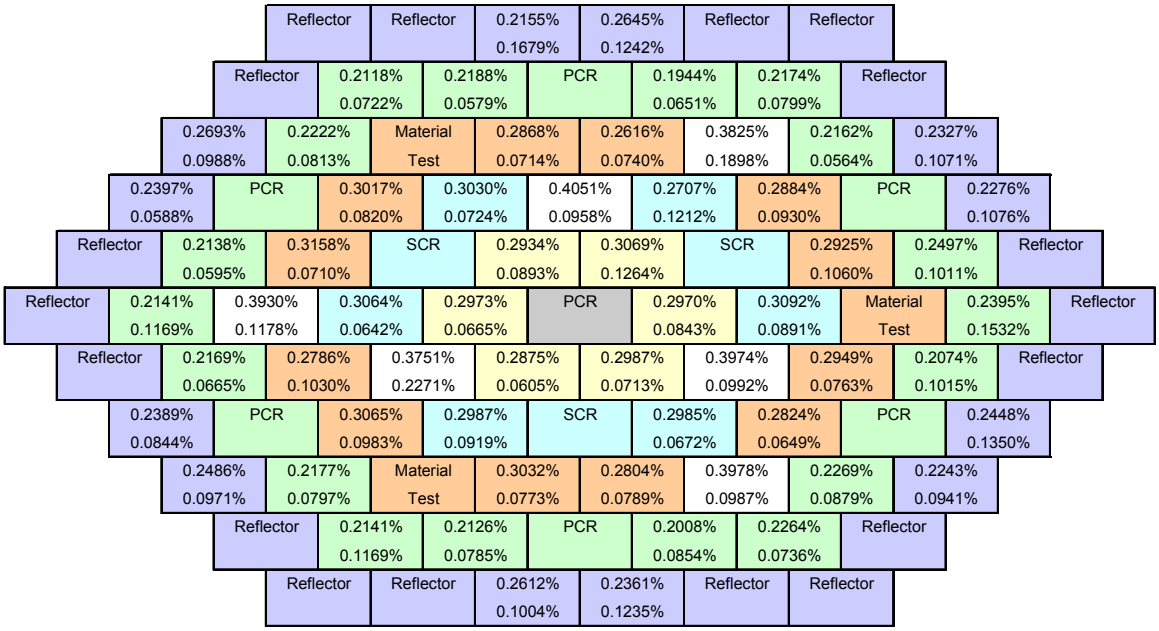

Figure 30 - Reactivity Change Resulting from 5% Clad Density Reduction in Axial Level 5

A 5% reduction in clad density tends to increase the net neutron production of the region by between 0.2% and 0.3%. Those hexes nearest the center of the core tended to show a larger relative effect on clad density reduction. However, relative errors on the clad density reduction perturbations are substantial. In hex (1,1) the relative error is (0.1264/0.3069) 41%.

4.2.2.3 Coolant Density Reduction

The change in net neutron production as a result of a 50% reduction in coolant density is presented in Figures 31-35. The coolant density in this case is reduced from 0.850272 g/cc to 0.425136 g/cc.

		Reflector	Reflector	0.4075% 0.4075%	0.5975% 0.2549%	Reflector	Reflector				
	Reflector	0.6381% 0.3486%	0.4540% 0.3392%	PCR	0.5224% 0.1444%	0.6025% 0.3529%	Reflector				
0.4317% 0.4123%	0.6444% 0.3371%	Material Test	0.7245% 0.3074%	0.5868% 0.3049%	1.4257% 0.3466%	0.3308% 0.2811%	0.4357% 0.3837%				
0.4798% 0.3688%	PCR	1.0321% 0.2975%	0.7588% 0.3211%	1.2408% 0.2393%	0.7811% 0.2733%	0.6585% 0.3141%	PCR	0.6299% 0.4128%			
Reflector	0.5940% 0.3333%	0.9740% 0.2586%	SCR	0.8352% 0.2875%	0.8187% 0.2703%	SCR	0.6631% 0.3462%	0.4751% 0.1819%	Reflector		
Reflector	0.4254% 0.3808%	1.0723% 0.3511%	0.7339% 0.2217%	0.8984% 0.2835%	PCR	0.9337% 0.1916%	0.9603% 0.2872%	Material Test	0.5292% 0.3886%	Reflector	
Reflector	0.4854% 0.1759%	0.8060% 0.2921%	1.3422% 0.2241%	0.7744% 0.2732%	0.6950% 0.2955%	1.5473% 0.3175%	0.6772% 0.2627%	0.5106% 0.3144%	Reflector		
0.3695% 0.3695%	PCR	0.6894% 0.3522%	0.7635% 0.2122%	SCR	0.8428% 0.2151%	0.7226% 0.2031%	PCR	0.5062% 0.3708%			
0.4078% 0.4078%	0.2859% 0.2859%	Material Test	0.8362% 0.3269%	0.8538% 0.3139%	1.2680% 0.2336%	0.5692% 0.2818%	0.6298% 0.2762%				
	Reflector	0.4254% 0.3808%	0.4971% 0.3122%	PCR	0.4377% 0.2903%	0.3507% 0.3507%	Reflector				
		Reflector	Reflector	0.5170% 0.4250%	0.6830% 0.4175%	Reflector	Reflector				

Figure 31 - Reactivity Change Resulting from 50% Coolant Density Reduction in Axial Level 1

		Reflector	Reflector	0.5418% 0.2884%	0.4195% 0.2761%	Reflector	Reflector				
	Reflector	0.3761% 0.2811%	0.4743% 0.2359%	PCR	0.4890% 0.2174%	0.6213% 0.2482%	Reflector				
0.3979% 0.2849%	0.5267% 0.2331%	Material Test	0.7694% 0.1728%	0.6287% 0.1999%	1.2145% 0.1442%	0.4913% 0.2081%	0.3642% 0.3113%				
0.4515% 0.3133%	PCR	0.7608% 0.2299%	0.8087% 0.1818%	1.1208% 0.1835%	0.6833% 0.1263%	0.6301% 0.2156%	PCR	0.5093% 0.2812%			
Reflector	0.4798% 0.2062%	0.8226% 0.2330%	SCR	0.7101% 0.1998%	0.6762% 0.2018%	SCR	0.6872% 0.2408%	0.5155% 0.2051%	Reflector		
Reflector	0.4168% 0.2832%	1.0607% 0.1471%	0.7050% 0.1128%	0.7081% 0.1959%	PCR	0.7148% 0.1999%	0.7325% 0.2211%	Material Test	0.4529% 0.2998%	Reflector	
Reflector	0.3862% 0.2125%	0.7251% 0.2001%	1.2027% 0.1602%	0.6636% 0.1990%	0.7609% 0.1995%	1.2126% 0.2330%	0.5305% 0.2536%	0.5498% 0.2368%	Reflector		
0.4983% 0.2804%	PCR	0.7612% 0.2205%	0.6564% 0.2326%	SCR	0.6977% 0.2020%	0.7140% 0.1544%	PCR	0.5649% 0.2313%			
0.5743% 0.2961%	0.4808% 0.2178%	Material Test	0.8389% 0.2538%	0.7762% 0.1928%	1.1516% 0.1551%	0.5426% 0.2017%	0.3573% 0.2881%				
	Reflector	0.4168% 0.2832%	0.4911% 0.2217%	PCR	0.5770% 0.1189%	0.4993% 0.2545%	Reflector				
		Reflector	Reflector	0.5740% 0.1846%	0.4849% 0.2540%	Reflector	Reflector				

Figure 32 - Reactivity Change Resulting from 50% Coolant Density Reduction in Axial Level 2

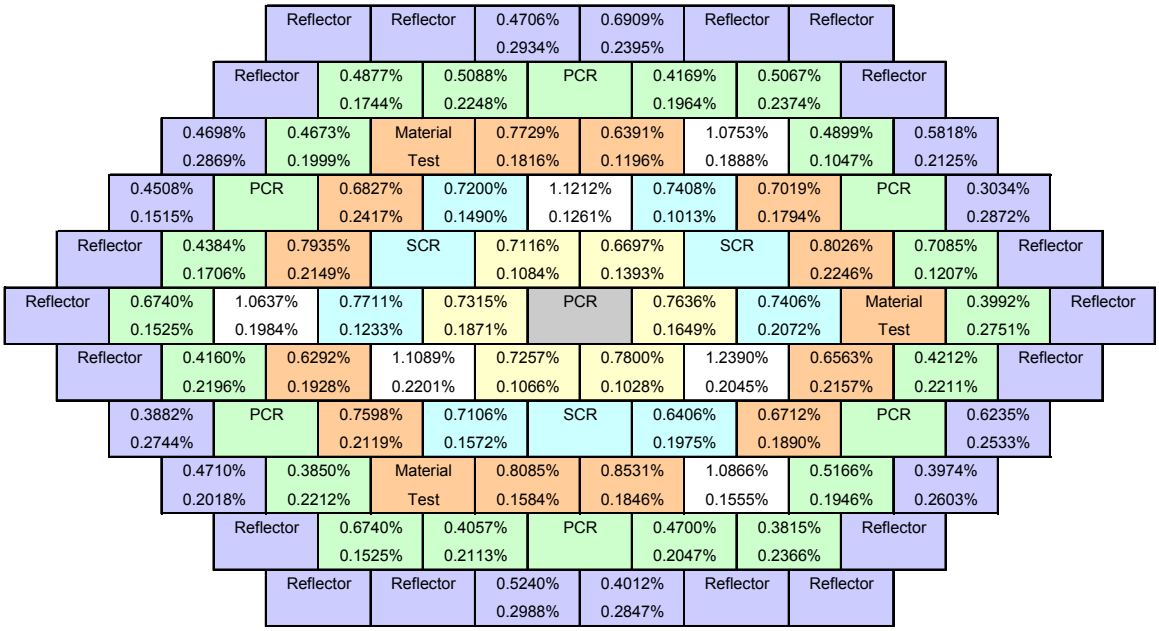

Figure 33 - Reactivity Change Resulting from 50% Coolant Density Reduction in Axial Level 3

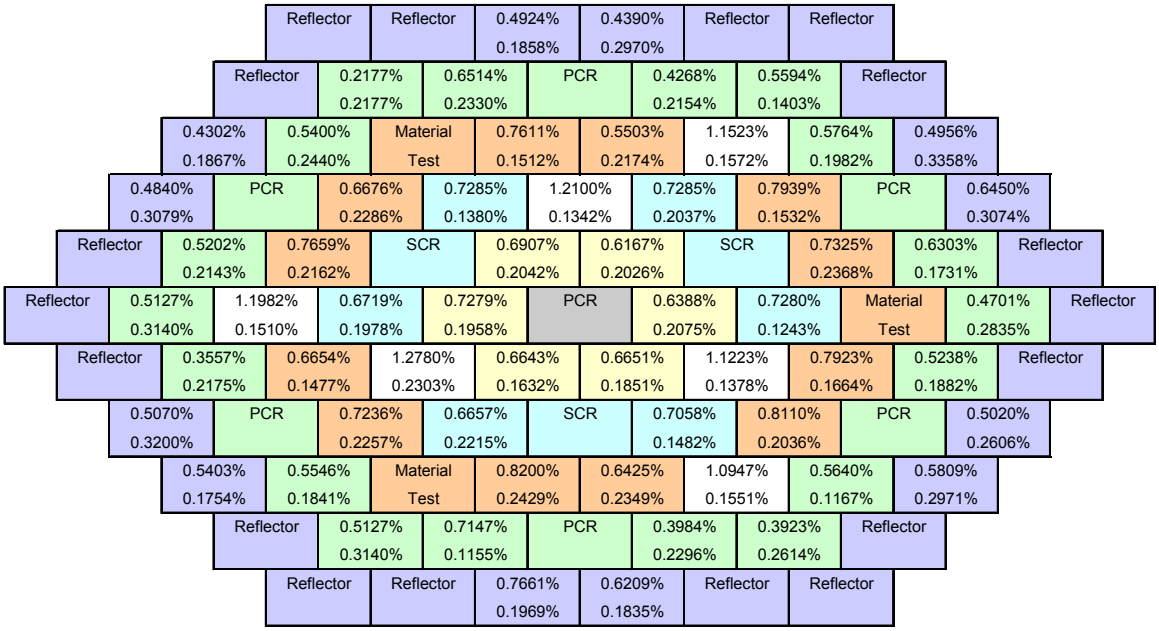

Figure 34 - Reactivity Change Resulting from 50% Coolant Density Reduction in Axial Level 4

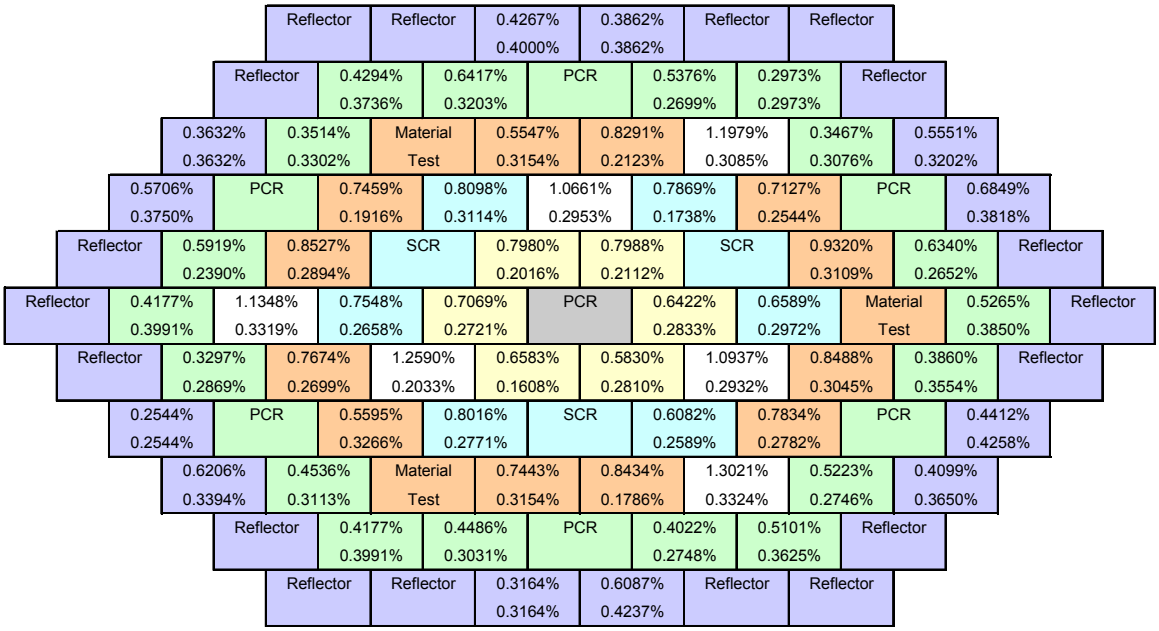

Figure 35 - Reactivity Change Resulting from 50% Coolant Density Reduction in Axial Level 5

A 50% reduction in coolant density tends to increase the net neutron production in the region, but the statistical error of the perturbations makes it difficult to assess the magnitude of the effect. While simply running more particle histories is one means of reducing statistical uncertainty, reducing the error by a factor of 2 generally requires increasing the number of neutron histories by a factor of 4 (in the absence of variance reduction techniques, such as particle splitting). So the coolant perturbation tallies that had errors of 100% would still be expected to have errors of ~50% if the calculation were run four times longer. In general, the fission rate does not change much as a result of coolant density reduction, but the parasitic capture rate decreases, increasing net neutron production in the region.

4.2.3 Fission Source Reconvergence

Perturbation theory allows one to assess the effect of a relatively small change without running a completely new calculation. However, one can run a new calculation, reconverging the fission source in the hopes of determining the effect of the change. The limitation to this technique is that in comparing two independent calculations that only differ by a small change, the statistical uncertainties of the calculations will often obscure any real effects introduced by the change. Nonetheless, reconverged neutron production calculations were performed for three fuel hexes, and the results compared to the perturbation calculations. The results are presented in Table 20. Again, absolute statistical uncertainties follow the net neutron production change.

Table 20 – Comparison of Reconverged Solution to Perturbation Calculations

	Axial Level	Calculation Type	Net neutron production change					
			Fuel Hex (2,4)		Fuel Hex (1,1)		Fuel Hex (4,1)	
Fuel density reduction	1	Perturbation	-1.8635%	0.0379%	-1.8910%	0.0320%	-1.8406%	0.0401%
		Reconverged	-1.4108%	1.0109%	-2.6235%	0.8049%	-2.5646%	0.9703%
	2	Perturbation	-1.8258%	0.0275%	-1.8603%	0.0242%	-1.8279%	0.0294%
		Reconverged	-2.3897%	0.7472%	-3.1721%	0.6117%	-3.8223%	0.7396%
	3	Perturbation	-1.8193%	0.0231%	-1.8568%	0.0205%	-1.8420%	0.0251%
		Reconverged	-2.9846%	0.7279%	-2.9227%	0.5936%	-4.2409%	0.7590%
	4	Perturbation	-1.8164%	0.0248%	-1.8643%	0.0217%	-1.8292%	0.0267%
		Reconverged	-0.9941%	0.7890%	-2.8970%	0.6545%	-5.3257%	0.7967%
	5	Perturbation	-1.8484%	0.0330%	-1.8807%	0.0276%	-1.8628%	0.0345%
		Reconverged	-3.9678%	1.0318%	-2.7364%	0.8341%	-4.9008%	1.0351%
Clad density reduction	1	Perturbation	0.4316%	0.0964%	0.3163%	0.0871%	0.2439%	0.0763%
		Reconverged	2.5071%	1.0340%	0.5745%	0.5745%	-0.3123%	-0.3123%
	2	Perturbation	0.3540%	0.0615%	0.2729%	0.0468%	0.2077%	0.0549%
		Reconverged	0.3099%	0.3099%	-0.1178%	-0.1178%	-0.2916%	-0.2916%
	3	Perturbation	0.3676%	0.0643%	0.2802%	0.0498%	0.2124%	0.0479%
		Reconverged	1.1664%	0.7194%	0.7488%	0.5892%	-1.8508%	0.7364%
	4	Perturbation	0.3512%	0.0671%	0.2954%	0.0470%	0.2102%	0.0490%
		Reconverged	2.7704%	0.7543%	-0.8208%	0.6488%	-1.3850%	0.7889%
	5	Perturbation	0.3974%	0.0992%	0.3069%	0.1264%	0.2174%	0.0799%
		Reconverged	1.0655%	1.0144%	0.5936%	0.5936%	-1.6708%	1.0254%
Coolant density reduction	1	Perturbation	1.5473%	0.3175%	0.8187%	0.2703%	0.6025%	0.3529%
		Reconverged	3.3671%	1.3423%	0.1670%	0.1670%	0.4234%	0.4234%
	2	Perturbation	1.2126%	0.2330%	0.6762%	0.2018%	0.6213%	0.2482%
		Reconverged	1.9277%	0.8540%	0.0268%	0.0268%	-0.3622%	-0.3622%
	3	Perturbation	1.2390%	0.2045%	0.6697%	0.1393%	0.5067%	0.2374%
		Reconverged	0.3517%	0.3517%	-0.0031%	-0.0031%	-1.9333%	0.9480%
	4	Perturbation	1.1223%	0.1378%	0.6167%	0.2026%	0.5594%	0.1403%
		Reconverged	2.8542%	0.9269%	0.1819%	0.1819%	-1.3655%	0.9466%
	5	Perturbation	1.0937%	0.2932%	0.7988%	0.2112%	0.2973%	0.2973%
		Reconverged	0.1461%	0.1461%	1.3857%	1.0282%	-2.1569%	1.2932%

This table confirms the limitations of reconverged calculations. Relative statistical uncertainties of the reconverged production rates are often above 50%, and in some cases reach 100%. These reconverged calculations ran 50,000 histories per cycle for 160 active cycles, each of which took about 1000 minutes on a 2.7-GHz Opitron processor.

4.2.4 Conclusions

Note the striking difference in statistical uncertainty between perturbed and reconverged calculations in Table 20. While the number of particle histories is the same for each, a key consideration is that the perturbation calculations actively calculate (and estimate the uncertainty of) the *difference* between the initial and perturbed configurations. The reconverged calculations calculate each value independently, each with its own associated statistical uncertainty. Thus, when calculating the effect of a small change, the perturbation result will yield a smaller statistical uncertainty than the comparison of two independent results.

There are limitations to the perturbation technique. If using the initial fission source distribution for the perturbed problem is insufficient, then the perturbed values will be

inaccurate. Preliminary calculations showed the 2nd order perturbations were less than 1% of the 1st order terms, indicating that the perturbation results are likely valid for the fuel density calculations. Future work would involve characterizing the 2nd order perturbation estimator for each difference that is evaluated, to support the validity of the perturbation model. Other future work would be to compare the results when using ENDF/B-VII cross-section evaluations instead of ENDF/B-V.

The perturbation model did very well in determining reactivity changes due to fuel density reduction. Relative statistical errors in this case were less than 2%. Determining the effect of clad density reduction on reactivity change showed promise, but statistical uncertainties were above 40% (relative error) in some cases. Judicious use of other variance reduction techniques, such as particle splitting, might still allow use of perturbation theory to evaluate clad density effects. Coolant density changes proved much more elusive. Relative statistical uncertainties in these cases were routinely over 50%, and in some cases reached 100%.

If the difference being analyzed were increased – for example, if the clad density were reduced by 10% instead of 5%, then the statistical error of the perturbation would be reduced. However, it is important to maintain a balance between analyzing changes that are large enough to be reliably determined using stochastic methods while not analyzing changes that are so large that the fission source is significantly altered, invalidating the perturbation model. By comparing 1st and 2nd order perturbation estimators, and tracking statistical uncertainties, the perturbation method can be used to determine reactivity effects results from small local changes in a reactor system.

5. ERROR PROPAGATION IN MONTE CARLO DEPLETION CALCULATIONS

5.1 Base Model and Depletion Study Case Matrix

The base model for this study is a partially-homogenized representation of the Advanced Breeder Reactor concept, generated in-house using ABRgen. In this model, fuel, clad, and coolant are homogenized as hexagonal assemblies with four axial zones. Symmetric fuel assemblies are grouped as a single burn material to improve statistics/runtime. Control rods are represented explicitly, with the main bank 50% inserted; control rods and reflector assemblies are not burned. A 2-year burn at 250 MWth is applied to all cases, along with an 800 K reference temperature for cross-section libraries. The MCNP cases are fixed at 10 inactive and 100 active kcode cycles.

For this study, there are three principal parameters to be considered: batch size (with the number of cycles fixed, this translates to total number of particles tracked), number of burn steps, and initial random number seed. Three batch sizes (5,000, 10,000, and 20,000) and 4 burn step lengths (2 years, 1 year, 6 months, and 3 months) make up the first 12 cases. Another forty cases are run varying only the initial random number seed for the MCNPX calculations, with 3-month steps, and with both 5,000 and 20,000 particles per batch.

Additionally, a set of standalone MCNP runs were executed varying the total number of cycles. The base deck here is a single MonteBurns-generated input deck with cross-section and energy spectrum tallies for all burn materials. These cases are intended to assess the variability of cross sections and k_{eff} as a function of runtime and relative error.

Table 21 - Case Matrix Summary

Test Parameter	Test Values	Sub-parameter	Sub-parameter Values	Description
Burn step size	30 days	Batch size (# of source neutrons per cycle)	5,000	
	60 days		10,000	
	120 days		20,000	
	360 days			
Batch/cycle length	25, 50, 100, 200, 400, 800 cycles			Quantify runtime impact relative to error, ensure stable cross sections. 5,000 particles per batch
Initial random number seed	40 random numbers	Batch size	5,000 20,000	Attempt to quantify the purely statistical variance in k_{eff} and isotopic concentrations. 4 burn steps, seed re-used for each step within case

5.1.1 MonteBurns Script Modification

In order to preserve tally files between MonteBurns steps, a modification to the Perl driver script was necessary. This could have been accomplished one of two ways—giving the MCNP tally file a unique name after each step, or appending the tally file to a "log" of tally data. The latter was chosen for simplicity. The driver script used for this study now creates two files, mbmco.log and mbmcm.log; these files are the combined MCNP output files and tally files, respectively.

The script has also been modified to make use of the *gstat* command to generate a machine file for parallel processing. The modification allows MonteBurns to identify the least-loaded compute nodes, with an ability to filter by type and/or CPU speed.

5.1.2 Post-processing Tools

5.1.2.1 Cross-section Postprocessor

The cross-section postprocessor collects a material, cell, isotope, and burn-step dependent structure of cross-sections and relative errors. The routine collects general information about the run from the *.chk* file (e.g. number of burn steps), then opens the *mbmcm.log* file to read tally data. All tally data (tally number, cell number, comment, values, and relative errors) contained in the problem is read into memory and stored in a data structure array:

```
Type TallyData
  TallyNum As Integer     'Tally number
  TallyComment As String
  CellNum As Integer      'Tally cell number
  Vals() As Double        'Tally data values
  Err() As Single         'Relative errors
  Mat() As Integer        'MCNP Material number
  Ebins() As Single       'Energy bin dividers
  ZAID() As Long          'Isotope identifier
  XSID() As Integer       'Cross-section identifier
End Type
```

The array is dimensioned according to the number of tallies and number of burn steps, with the arrays within the structure sized to match each individual tally. Since the tally file contains only data (tally values and errors), and not the tally multiplier card information, this must be read from the MCNP input decks preserved in the tmpfile directory. From these decks, material information and the tally multiplier *fm* card are processed. Material cards are used to populate an array matching ZAIDs to MonteBurns materials, while the fm cards supply material and cross-section identifiers to populate Mat, and XSID entries. A lookup function then uses the Mat numbers in the TallyData structure to fill in the corresponding ZAID.

This allows for a very simple (<30 lines) and flexible routine to arrange data on the spreadsheet in a convenient form. Currently, it is set to generate a sheet with columnar data containing burn step, ZAID, and cross-section values and errors.

5.1.2.2 MonteBurns CHK File Processor

The CHK file processor reads the CHK file generated by MonteBurns primarily to collect mass and atom density data. It also reads capture and fission cross-section data, though MonteBurns presents this data without the associated relative errors; the cross-section processor described in the previous section should be used instead. Unlike the cross-section postprocessor, this utility requires only the CHK file. Code structure is similar, with all data first being read into a custom data structure, organized by burn step and material. Totals by isotope and cell are generated by default.

5.2 Effect of Number of Particles Tracked

The average value of the system k_{eff} and the associated standard error are readily characterized in the MCNP output file. Figure 36 shows the value of k_{eff}, along with bands representing the range included by one standard deviation, for each of 800 active *kcode* cycles (5,000 source neutrons per cycle). It is obvious that the error is steadily decreasing, while the value continues drifting. Worth noting, however, is that the uncertainty window almost continuously includes the final window beyond 60 cycles (the exception being between 400 and 500 cycles).

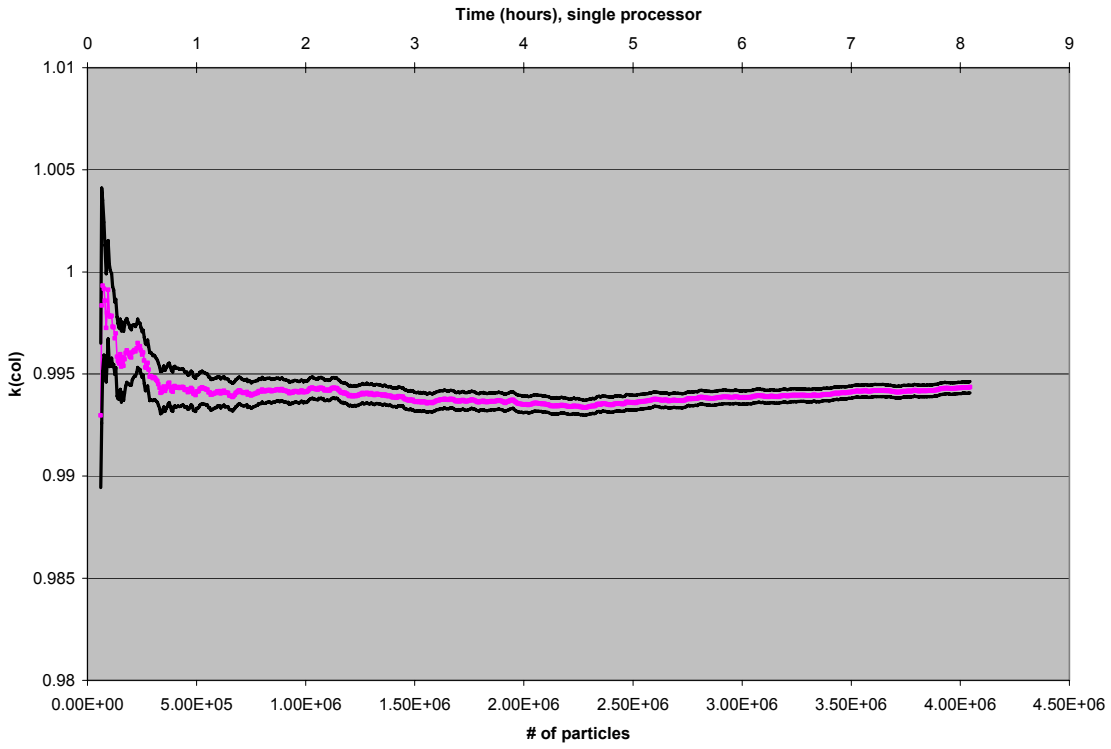

Figure 36 - k_{eff} with Error Bands Over 800 Active Cycles, 5,000 Neutron Batch Size

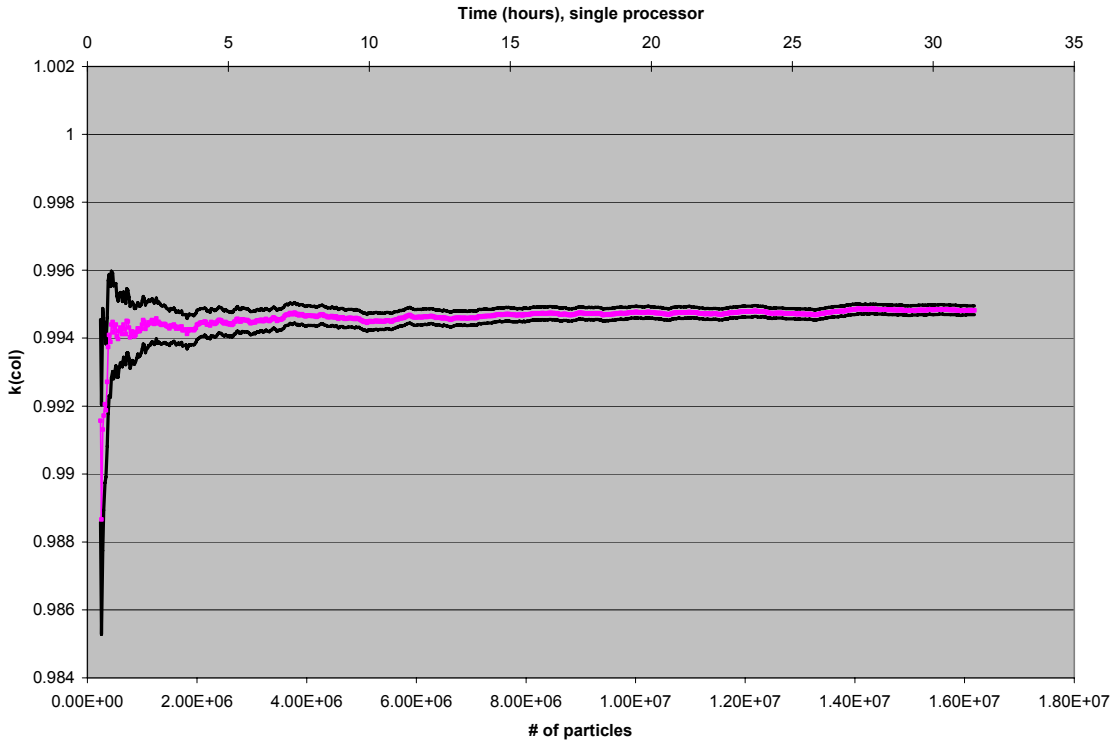

Figure 37 - k_{eff} with Error Bands for 20,000 Neutron Batch Size

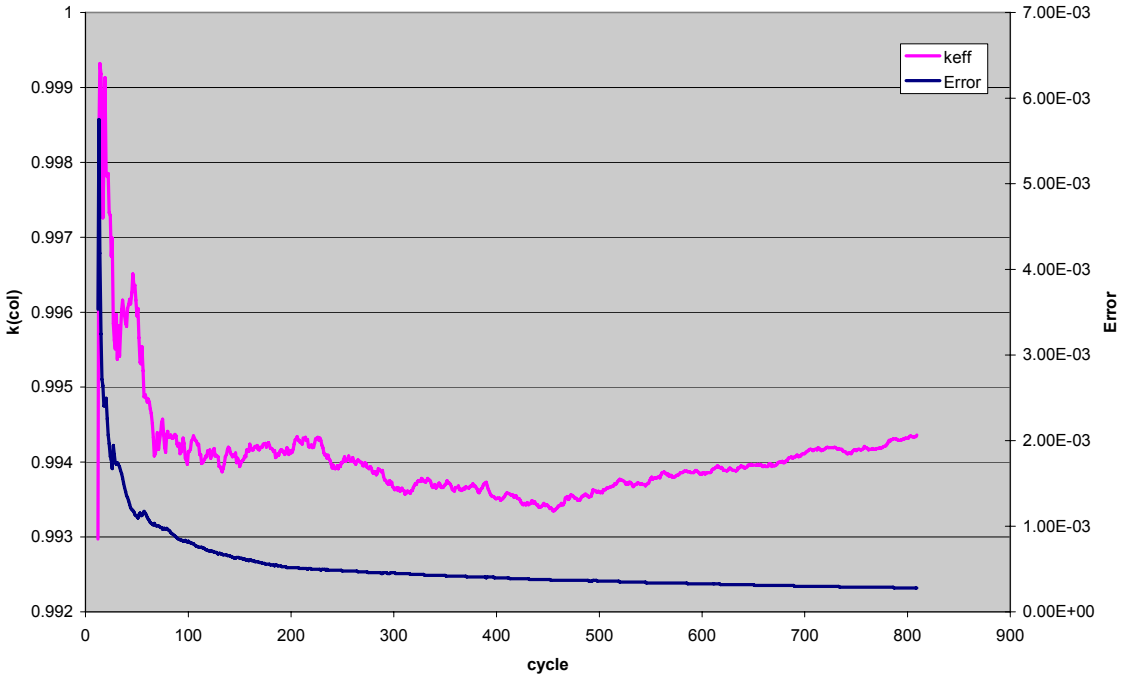

Figure 38 - k_{eff} and Error over 800 Active Cycles, 5,000 Neutron Batch Size

The functional form of the error can be seen in figure 38. Observe that from cycle 450 to the end of the run that the deviation of the mean k_{eff} is more than double the MCNP-calculated standard error, and that there is an obvious oscillation with a very long (i.e. hundreds of cycles) period. This could be reduced by increasing the number of particles per cycle, reducing the deviation of individual *kcode* calculations. The effect, as a function of particles tracked, is shown in figure 39. Notice that while the MCNP-reported error decreases faster with the smaller batch size, the reliability of the error statistic obviously increases (notice significantly flatter shape in figure 37). For both performance and statistical reliability, larger batch sizes with fewer active cycles are recommended.

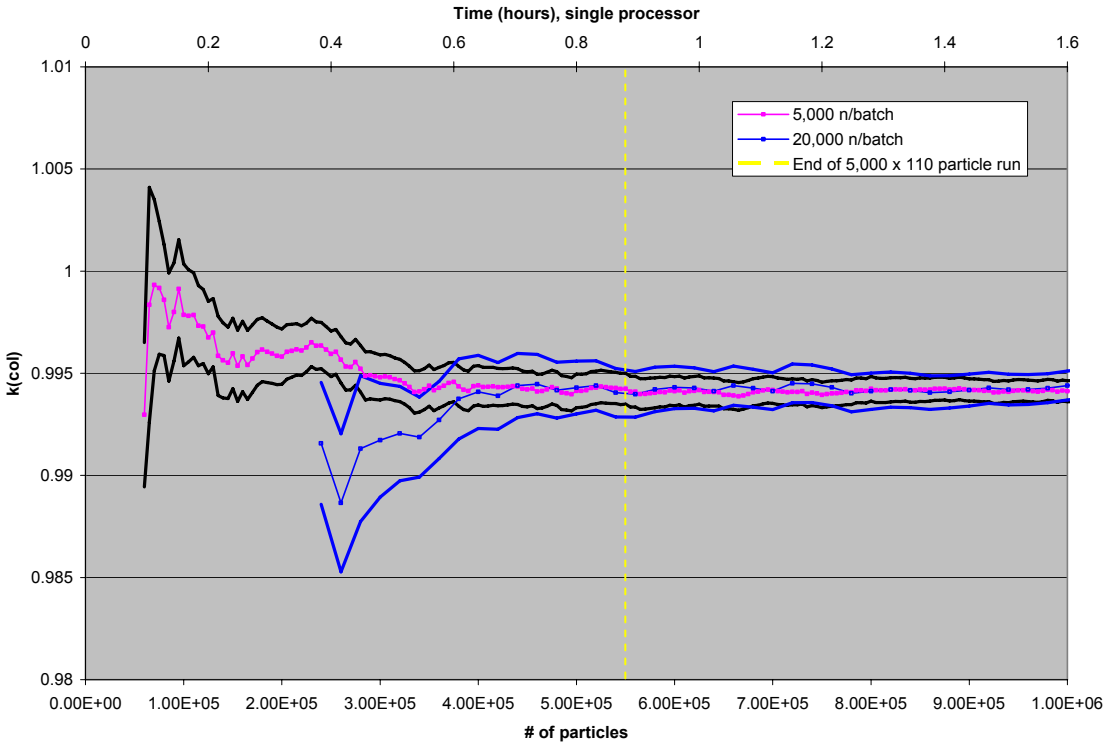

Figure 39 - k_{eff} with Error Bands for Small and Large Batch Sizes

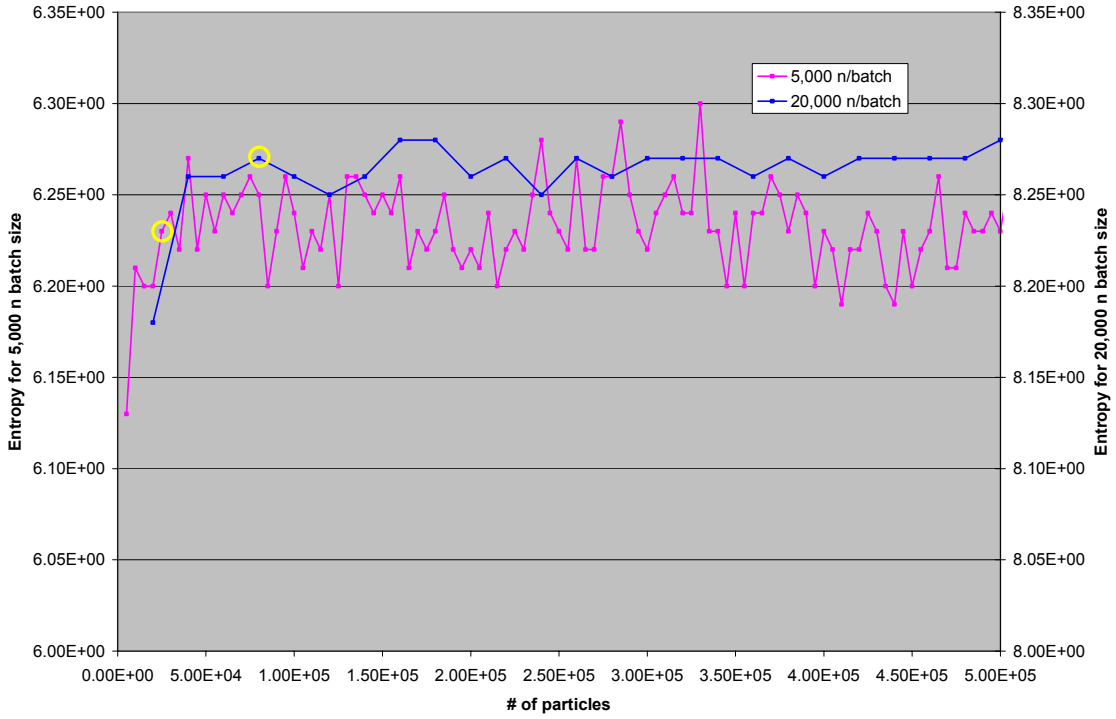

Figure 40 - Shannon Entropy

Figure 40 shows the Shannon entropy—a parameter for assessing fission source convergence—as calculated by MCNP5 for two different batch sizes. The code reports that the fifth and fourth cycles are the first to fall within the standard deviation for the small and large batch sizes. This suggests, as highlighted on the figure, that a converged source is actually achieved more quickly with the smaller batch size.

5.2.1 Localized Effects

- In general, cross section values are relatively constant as the number of *kcode* cycles is increased
- In many cases, cross section value after 25 cycles falls within one standard deviation of value after 800 cycles

Of equal or greater importance for depletion calculations with MCNP is the effect of error on cross section tallies. To a certain extent, variations in cross section values as a function of the number of active cycles can be ascertained from the tally fluctuation charts included in the MCNP output files. Alternatively, *kcode* runs can be carried out for varying numbers of active cycles, with the normal tally files containing cross sections and associated relative errors. The latter method is the basis for data in this section, primarily for convenience, being compatible with the post-processing tools already described.

Since there are 44 burned-material regions in the model, with nearly two-dozen isotopes each at beginning of life, it is not practical to discuss every cross section/reaction rate for every node and/or isotope in the problem. Instead, data for select isotopes and cells will

be used to show general trends. In this section, one of the fuel test assemblies (loaded with LWR-recycle fuel) will be discussed. Further, in consideration of its impact on the depletion process, the capture-to-fission ratio will be used to discuss the combined effect of changes to both cross sections. The error in the ratio is calculated from the relative error in each cross section, using the following relationship:

$$\left(\frac{\Delta CF}{CF}\right) = \sqrt{\left(\frac{\Delta(n,f)}{(n,f)}\right)^2 + \left(\frac{\Delta(n,\gamma)}{(n,\gamma)}\right)^2}$$

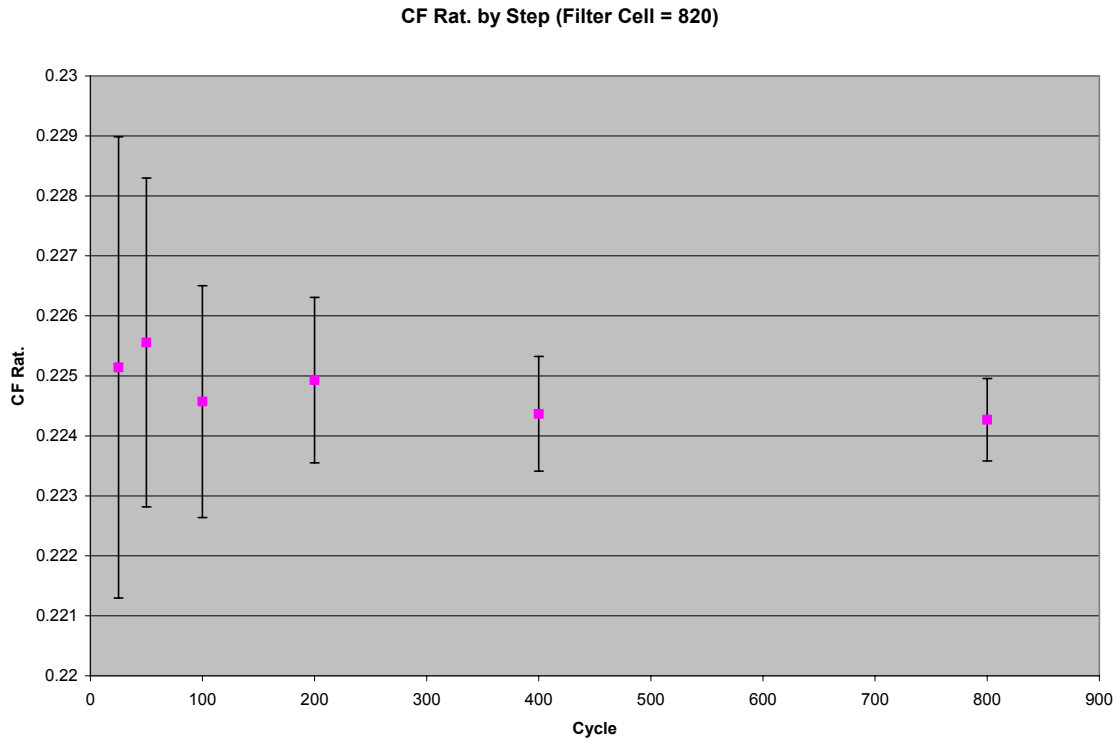

Figure 41 - Capture-to-fission ratio for ^{235}U in Controlled Upper-middle Fuel Test Node

For a large number of cells and fissionable isotopes in the analysis, the behavior of the microscopic capture-to-fission ratio is similar to that shown in figure 41, and relatively constant as a function of the number of cycles run. This ratio is not constant as a function of exposure; this dependence is discussed later in this document. It is also interesting that for most capture-to-fission ratios in internal nodes examined so far, the very first data point (25 active cycles) is within or only slightly outside the error bars at the end of 800 active cycles.

Figures 42 and 43 show similar behavior for the two nodes axially adjacent to the node shown in figure 41, except that in these cases, the 25-cycle value is within the 800-cycle error bars. This stability may break down in uncontrolled, outer (bottom) node locations, as can be seen in figure 44. It not clear at this point to what extent any location-based correlation may exist, or what the underlying cause of the behavior might be.

It can be seen in these figures that there are significant changes in converged microscopic cross sections and capture-to-fission ratios. There is little difference in the two internal nodes (approximately one standard deviation). Yet the ratios for the top and bottom node locations are greater by 4.2% and 11%, respectively.

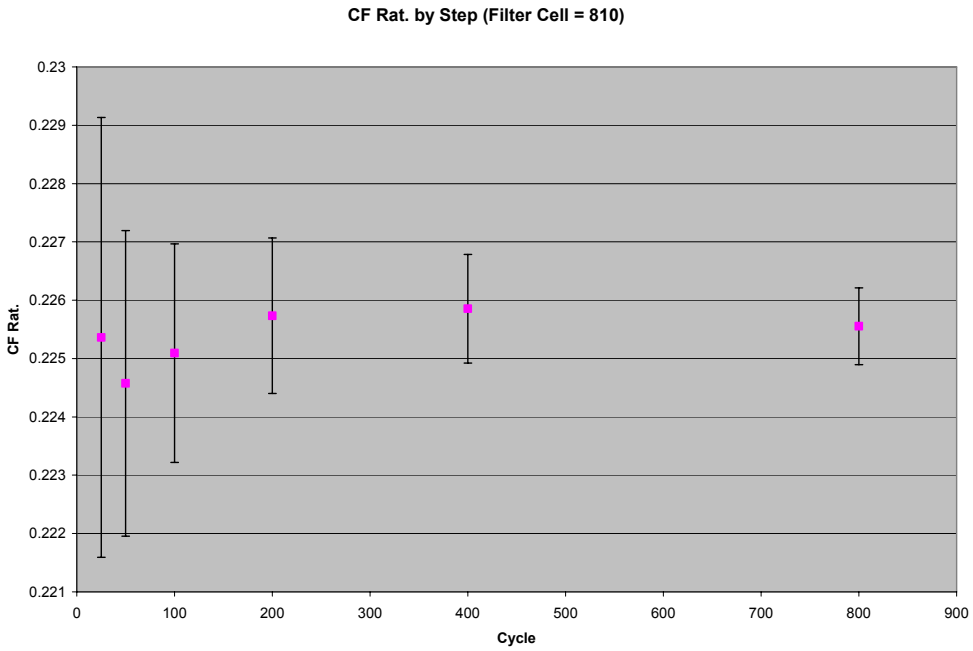

Figure 42 - Capture-to-fission ratio for ^{235}U in Uncontrolled Lower-middle Fuel Test Node

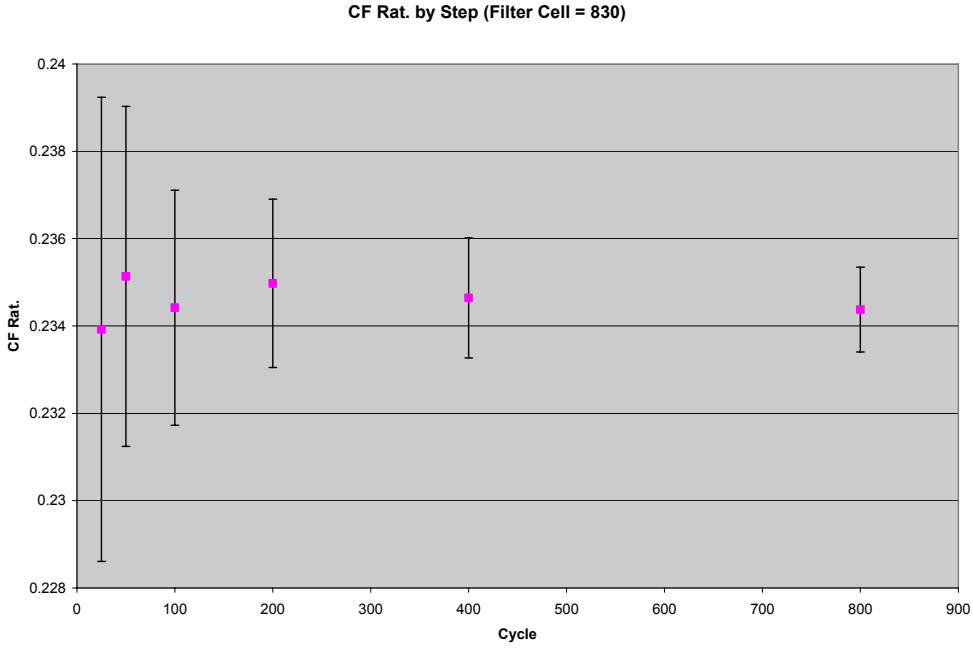

Figure 43 - Capture-to-fission Ratio for ^{235}U in Controlled Top-of-core Fuel Test Node

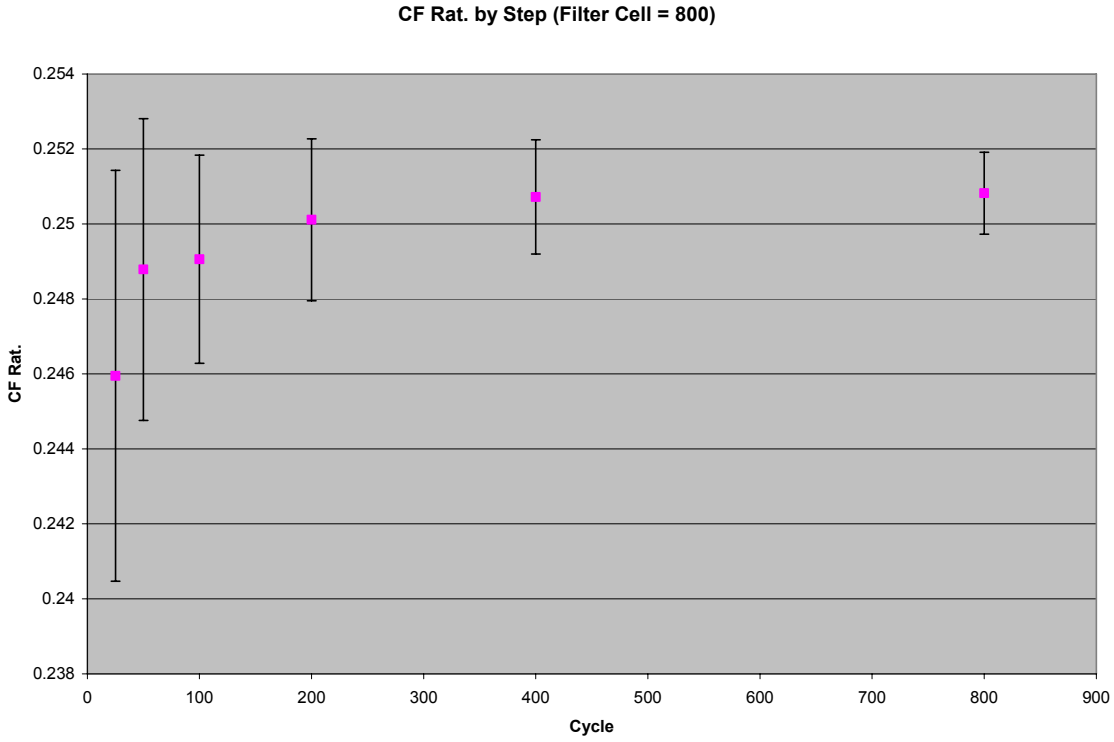

Figure 44 - Capture-to-fission Ratio for ^{235}U in Uncontrolled Bottom-of-core Fuel Test Node

5.3 Burn Step Size and Number of Particles Per Batch

The burn step size and the number of particles tracked in the Monte Carlo solution are the two primary parameters of interest in this study. Higher fidelity in either case results in a linear runtime penalty, such that it is important to understand the level of fidelity necessary to achieve satisfactory results and avoid excessive computation time. Discussion is separated into system-wide effects, namely k_{eff} and total end-of-cycle isotopic inventories, and localized effects, including trends in microscopic cross sections and individual cell composition.

5.3.1 Core-wide Trends

- k_{eff} and EOC inventories are sensitive to number of burn steps, insensitive to batch size
- *Smaller (in time) burn steps and smaller batch sizes give best results, so long as batch size is large enough for converged fission source*

5.3.1.1 System k_{eff}

It should be expected that the system k_{eff} is the first parameter (ahead of any tallies) to reach a converged solution in this Monte Carlo depletion process. In the figures that follow, eigenvalue data is presented for both full and half step MCNP runs (i.e. $2n$+1 data points, where n is the number of burn steps). Figure 45 shows that for the cases with four or eight burn steps, k_{eff} is very consistent, regardless of the number of source neutrons

tracked at each step. Notice, however, that deviations begin to appear as the number of burn steps is further reduced. To show the independence of k_{eff} and batch size, figure 46 shows the same data again, only filtering to the three cases with eight burn steps. There is no discernable difference in the value at this level; the only difference between these cases is a reduction in the reported relative errors (see figure 47).

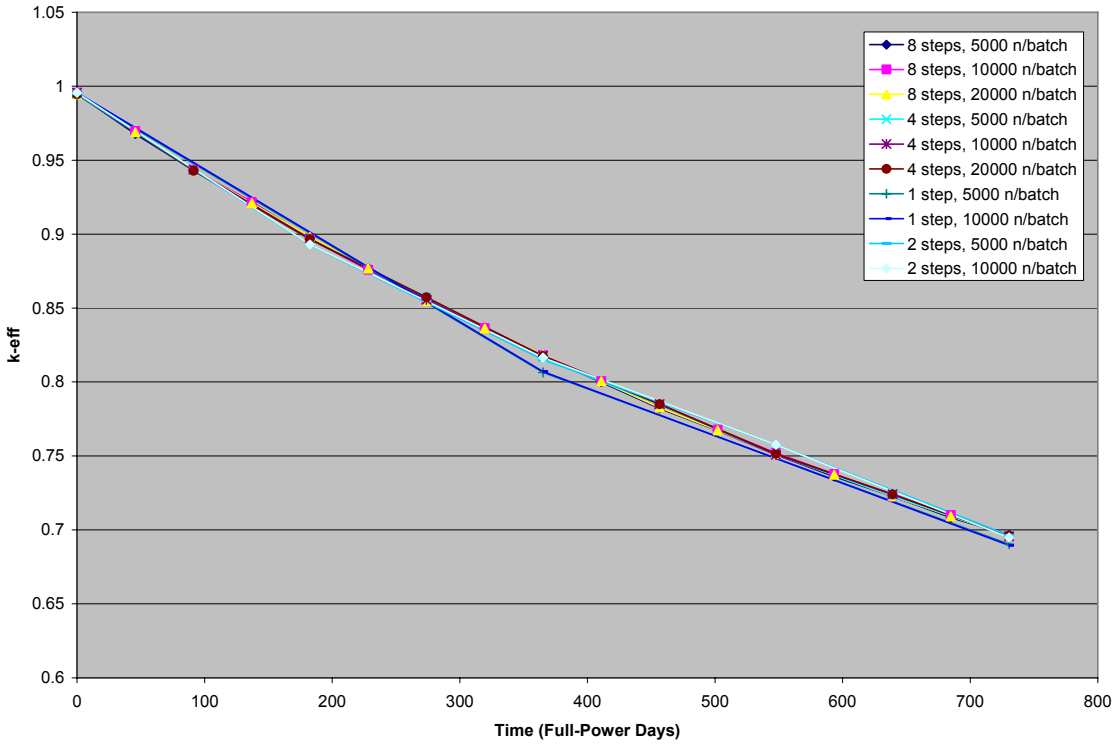

Figure 45 - System k_{eff} for Various Combinations of Burn Step and Batch Sizes (includes ½-steps)

As expected, the reported relative errors are halved when the number of particles is quadrupled (shown in figure 47). It is not necessarily obvious why the relative error consistently decreases with exposure, but it is instead far more important to note that the error reported in any one MCNP calculation is not influenced by the cumulative errors included in the inputs to that calculation. In other words, the reported errors are the same regardless of the number of burn steps as far as the MCNP errors are concerned. As a result, it is necessary for further comparisons to examine differences between these cases at isotopic and nodal levels.

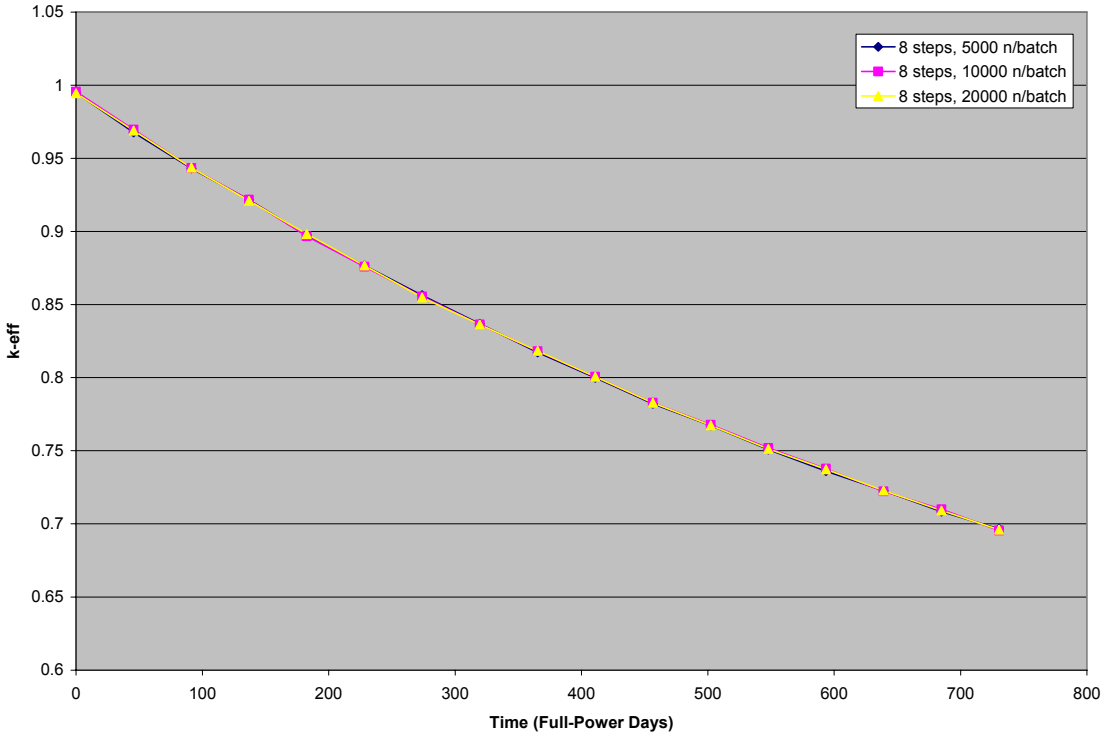

Figure 46 - System k_{eff} for 8 Burn Steps, Varying Batch Sizes (includes ½-steps)

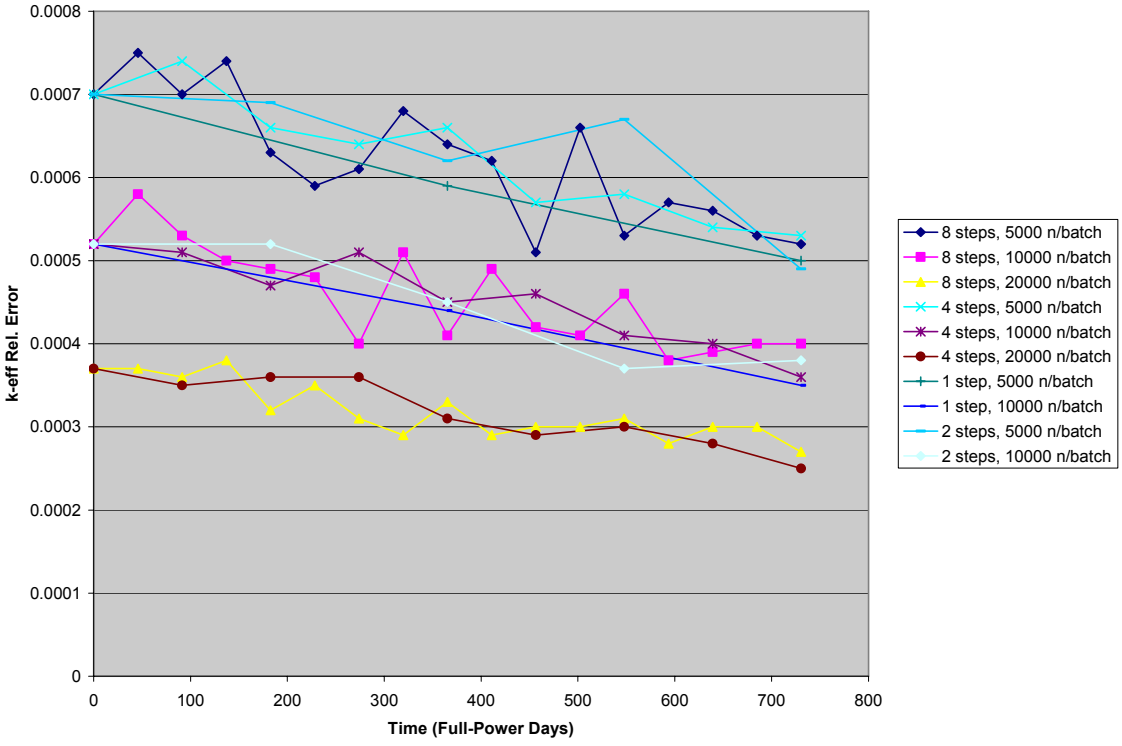

Figure 47 - Relative Error in System k_{eff} for Varying Burn Step and Batch Sizes (includes ½-steps)

5.3.1.2 Inventories

For the Advanced Burner Reactor concept, it is obvious that knowing end-of-cycle inventories for important isotopes will be critical. Tables 22 and 23 provide a summary of end-of-cycle mass inventories as a function of burn step and batch sizes. For reference, the first data column contains the inventories for isotopes present at the beginning of the burn.

For a large number of isotopes, there is little significant difference in inventory with changes in burn fidelity (i.e. number of steps, batch size). In general, differences are much larger as the number of burn steps is varied than with the number of particles per step. For a fixed total number of particles tracked, it will be beneficial to take a smaller time-step with fewer particles in each step.

In some cases, there is a significant difference in the end-of-cycle inventory as a function of the number of burn steps. ^{239}Np provides a compelling example where cross section changes, both microscopic (as spectrum changes) and macroscopic (self-shielding), induce error. With eight burn steps, the ^{239}Np inventory is 5.1% larger than the inventory calculated with 4 steps, and 25.1% larger than with 2 steps. Yet, for a fixed number of burn steps, the largest deviation is 1.9% (8 steps). Furthermore, within three of four step sizes, the masses for ^{239}Np differ by 0.3% or less.

The uncertainty associated with burn step size can also be seen in ^{95}Nb, which does not clear the reactivity threshold for 8, 4, or 1 burn step, but all three cases with two burn steps include it.

Table 22 - Total Inventories at End-of-Cycle (1 of 2)

Source Neutrons Per Batch / Isotope		8 burn steps			4 burn steps			2 burn steps			1 burn step		
	BOC	5000	10000	20000	5000	10000	20000	5000	10000	20000	5000	10000	20000
92-U-235	1200	229.76	229.89	230.1	230.27	230.29	230.59	230.29	230.62	230.76	223.78	224.96	224.39
92-U-238	750000	598200	598400	598400	598700	598400	598500	598700	598500	598800	595700	595900	595800
93-Np-237	1248	1131.6	1134.8	1135.9	1133.7	1129	1131.9	1139.3	1137.8	1135.2	1129.7	1141.8	1132
93-Np-239		514.35	524.57	524.18	498.61	498.95	498.74	418.94	419.69	418.79	374.49	373.84	373.36
94-Pu-238	625	1077.43	1078.41	1077.73	1081.77	1081.28	1076.65	1081.87	1081.94	1080.33	1090.37	1092.16	1094.28
94-Pu-239	139400	81870	81860	81850	81850	81920	81870	81790	81880	81850	81120	81190	81160
94-Pu-240	20732	30989	31012	31000	30980	30990	30956	30963	30949	30942	31092	31001	31034
94-Pu-241	2916	4230.2	4233.7	4236	4228.3	4232.9	4229.101	4236	4223.6	4229.399	4268	4250.1	4254.6
94-Pu-242	1536	1810.2	1811.3	1811.3	1811.5	1825.1	1811.3	1805.6	1806.1	1809	1828.6	1826.4	1827.4
95-Am-241	1488	658.6	658.8	659.2	660	659.9	661.2	660.6	661.4	661.4	651.1	649.7001	650.5
95-Am-242	41	72.43999	72.47	72.4	72.48	72.41	72.43	72.32999	72.27	72.42	71.46	71.37	71.53
95-Am-243	308	334.5	333.8	334.2	335.1	332.8	333.2	333.8	334.7	334	334.6	335.3	334.6
96-Cm-244		186.2	186.2	186.1	185.7	185.8	186	185.5	186.5	185.5	187.4	187.5	187.2
96-Cm-245		21.35	23.43	23.41	23.35	23.41	21.37	21.15	23.3	21.15	23.61	23.73	23.8

Table 23 - Total Inventories at End-of-Cycle (2 of 2)

Source Neutrons per Batch / Isotope		8 burn steps			4 burn steps			2 burn steps			1 burn step		
	BOC	5000	10000	20000	5000	10000	20000	5000	10000	20000	5000	10000	20000
11-Na-023	60280	60280	60280	60280	60280	60280	60280	60280	60280	60280	60280	60280	60280
24-Cr-052	45760	45360	45370	45360	45360	45360	45360	45360	45360	45360	45360	45360	45360
25-Mn-055	2024	1984.5	1984.5	1984.5	1984.8	1984.6	1984.7	1984.8	1984.3	1984.7	1983.6	1984.3	1983.9
26-Fe-056	307120	305490	305490	305500	305500	305490	305500	305500	305490	305500	305470	305470	305490
26-Fe-057		1516.6	1520.8	1518.1	1520.3	1518.2	1515.2	1514.4	1516.8	1513.6	1579.8	1549.1	1550.5
28-Ni-058	1892	1835.8	1835.7	1835.7	1836.1	1835.8	1835.9	1835.8	1836	1835.9	1835	1835.2	1835.2
36-Kr-083		15.62	15.03	10.59	30.26	35.34	45.49	73.92001	74.03	74.03999	124.12	124.07	123.98
38-Sr-088		345.6	345.8	346	344.9	345.4	344.5	375.1	376	344.6	413.6	413.5	412.2
38-Sr-090		1363.2	1363	1363.3	1361.1	1361.7	1360.9	1359.6	1329.7	1359.9	1382.5	1380.7	1379.7
39-Y-089		668.4	668.7	668.9	668.1	668.8	667.8	669.9	671.1	669.9	749.5001	718.9	717.0001
40-Zr-090	106040	210440	210450	210450	210450	210430	210440	210430	210440	210440	210420	210410	210430
40-Zr-091		1621.1	1621.5	1621.4	1606.2	1576.5	1574.6	1676.1	1613.6	1611.9	1810.3	1741.6	1738.8
40-Zr-092		2352.5	2352.1	2351.4	2349	2350	2347.699	2348.1	2348.8	2347.5	2400.6	2398.6	2397.3
40-Zr-093		2963.7	2962.599	2962.599	2961.2	2962	2959.3	2959.8	2960.2	2958	2982.1	3009.4	3007.9
40-Zr-094		3308.9	3307.2	3307.3	3302.2	3305.1	3302	3303	3303.3	3302.5	3364.6	3361.1	3359.5
41-Nb-095		0	0	0	0	0	0	7.69	7.72	7.71	0	0	0
42-Mo-095		2704.5	2703.7	2703.9	2708	2708.401	2707.7	2734.7	2734.4	2733.599	2845.7	2842.6	2841.8
42-Mo-097		3906.1	3903.5	3905.4	3869.3	3871.7	3870.2	3819.3	3817.9	3814.7	3881.1	3879.1	3875.8
42-Mo-098	15972	34997	35001	35001	34994	34995	34995	34990	34994	34985	35042	35038	35032
42-Mo-100		5170.5	5169.399	5171.3	5165.1	5166.5	5161.699	5165.4	5159.2	5160.1	5259.3	5251	5248
43-Tc-099		3925.8	3926.8	3924.7	4044.8	4044	4041.9	4026.5	4022.7	4023.3	4051.2	4048.5	4049.6
44-Ru-100		689.1	690.5	690.5001	707.8	710.2001	707.3	701.2001	703.8	701.7001	719.6	718.1	714.5
44-Ru-101		4348.8	4348.5	4347.599	4348.3	4348	4345.399	4348.6	4350.8	4347.1	4414.1	4410	4408.5
44-Ru-102		6336.3	6333.5	6333.6	6321.1	6329	6319.399	6318.8	6325.3	6321.7	6453.2	6440.6	6434.601
44-Ru-103		420.19	411.96	403.59	412.36	395.89	404.57	358.54	367.94	367.66	310.28	318.06	293.88
44-Ru-104		5217.1	5214.7	5217.1	5209.3	5210	5204.2	5205	5205.501	5205.4	5301.6	5294.3	5289
44-Ru-106		1821.5	1821.5	1820.9	1813.3	1814.2	1812.7	1792.6	1793.2	1792.5	1701.1	1698.1	1696.2
45-Rh-103		4381.5	4383.1	4384.3	4387.7	4390.7	4386.299	4410	4412.9	4411.5	4526.6	4518.2	4517.2
46-Pd-104		808.8	808.9999	808.9	817.1	818.5001	815.9001	815.5001	815.6999	814.6	839.4999	839.1999	836
46-Pd-105		3387.7	3387.2	3387.3	3355.2	3356.901	3354.299	3345.8	3344.1	3343.7	3386.3	3385.2	3383.801
46-Pd-106		2806.4	2805.5	2805.1	2793.4	2796.3	2791.5	2805.6	2807.5	2804.5	2947.4	2938.8	2935.8
46-Pd-107		2034.5	2034	2034.1	2031.2	2031.4	2031	2032.2	2031.3	2030.9	2061	2059.6	2058.4
46-Pd-108		2474.3	2474.3	2474.4	2470.9	2471.1	2467.8	2468.9	2470.5	2468	2523.6	2519.9	2515.2
47-Ag-109		1260	1259.7	1259.5	1257.1	1259.5	1257.9	1259.5	1258.4	1258.4	1283.3	1280.8	1282.3
48-Cd-110		26.9	25.1	26.9	26.6	37.8	26.4	37.8	37.8	26.4	40.4	39.8	39
48-Cd-111		192.61	183.42	183.63	183.93	184.04	192.38	193.9	201.39	194.03	211.66	211.59	218.65
52-Te-130		2458.7	2457.9	2457.7	2454.601	2455.601	2453.4	2454.2	2454.6	2452.6	2499.799	2496.2	2494.9
53-I-127		445.24	445.11	445.25	483.3701	483.1101	483.1001	482.01	474.14	481.6701	480.48	487.49	487.58
53-I-129		1385.1	1384.6	1384.5	1383.5	1383.7	1382.6	1383.6	1383.2	1383.2	1410.6	1409.2	1408.8
54-Xe-131		3775.3	3772.5	3774	3771.8	3774.3	3773	3778.2	3772.5	3775.1	3854.9	3851.2	3846.8
54-Xe-132		6046.2	6044.5	6042.6	6031.3	6033.2	6022.899	6019.7	6024.1	6016.1	6129.1	6114.8	6114.8
54-Xe-134		7900.5	7907.1	7898.6	7891	7894.6	7886.2	7891.9	7891.8	7890.8	8036.2	8027.6	8023.9
54-Xe-136		7603.4	7603	7602.5	7590.8	7595.6	7586.1	7586.7	7589.7	7587.6	7731.9	7717.4	7716.5
55-Cs-133		6332.2	6330.7	6327.7	6327.3	6322	6322	6520.6	6514.1	6512	6531	6526	6527.6
55-Cs-134		673.5299	675.1799	675.01	671.04	673.6901	670.74	687.2	690.7899	688.96	701.98	702.75	698.78
55-Cs-135		7719.7	7723.3	7727.7	7716.2	7713.8	7712.5	7704	7707	7703.9	7833.8	7824.1	7814.4
55-Cs-137		6830.6	6827.3	6828.4	6817.2	6822.8	6815.3	6814.4	6815.4	6813.8	6935.7	6921.601	6920.6
56-Ba-138		7084.2	7083.1	7081.3	7073.3	7077.8	7067.9	7072.3	7075.7	7068.9	7203.9	7197.8	7190.3
57-La-139		6528.8	6527.3	6526.4	6514.5	6521.601	6518.4	6518.8	6517.4	6516	6638.7	6629.5	6627.5
58-Ce-140		6008.6	6008.8	6007	6004	6008.9	5999.4	6011.6	6013.2	6008.7	6453.7	6444.3	6438.7
58-Ce-142		5647.299	5648	5647.101	5640.4	5640.7	5635.8	5637.6	5638.7	5635.9	5748.6	5738	5734.1
58-Ce-144		1883.4	1882.9	1882.6	1872.8	1873.8	1872.2	1844.9	1845.2	1844.7	1802.8	1767.1	1798.5
59-Pr-141		5718.2	5715.9	5714.8	5714.1	5714.6	5715.7	5731.9	5733.7	5731	5882.5	5871.1	5868.101
60-Nd-143		4633.7	4636.5	4634.699	4634.5	4634.199	4632.4	4644.2	4640.8	4642.4	4798.299	4795.1	4792.3
60-Nd-144		2672.5	2673.8	2672.2	2675.1	2678.4	2673.8	2696.3	2699.1	2695.6	2833.9	2828.5	2825
60-Nd-145		3355.7	3353.4	3354.201	3354.3	3352.6	3353.499	3356.9	3357.4	3356	3425.9	3421.3	3419.2
60-Nd-146		3499.5	3499.7	3499.9	3494	3497.3	3490.199	3489.6	3489.701	3489.3	3566.199	3561.099	3558.6
60-Nd-148		1901.3	1922.2	1922.4	1919.3	1920.2	1919.2	2028.3	2028.3	2027.4	2103.9	2099.4	2100.3
60-Nd-150		492.6	513.4	513.2	530.6	551.9	551.3	817.9	763.9	791.2001	1120.9	1121.3	1120.4
61-Pm-147		1493	1491.2	1492.1	1494.2	1493.3	1493.7	1493.5	1492.3	1493.6	1493.4	1495.6	1495
62-Sm-147		360.67	354.7199	360.95	365.27	358.9	359.29	372.63	371.6299	372.69	400.2101	400.7701	400.76
62-Sm-148		241.8	254	253.5	324.7	349.6	333.3	394.5	383.7	393.8	436.9	407.9	420.7
62-Sm-149		1099.9	1099.8	1099	1099.4	1097.9	1099	1103.8	1103.2	1103.2	1115	1115.5	1113
62-Sm-150		613.9	615	615	634.3001	637.0001	633.9001	634.4	636.6	634.3	644.3001	641.2001	640.9
62-Sm-151		601.0999	600.4799	600.28	601.42	600.47	601.4301	604.33	604.5699	604.27	622.34	621.4301	621.25
62-Sm-152		1173.9	1187.1	1173.3	1180.3	1196.8	1193.8	1192.6	1190.5	1191.3	1216	1211.9	1211.3
63-Eu-153		398.04	397.41	398.25	399.15	397.7801	397.39	400.8799	401.58	400.61	408.2699	409.63	409.2001
63-Eu-154		169.5699	169.57	169.49	171.23	171.36	171.08	168.6	168.85	170.07	175.53	175.27	174.7
63-Eu-155		229.81	225.68	220.34	224.16	220.11	224.4	219.73	232.84	228.96	262.63	256.63	255.39
64-Gd-156		9.99	10	10	9.94	10.1	9.93	9.85	9.97	9.86	10.2	10.2	10.1
64-Gd-157		7.65	6.23	4.47	14.26	17.23	14.16	26.49	21.1	24.3	48.35	48.3	48.3

5.3.2 Local Cross Sections and Composition

- Significant change in microscopic cross sections with exposure (generally increasing)
- Greater deviation with increased step size (fewer steps) than with reduced batch size (fewer particles per burn step)

As suggested in the previous section, some of the variation in end-of-cycle masses aligns with the expectation that cross sections change as a function of exposure. The magnitude of such a change is obviously system dependent, but quite significant for the ABR concept studied here.

Once again, it is not practical or useful to present data for every isotope at every node in this discussion. Figure 48 begins to provide a sense of the extent of fission cross section changes as a function of time and number of burn steps. In this case, ^{239}Pu in cell 810 (second quarter-height from core bottom in a fuel test location) is shown. The 8-step case shows a 10% increase in the microscopic fission cross section; this change is far greater in magnitude than the MCNP standard error associated with any data point. It is also important to notice the effect of changing cross sections as a function of the number of burn steps taken. Cross-section differences as a function of the three batch sizes studied are generally negligible.

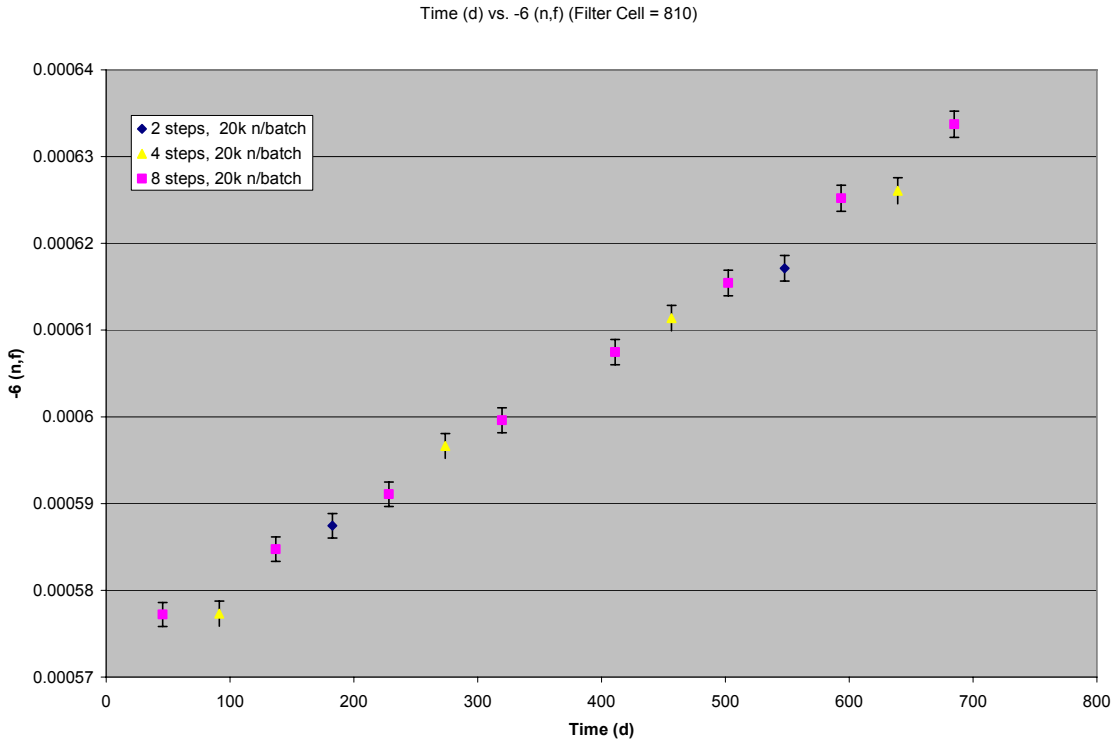

Figure 48 - ^{239}Pu Fission Cross Section with Time (note that cross sections are tallied at the ½-step time point)

The magnitude of the change in ^{239}Pu fission cross section is representative of most of the minor actinides. Associated uncertainties increase as inventories decrease, and some isotopes introduced to the problem in later burn steps can be large.

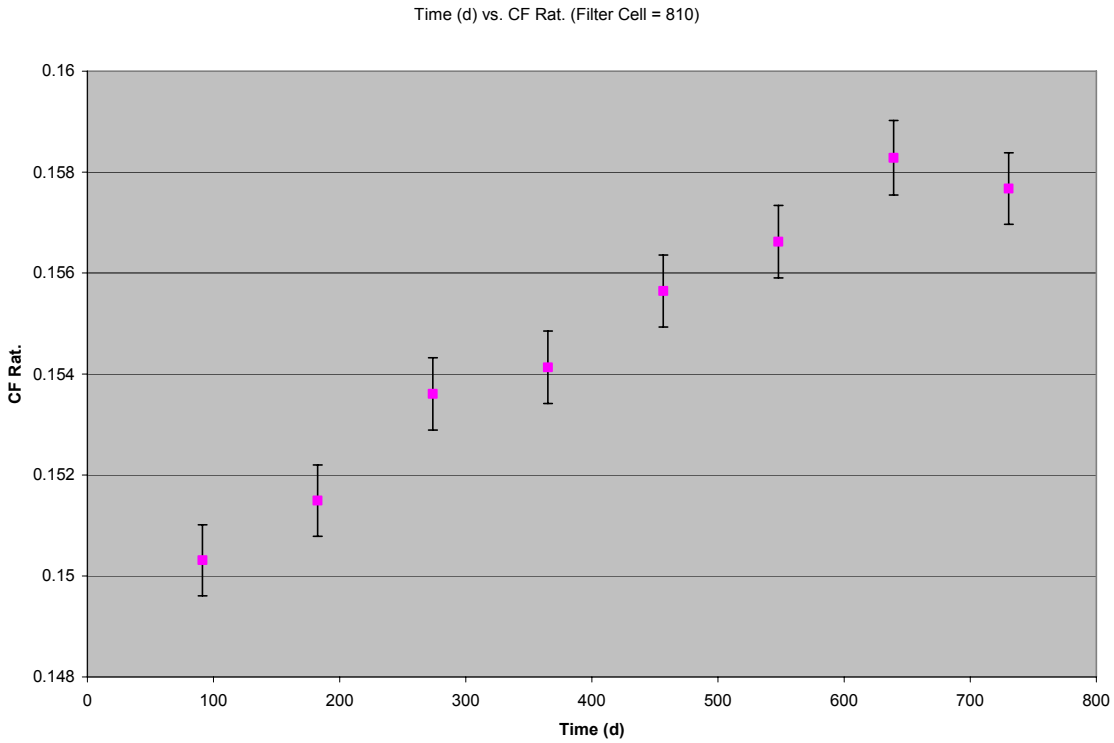

Figure 49 - Capture-to-Fission Ratio for ^{239}Pu

With regard to material composition, there are two effects worth noting. First, the 239Pu densities with a two-step burn differ only slightly (less than 0.5%) from the average densities for the first and last halves of the eight-step burn, shown in figure 50. Separately, and perhaps more significantly, the average difference (in magnitude) is approximately 1.2%.

This begins to suggest that changes, whether 1-group cross-sections or material composition, over relatively small time intervals contribute significantly to the observed differences in k_{eff} and end-of-cycle aggregate material composition. It appears that these very localized parameters do indeed play a significant role in the macroscopic nodal cross sections. The combined effects of increasing cross sections and decreasing density observed with ^{239}Pu is likely indicative of significant self-shielding. In fact, the macroscopic cross section in this case only slightly decreases with exposure (6%, compared to changes of 10% and 16% for microscopic cross section and density).

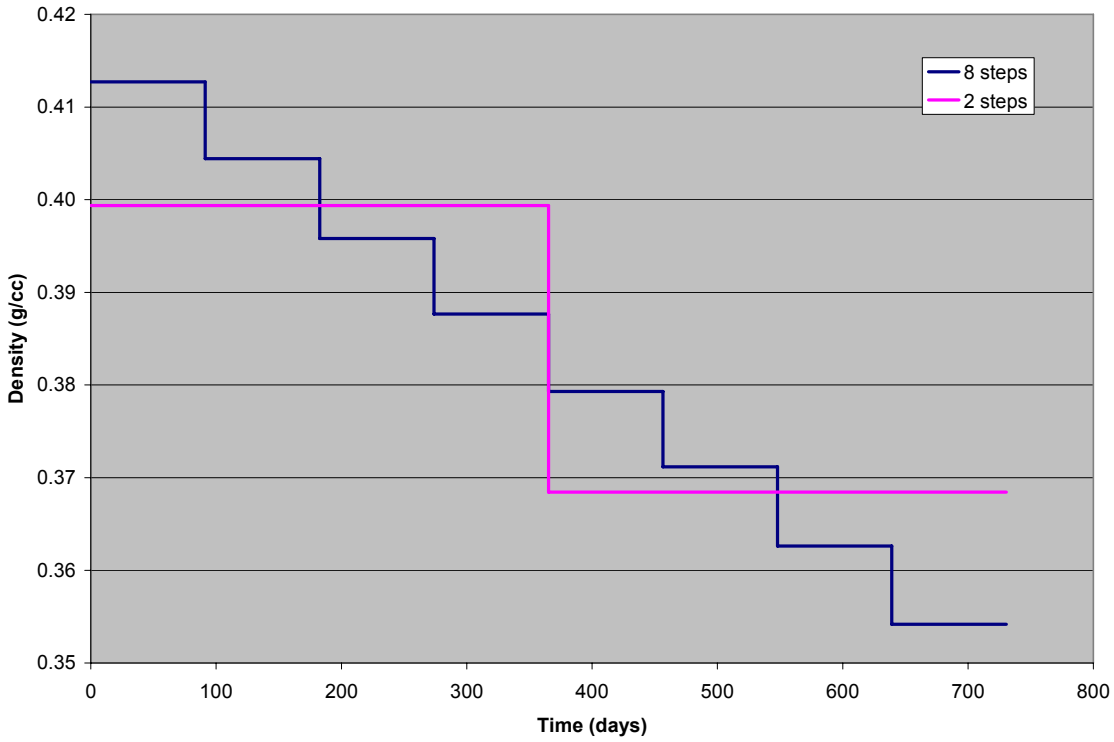

Figure 50 - ^{239}Pu Density for Lower-middle Fuel Test Cell Location (cell 810)

5.3.3 Conclusions

Ultimately, final composition and reactivity parameters are fundamentally dependent on time-dependent cross sections, fluxes, and material composition. It appears from the observed trends that the impact of the number (or size) of burn steps is a far more significant area of concern than the accumulated errors in the Monte Carlo calculations.

5.4 Variations Associated with Starting Random Number Seed

- Decreased deviation with larger batch size
- Variations generally small and consistent

Using a perl script to generate random numbers, 40 MonteBurns cases were generated with unique random number seeds for each of 5,000 and 20,000 particle batch sizes, with 4 burn steps. This section presents a statistical summary of observations in k_{eff}, end-of-cycle inventories, and inventories in a single cell.

5.4.1 System k_{eff}

The behavior of k_{eff} is largely as expected, with smaller reported errors and smaller variations between case sets as the number of particles per batch is increased. Nine steps are shown for each statistic, made up of 4-pairs of mid- and end-steps, and an extra predictor step. There is very little difference between mean and median at any point (table 24), suggesting a normal distribution. Differences between 5,000 and 20,000 particle cases are also small.

Table 24 - k_{eff} Statistics by Step: (a) Means and **(b)** Medians, varying starting random number seed, for each MCNP calculation in a 4-step burn; 5,000 and 20,000 source neutron batch sizes shown.

Mean

	5k	20k
1	0.99464	0.99473
2	0.94571	0.94559
3	0.94340	0.94317
4	0.89721	0.89725
5	0.85770	0.85781
6	0.81719	0.81747
7	0.78500	0.78480
8	0.75131	0.75158
9	0.72405	0.72419

(a)

Median

	5k	20k
1	0.99469	0.99466
2	0.94572	0.94560
3	0.94318	0.94322
4	0.89706	0.89727
5	0.85767	0.85783
6	0.81712	0.81744
7	0.78496	0.78479
8	0.75141	0.75151
9	0.72403	0.72416

(b)

Examining minimum and maximum eigenvalues begins to show the statistical effect of a larger batch size, with the range (difference between maximum and minimum) of the set roughly half with the larger batch size (table 25c). In either case, the impact of the statistical randomness is minimal with regard to k_{eff}, as at the end of the burn, batch size separates the maximums, minimums, and means by about one standard deviation (or less).

The MCNP-reported standard error is almost always less than the actual standard deviation calculated with the 40-case set. In all but two of the 18 entries in table 26, the MCNP error is less than the set error. In some cases, the difference is as much as 40%. Again, this impact on the final analysis is minimal, but deserves some consideration when assessing the single-point uncertainties.

Table 25 - k_{eff} Statistics by Step: (a) Maximums, **(b)** Minimums, and **(c)** Difference (spread) between Max. and Min.

Max.

	5k	20k
1	0.99643	0.99528
2	0.94757	0.94684
3	0.94501	0.94380
4	0.89936	0.89796
5	0.85943	0.85857
6	0.81844	0.81846
7	0.78632	0.78553
8	0.75211	0.75239
9	0.72588	0.72484

(a)

Min.

	5k	20k
1	0.99327	0.99407
2	0.94360	0.94417
3	0.94222	0.94199
4	0.89553	0.89628
5	0.85548	0.85692
6	0.81594	0.81676
7	0.78346	0.78417
8	0.74993	0.75092
9	0.72281	0.72362

(b)

Spread

	5k	20k
1	0.00316	0.00121
2	0.00397	0.00267
3	0.00279	0.00181
4	0.00383	0.00168
5	0.00395	0.00165
6	0.00250	0.00170
7	0.00286	0.00136
8	0.00218	0.00147
9	0.00307	0.00122

(c)

Table 26 - k_{eff} Statistics by Step: (a) Standard deviation of 40-case set, **(b)** average of standard errors reported by MCNP, and **(c)** ratio of **(a)** and **(b)**.

St. Dev.

	5k	20k
1	0.000896	0.000326
2	0.000959	0.000520
3	0.000738	0.000464
4	0.000990	0.000348
5	0.000831	0.000387
6	0.000717	0.000418
7	0.000662	0.000316
8	0.000563	0.000375
9	0.000765	0.000315

(a)

Mean MCNP St. Dev.

	5k	20k
1	0.000772	0.000374
2	0.000706	0.000362
3	0.000719	0.000367
4	0.000691	0.000331
5	0.000664	0.000331
6	0.000648	0.000314
7	0.000621	0.000303
8	0.000581	0.000282
9	0.000562	0.000282

(b)

St. Dev. Ratio

	5k	20k
1	0.861527	1.146716
2	0.736054	0.695713
3	0.974849	0.790729
4	0.698636	0.951441
5	0.798627	0.854595
6	0.903503	0.752222
7	0.938439	0.959525
8	1.030548	0.750623
9	0.735083	0.893204

(c)

5.4.1.1 Inventories

One measure of looking at the cumulative effect of propagating MCNP errors is the variance in the end-of-cycle core isotopics. Table 27 provides a top-level summary of these variances. Note that the reported statistics are not mass-weighted; an isotope present in very small quantities will have a large error and a significant impact on the mean of standard deviations.

In this table, it becomes clear that a few isotopes with large errors have a significant effect on the mean (which shows errors 20 times greater than the median). It is also clear that only about a dozen isotopes have errors greater than 1%, even when a 5,000-particle batch size is used. It is not until an error threshold of 0.05% is applied that there is a substantial difference in the number of isotopes above/below with batch size.

Table 27 - End-of-Cycle Inventory Statistics

	20k	5k
Avg.	0.79%	1.29%
Median	0.04%	0.06%
#	84	84
# < 1%	75	72
# < 0.5%	72	69
# < 0.1%	62	51
# < 0.05%	49	18

Tables 28 and 29 provide a much more detailed look at system-wide isotopic variations. Some of the large variances are likely a result of when a particular isotope crossed the worth threshold in the MonteBurns calculation at the cell level. In any case, values with errors greater than 10% have little value unless amassed as part of a larger dataset.

Table 28 - Isotopic Mass Statistics at End of Cycle

Isotope	BOC	5,000 n/batch						20,000 n/batch					
		Max	Min	Mean	Median	Std. Dev.	Rel. Std. Dev.	Max	Min	Mean	Median	Std. Dev.	Rel. Std. Dev.
11-Na-023	60280	60280	60280	60280	60280	0	0.00%	60280	60280	60280	60280	0	0.00%
24-Cr-052	45760	45380	45360	45362.333	45360	5.683208	0.01%	45370	45360	45360.25	45360	1.581139	0.00%
25-Mn-055	2024	1984.8	1984.3	1984.5401	1984.6	0.142881	0.01%	1984.8	1984.4	1984.623	1984.6	0.094709	0.00%
26-Fe-056	307120	305520	305490	305500	305500	7.427814	0.00%	305510	305480	305498.8	305500	5.633007	0.00%
26-Fe-057		1521.9	1508.8	1516.0934	1516.15	3.098214	0.20%	1518.2	1514	1516.335	1516.4	1.120758	0.07%
28-Ni-058	1892	1836.1	1835.6	1835.8699	1835.9	0.123589	0.01%	1836.1	1835.8	1835.895	1835.9	0.090418	0.00%
36-Kr-083		45.45	24.78	35.822667	35.655	4.945059	13.80%	45.49	29.86	37.936	40.22	4.099614	10.81%
38-Sr-088		376	344.1	349.22002	345.25	10.53907	3.02%	345.6	344.7	345.1775	345.2	0.217785	0.06%
38-Sr-090		1362.4	1329.3	1357.0234	1360.75	10.53366	0.78%	1361.8	1359.9	1361.063	1361.1	0.40617	0.03%
39-Y-089		669.2001	667.3	668.35668	668.35	0.541814	0.08%	668.9001	667.7	668.3476	668.4001	0.310488	0.05%
40-Zr-090	106040	210450	210430	210443.33	210440	6.064784	0.00%	210450	210430	210445.3	210450	5.986095	0.00%
40-Zr-091		1669.9	1574	1602.22	1605.7	24.23191	1.51%	1606.8	1574.7	1593.865	1605.85	15.25543	0.96%
40-Zr-092		2350.7	2346	2348.48	2348.4	1.057476	0.05%	2349.4	2347.3	2348.365	2348.5	0.637555	0.03%
40-Zr-093		2962.4	2926.6	2954.5134	2958.9	11.87739	0.40%	2961	2928.9	2957.915	2959.3	6.69025	0.23%
40-Zr-094		3306	3298.5	3302.6534	3302.85	1.677495	0.05%	3305.1	3300.8	3302.847	3302.75	1.058561	0.03%
42-Mo-095		2709.4	2705.1	2707.0134	2707.1	1.06468	0.04%	2708.6	2705.8	2706.975	2706.95	0.670588	0.02%
42-Mo-097		3875.4	3866.6	3870.61	3870.25	2.363848	0.06%	3874.1	3866.7	3870.55	3870.25	1.787293	0.05%
42-Mo-098	15972	35000	34983	34991.433	34991.5	3.539758	0.01%	34997	34988	34992.53	34992	2.253061	0.01%
42-Mo-100		5168.3	5157.3	5162.45	5163	2.737643	0.05%	5164.699	5158.2	5161.285	5161.201	1.539796	0.03%
43-Tc-099		4047.3	4035.9	4043.4567	4043.4	2.239371	0.06%	4045.9	4039.8	4043.005	4043.149	1.616603	0.04%
44-Ru-100		710.9999	706.7001	708.63002	708.65	1.140829	0.16%	710.1	707.6	708.825	708.9001	0.566927	0.08%
44-Ru-101		4349.1	4338.3	4345.2632	4345.9	2.292954	0.05%	4348.1	4341.9	4344.99	4344.6	1.594254	0.04%
44-Ru-102		6332.2	6317.7	6324.2266	6324.55	4.112168	0.07%	6328	6319.7	6323.463	6323.25	1.87311	0.03%
44-Ru-103		413.16	386.6	405.02267	404.605	6.1432	1.52%	413.0001	396.26	407.55	404.885	4.33931	1.06%
44-Ru-104		5214	5201.799	5206.2101	5206.15	2.776372	0.05%	5210.7	5203.2	5206.72	5206.55	1.908439	0.04%
44-Ru-106		1815.6	1811.3	1813.4833	1813.6	1.042884	0.06%	1814.5	1812.6	1813.557	1813.5	0.503289	0.03%
45-Rh-103		4392	4383.7	4387.6	4387.8	2.294743	0.05%	4391.101	4383.3	4387.43	4387.75	2.061344	0.05%
46-Pd-104		819.7999	814.9	817.21334	817.2	1.11596	0.14%	818.4	816.2001	817.52	817.55	0.531669	0.07%
46-Pd-105		3358	3351.1	3355.4501	3355.55	1.422372	0.04%	3356.7	3354	3355.39	3355.3	0.779828	0.02%
46-Pd-106		2798.7	2788.7	2793.2468	2793.35	2.173744	0.08%	2797.199	2791.3	2793.447	2793.549	1.234667	0.04%
46-Pd-107		2032.5	2029	2030.6666	2030.7	0.94775	0.05%	2031.6	2029.8	2030.722	2030.7	0.483825	0.02%
46-Pd-108		2472.2	2463.6	2469.2667	2469.5	1.975411	0.08%	2471.1	2467.4	2469.19	2469.25	0.899484	0.04%
47-Ag-109		1260.7	1255.4	1257.8034	1257.7	1.189769	0.09%	1259.2	1256.9	1257.89	1258	0.529991	0.04%
48-Cd-110		38.4	12.8	23.473333	26.5	7.867653	33.52%	37.9	12.9	24.1925	26.6	5.945453	24.58%
48-Cd-111		192.76	183.37	187.99867	187.51	4.384847	2.33%	192.79	183.42	187.5247	184	4.378152	2.33%
52-Te-130		2456.4	2451.9	2454.0934	2453.9	1.095217	0.04%	2455.3	2452.9	2454.025	2454	0.636402	0.03%
53-I-127		483.57	474.86	478.66074	475.7151	3.866943	0.81%	483.2901	474.98	479.0906	479.1301	3.902698	0.81%
53-I-129		1383.9	1381.5	1382.9333	1383	0.645564	0.05%	1383.8	1382.2	1382.917	1382.9	0.427795	0.03%
54-Xe-131		3776.3	3766.7	3772.38	3772.45	2.422638	0.06%	3775.3	3768.8	3772.052	3772	1.360239	0.04%
54-Xe-132		6033.1	6020.7	6027.4567	6028.65	3.693971	0.06%	6032.5	6022.9	6028.155	6028	2.385459	0.04%
54-Xe-134		7897.4	7881.2	7889.3233	7889.2	3.984098	0.05%	7894.2	7885.4	7889.56	7889.5	2.476647	0.03%
54-Xe-136		7594.4	7579.3	7588.6566	7588.9	3.794965	0.05%	7594	7582.6	7587.4	7587.25	2.726678	0.04%
55-Cs-133		6326.8	6315.299	6322.7566	6323.75	3.166789	0.05%	6325.8	6316.1	6322.005	6322.65	2.657703	0.04%
55-Cs-134		676.1901	663.3101	671.79069	672.17	2.528093	0.38%	673.4902	664.5701	671.8496	672.47	2.075892	0.31%
55-Cs-135		7718	7703.4	7711.8799	7712.2	3.881526	0.05%	7716	7705.8	7710.993	7711.15	2.853469	0.04%
55-Cs-137		6823.3	6809.3	6817.2501	6817.9	3.456158	0.05%	6822	6812.6	6818.005	6818.65	2.372213	0.03%
56-Ba-138		7078.7	7063	7070.3834	7069.95	4.191028	0.06%	7075.7	7064.4	7070.71	7070.7	2.562734	0.04%
57-La-139		6521.3	6507.3	6516.86	6517.6	3.471711	0.05%	6520.7	6512.2	6516.688	6516.6	1.64534	0.03%
58-Ce-140		6011	5996.7	6003.1099	6003.45	3.592903	0.06%	6006.8	5998.6	6002.508	6002.4	2.063896	0.03%
58-Ce-142		5646.1	5632.6	5638.72	5638.3	3.17837	0.06%	5641.7	5634.4	5637.667	5637.65	1.805905	0.03%
58-Ce-144		1875.1	1871	1873.2134	1873.2	1.001622	0.05%	1874.2	1872.2	1873.128	1873	0.523309	0.03%
59-Pr-141		5719.8	5707.9	5713.6	5714.051	3.100448	0.05%	5717.2	5707.8	5713.275	5713.45	2.33666	0.04%
60-Nd-143		4637.7	4628	4632.3333	4632.2	2.259453	0.05%	4635.7	4629.1	4632.902	4632.9	1.289157	0.03%
60-Nd-144		2677.6	2670.6	2674.6499	2674.4	1.589973	0.06%	2676.7	2672	2674.35	2674.55	1.05414	0.04%
60-Nd-145		3355.7	3349.4	3352.6034	3352.75	1.742439	0.05%	3354	3350	3351.975	3351.95	0.86546	0.03%
60-Nd-146		3498	3488.601	3493.2967	3493.15	2.068378	0.06%	3496.7	3489.8	3493.18	3493.6	1.625904	0.05%
60-Nd-148		1921.2	1917.6	1919.45	1919.5	0.834913	0.04%	1920.3	1918.4	1919.353	1919.35	0.50636	0.03%
60-Nd-150		576.6	506.6	543.22665	551.3	13.73973	2.53%	552.6	531	548.585	551.6	7.428933	1.35%
61-Pm-147		1494.7	1491.1	1492.8533	1492.9	0.95183	0.06%	1494.2	1492.1	1493.07	1493.05	0.501909	0.03%
62-Sm-147		365.3601	358.14	361.32532	359.23	3.03646	0.84%	365.3	358.7599	360.2152	359.065	2.437192	0.68%
62-Sm-148		348.8	293.9	322.73334	322.35	13.59481	4.21%	348.3	294	316.425	314.8	10.62114	3.36%
62-Sm-149		1099.4	1096.5	1097.9099	1097.85	0.710195	0.06%	1099	1096	1097.845	1097.8	0.633632	0.06%
62-Sm-150		637.4999	634.0001	635.40002	635.2501	0.91649	0.14%	636.4001	634.0001	635.2325	635.2	0.582825	0.09%
62-Sm-151		602.1901	599.43	600.95701	600.895	0.579742	0.10%	601.86	600.21	600.9945	601.005	0.401831	0.07%
62-Sm-152		1195.6	1177.8	1183.3767	1181.7	5.062629	0.43%	1195	1179.4	1183.992	1181.6	5.264667	0.44%
63-Eu-153		400.4401	396.46	398.26501	398.32	1.044927	0.26%	399.4	397.2001	398.3525	398.295	0.526923	0.13%
63-Eu-154		171.94	169.2	170.88899	171.1	0.83367	0.49%	171.88	169.63	171.3763	171.42	0.3604	0.21%
63-Eu-155		238.08	220.41	227.20434	225.42	4.412829	1.94%	233.93	219.91	226.2043	225.28	3.695358	1.63%
64-Gd-156		10.1	0	9.6686667	9.99	1.826743	18.89%	10.1	9.96	9.99975	10	0.031662	0.32%
64-Gd-157		17.53	10.82	14.599	14.385	1.53177	10.49%	17.46	12.62	14.176	14.155	1.368424	9.65%
92-U-235	1200	231.17	229.9	230.575	230.59	0.354147	0.15%	230.94	230.3	230.6445	230.655	0.147912	0.06%
92-U-238	750000	598900	598300	598620	598600	182.7001	0.03%	598900	598400	598632.5	598600	102.2503	0.02%
93-Np-237	1248	1142.1	1126.3	1134.5133	1134.6	4.067421	0.36%	1140.7	1129.8	1135.325	1135.65	2.312246	0.20%
93-Np-239		510.41	498.44	499.67934	499.155	2.153104	0.43%	500.0701	498.2801	499.2758	499.275	0.410859	0.08%
94-Pu-238	625	1089.73	1074.07	1080.1043	1079.895	3.345503	0.31%	1085.04	1075.65	1079.11	1078.05	2.726066	0.25%
94-Pu-239	139400	81940	81820	81892.333	81890	32.8721	0.04%	81940	81860	81899.25	81900	18.99899	0.02%
94-Pu-240	20732	31009	30957	30982.733	30981.5	15.30592	0.05%	30991	30964	30976.85	30976	7.412913	0.02%
94-Pu-241	2916	4242.899	4221.2	4230.1266	4230.6	4.326849	0.10%	4235.8	4225.3	4230.47	4230.05	2.36175	0.06%
94-Pu-242	1536	1827.5	1808.9	1814.7267	1811.8	5.752149	0.32%	1823.8	1809.8	1813.938	1811.75	5.050854	0.28%
95-Am-241	1488	663.5	659.1	660.92334	660.7	1.034805	0.16%	662.5	659.5	660.7675	660.75	0.778688	0.12%
95-Am-242	41	72.57	72.36	72.435333	72.43	0.056246	0.08%	72.56001	72.36	72.43525	72.42	0.057244	0.08%
95-Am-243	308	335.6	332.2	333.91	333.9	0.726038	0.22%	334.7	333.6	334.085	334	0.328591	0.10%
96-Cm-244		186.7	185.2	185.81333	185.75	0.41083	0.22%	186.1	185.5	185.835	185.85	0.164162	0.09%
96-Cm-245		23.51	21.19	21.953	21.4	0.952775	4.34%	23.47	21.22	21.9075	21.355	0.940149	4.29%

Table 29 - Atom Fraction Statistics at End of Cycle

Isotope	BOC	5,000 n/batch						20,000 n/batch					
		Max	Min	Mean	Median	Std. Dev.	Rel. Std. Dev.	Max	Min	Mean	Median	Std. Dev.	Rel. Std. Dev.
11-Na-023	60280	0.173727	0.173682	0.1737053	0.173705	7.27E-06	0.00%	0.173705	0.173705	0.173705	0.173705	0	0.00%
24-Cr-052	45760	0.058025	0.058011	0.0580173	0.058017	3.75E-06	0.01%	0.05802	0.058009	0.058015	0.058016	2.57E-06	0.00%
25-Mn-055	2024	0.002395	0.002394	0.0023947	0.002395	2.42E-07	0.01%	0.002395	0.002394	0.002395	0.002395	1.76E-07	0.01%
26-Fe-056	307120	0.362068	0.361977	0.3620114	0.362011	2.78E-05	0.01%	0.362023	0.361977	0.361999	0.362	1.26E-05	0.00%
26-Fe-057		0.00176	0.001745	0.0017534	0.001753	3.54E-06	0.20%	0.001756	0.00175	0.001754	0.001754	1.42E-06	0.08%
28-Ni-058	1892	0.002101	0.0021	0.0021009	0.002101	2.61E-07	0.01%	0.002101	0.002101	0.002101	0.002101	1.21E-07	0.01%
36-Kr-083		3.62E-05	1.97E-05	2.852E-05	2.84E-05	3.94E-06	13.82%	3.62E-05	2.38E-05	3.02E-05	3.2E-05	3.26E-06	10.80%
38-Sr-088		0.000278	0.000254	0.0002579	0.000255	7.81E-06	3.03%	0.000255	0.000255	0.000255	0.000255	1.72E-07	0.07%
38-Sr-090		0.000996	0.000972	0.000992	0.000995	7.83E-06	0.79%	0.000996	0.000994	0.000995	0.000995	3.73E-07	0.04%
39-Y-089		0.000491	0.000489	0.0004904	0.00049	4.28E-07	0.09%	0.000491	0.00049	0.000491	0.000491	2.3E-07	0.05%
40-Zr-090	106040	0.077607	0.077584	0.0775949	0.077593	5.27E-06	0.01%	0.0776	0.077584	0.077594	0.077595	3.79E-06	0.00%
40-Zr-091		0.001134	0.001088	0.0011061	0.001111	1.28E-05	1.15%	0.001113	0.001088	0.001102	0.001111	1.13E-05	1.02%
40-Zr-092		0.001687	0.001684	0.0016857	0.001686	8.45E-07	0.05%	0.001687	0.001685	0.001686	0.001686	5.54E-07	0.03%
40-Zr-093		0.002105	0.002079	0.0020995	0.002103	8.82E-06	0.42%	0.002104	0.00208	0.002102	0.002103	4.96E-06	0.24%
40-Zr-094		0.002324	0.002319	0.002322	0.002322	1.11E-06	0.05%	0.002323	0.00232	0.002322	0.002322	7.77E-07	0.03%
42-Mo-095		0.001885	0.001882	0.0018836	0.001884	7.41E-07	0.04%	0.001885	0.001882	0.001884	0.001884	5.83E-07	0.03%
42-Mo-097		0.00264	0.002635	0.0026378	0.002638	1.27E-06	0.05%	0.002639	0.002636	0.002638	0.002638	6.2E-07	0.02%
42-Mo-098	15972	0.013459	0.013451	0.0134554	0.013456	2.61E-06	0.02%	0.013459	0.013451	0.013455	0.013455	2.03E-06	0.02%
42-Mo-100		0.003415	0.003408	0.0034117	0.003412	1.71E-06	0.05%	0.003413	0.00341	0.003412	0.003412	7.45E-07	0.02%
43-Tc-099		0.002703	0.002699	0.0027011	0.002701	1.07E-06	0.04%	0.002702	0.0027	0.002701	0.002701	7.35E-07	0.03%
44-Ru-100		0.000465	0.000462	0.0004632	0.000463	8.58E-07	0.19%	0.000464	0.000462	0.000463	0.000463	4.76E-07	0.10%
44-Ru-101		0.002847	0.002843	0.0028454	0.002845	1.02E-06	0.04%	0.002847	0.002844	0.002845	0.002845	7.62E-07	0.03%
44-Ru-102		0.0041	0.00409	0.0040947	0.004095	2.26E-06	0.06%	0.004097	0.004092	0.004095	0.004095	1.13E-06	0.03%
44-Ru-103		0.000264	0.000247	0.0002589	0.000259	4.01E-06	1.55%	0.000264	0.000253	0.000261	0.000259	2.87E-06	1.10%
44-Ru-104		0.003311	0.003305	0.0033083	0.003308	1.59E-06	0.05%	0.00331	0.003307	0.003308	0.003308	9.18E-07	0.03%
44-Ru-106		0.00113	0.001127	0.0011282	0.001128	7.81E-07	0.07%	0.001129	0.001127	0.001128	0.001128	4.42E-07	0.04%
45-Rh-103		0.002818	0.002813	0.0028162	0.002816	1.33E-06	0.05%	0.002818	0.002814	0.002816	0.002816	9.06E-07	0.03%
46-Pd-104		0.000518	0.000515	0.0005159	0.000516	7.01E-07	0.14%	0.000517	0.000515	0.000516	0.000516	3.17E-07	0.06%
46-Pd-105		0.002116	0.002111	0.0021137	0.002114	1.11E-06	0.05%	0.002115	0.002112	0.002114	0.002114	6.23E-07	0.03%
46-Pd-106		0.001741	0.001736	0.0017385	0.001739	1.15E-06	0.07%	0.00174	0.001737	0.001738	0.001738	7.42E-07	0.04%
46-Pd-107		0.001257	0.001254	0.0012553	0.001255	6.75E-07	0.05%	0.001256	0.001254	0.001255	0.001255	4.4E-07	0.04%
46-Pd-108		0.001511	0.001506	0.0015094	0.001509	1.3E-06	0.09%	0.001511	0.001508	0.001509	0.001509	6.36E-07	0.04%
47-Ag-109		0.000765	0.000761	0.0007627	0.000763	7.52E-07	0.10%	0.000764	0.000762	0.000763	0.000763	3.31E-07	0.04%
48-Cd-110		2.25E-05	7.5E-06	1.376E-05	1.56E-05	4.63E-06	33.62%	2.22E-05	7.57E-06	1.42E-05	1.56E-05	3.5E-06	24.68%
48-Cd-111		0.000113	0.000108	0.0001107	0.00011	2.61E-06	2.36%	0.000114	0.000108	0.00011	0.000108	2.59E-06	2.34%
52-Te-130		0.001248	0.001245	0.0012463	0.001246	5.75E-07	0.05%	0.001247	0.001245	0.001246	0.001246	4.4E-07	0.04%
53-I-127		0.000252	0.000247	0.000249	0.000247	2.06E-06	0.83%	0.000251	0.000247	0.000249	0.000249	2.08E-06	0.83%
53-I-129		0.000709	0.000708	0.0007085	0.000708	3.19E-07	0.05%	0.000709	0.000708	0.000708	0.000708	1.7E-07	0.02%
54-Xe-131		0.001905	0.0019	0.001903	0.001903	1.33E-06	0.07%	0.001905	0.001902	0.001903	0.001903	7.05E-07	0.04%
54-Xe-132		0.003019	0.003013	0.0030161	0.003016	1.57E-06	0.05%	0.003018	0.003014	0.003016	0.003016	9.7E-07	0.03%
54-Xe-134		0.003893	0.003887	0.0038897	0.00389	1.78E-06	0.05%	0.003892	0.003888	0.00389	0.00389	9.95E-07	0.03%
54-Xe-136		0.003689	0.003682	0.0036862	0.003686	1.7E-06	0.05%	0.003688	0.003684	0.003686	0.003686	8.59E-07	0.02%
55-Cs-133		0.003144	0.003139	0.0031423	0.003143	1.36E-06	0.04%	0.003144	0.003141	0.003142	0.003142	7.55E-07	0.02%
55-Cs-134		0.000332	0.000326	0.0003297	0.00033	1.26E-06	0.38%	0.000331	0.000326	0.00033	0.00033	1.03E-06	0.31%
55-Cs-135		0.003777	0.00377	0.0037743	0.003774	1.86E-06	0.05%	0.003776	0.003772	0.003774	0.003774	9.72E-07	0.03%
55-Cs-137		0.00329	0.003284	0.0032875	0.003287	1.61E-06	0.05%	0.003289	0.003286	0.003287	0.003287	8.03E-07	0.02%
56-Ba-138		0.003387	0.003381	0.0033849	0.003385	1.58E-06	0.05%	0.003387	0.003383	0.003385	0.003385	8.68E-07	0.03%
57-La-139		0.0031	0.003094	0.0030978	0.003098	1.53E-06	0.05%	0.003099	0.003095	0.003097	0.003097	8.55E-07	0.03%
58-Ce-140		0.002836	0.00283	0.0028328	0.002833	1.38E-06	0.05%	0.002835	0.002831	0.002833	0.002833	8.48E-07	0.03%
58-Ce-142		0.002626	0.00262	0.0026231	0.002623	1.33E-06	0.05%	0.002625	0.002622	0.002623	0.002623	8.15E-07	0.03%
58-Ce-144		0.000859	0.000856	0.0008575	0.000858	6.4E-07	0.07%	0.000858	0.000857	0.000858	0.000858	2.79E-07	0.03%
59-Pr-141		0.002679	0.002674	0.002677	0.002677	1.18E-06	0.04%	0.002679	0.002676	0.002677	0.002677	7.55E-07	0.03%
60-Nd-143		0.002143	0.002139	0.0021407	0.002141	8.63E-07	0.04%	0.002142	0.002139	0.002141	0.002141	7.19E-07	0.03%
60-Nd-144		0.001227	0.001223	0.0012253	0.001225	8.19E-07	0.07%	0.001226	0.001224	0.001225	0.001225	4.95E-07	0.04%
60-Nd-145		0.001529	0.001526	0.0015281	0.001528	8.85E-07	0.06%	0.001529	0.001527	0.001528	0.001528	4.86E-07	0.03%
60-Nd-146		0.001581	0.001577	0.0015798	0.00158	9.79E-07	0.06%	0.001581	0.001578	0.00158	0.00158	6.77E-07	0.04%
60-Nd-148		0.000856	0.000854	0.0008552	0.000855	4.79E-07	0.06%	0.000856	0.000854	0.000855	0.000855	3.47E-07	0.04%
60-Nd-150		0.000252	0.000221	0.0002369	0.000241	6.14E-06	2.59%	0.000241	0.000231	0.000239	0.000241	3.34E-06	1.40%
61-Pm-147		0.000672	0.000671	0.0006716	0.000672	4.19E-07	0.06%	0.000672	0.000671	0.000672	0.000672	2.04E-07	0.03%
62-Sm-147		0.000164	0.000161	0.0001625	0.000161	1.4E-06	0.86%	0.000164	0.000161	0.000162	0.000161	1.12E-06	0.69%
62-Sm-148		0.000154	0.00013	0.0001425	0.000142	6E-06	4.21%	0.000154	0.00013	0.00014	0.000139	4.7E-06	3.36%
62-Sm-149		0.000488	0.000487	0.0004873	0.000487	3.07E-07	0.06%	0.000488	0.000487	0.000487	0.000487	2.56E-07	0.05%
62-Sm-150		0.000279	0.000277	0.000278	0.000278	4.11E-07	0.15%	0.000279	0.000277	0.000278	0.000278	2.35E-07	0.08%
62-Sm-151		0.000264	0.000263	0.0002633	0.000263	2.32E-07	0.09%	0.000264	0.000263	0.000263	0.000263	1.36E-07	0.05%
62-Sm-152		0.000519	0.000511	0.0005136	0.000513	2.24E-06	0.44%	0.000519	0.000512	0.000514	0.000513	2.36E-06	0.46%
63-Eu-153		0.000173	0.000171	0.0001721	0.000172	4.21E-07	0.24%	0.000173	0.000172	0.000172	0.000172	2.14E-07	0.12%
63-Eu-154		7.36E-05	7.24E-05	7.313E-05	7.32E-05	3.7E-07	0.51%	7.36E-05	7.25E-05	7.33E-05	7.34E-05	1.64E-07	0.22%
63-Eu-155		0.000101	9.32E-05	9.614E-05	9.53E-05	1.9E-06	1.98%	9.91E-05	9.3E-05	9.57E-05	9.53E-05	1.6E-06	1.67%
64-Gd-156		4.18E-06	0	3.986E-06	4.11E-06	7.53E-07	18.89%	4.14E-06	4.11E-06	4.12E-06	4.11E-06	1.15E-08	0.28%
64-Gd-157		7.42E-06	4.59E-06	6.181E-06	6.08E-06	6.48E-07	10.48%	7.38E-06	5.34E-06	6E-06	5.99E-06	5.77E-07	9.62%
92-U-235	1200	6.58E-05	6.54E-05	6.563E-05	6.56E-05	1.06E-07	0.16%	6.58E-05	6.55E-05	6.57E-05	6.57E-05	4.89E-08	0.07%
92-U-238	750000	0.167023	0.166795	0.1668841	0.166886	5.67E-05	0.03%	0.166955	0.166795	0.166892	0.166886	3.7E-05	0.02%
93-Np-237	1248	0.000322	0.000318	0.0003198	0.00032	1.12E-06	0.35%	0.000322	0.000318	0.00032	0.00032	6.49E-07	0.20%
93-Np-239		0.000141	0.000137	0.0001375	0.000137	6.05E-07	0.44%	0.000138	0.000137	0.000137	0.000137	1.02E-07	0.07%
94-Pu-238	625	0.000307	0.000303	0.0003041	0.000304	9.05E-07	0.30%	0.000305	0.000303	0.000304	0.000304	6.4E-07	0.21%
94-Pu-239	139400	0.022761	0.022718	0.0227374	0.022736	1.05E-05	0.05%	0.02275	0.02273	0.02274	0.022741	4.93E-06	0.02%
94-Pu-240	20732	0.008572	0.008557	0.0085642	0.008564	4.56E-06	0.05%	0.008567	0.008559	0.008563	0.008563	2.05E-06	0.02%
94-Pu-241	2916	0.001169	0.001163	0.0011654	0.001165	1.14E-06	0.10%	0.001167	0.001164	0.001165	0.001165	6.15E-07	0.05%
94-Pu-242	1536	0.000506	0.000501	0.0005025	0.000502	1.57E-06	0.31%	0.000505	0.000501	0.000502	0.000502	1.4E-06	0.28%
95-Am-241	1488	0.000186	0.000185	0.0001852	0.000185	2.55E-07	0.14%	0.000186	0.000185	0.000185	0.000185	2.08E-07	0.11%
95-Am-242	41	2.02E-05	2.02E-05	2.02E-05	2.02E-05	2.25E-08	0.11%	2.03E-05	2.02E-05	2.02E-05	2.02E-05	2.3E-08	0.11%
95-Am-243	308	9.31E-05	9.21E-05	9.264E-05	9.26E-05	2E-07	0.22%	9.29E-05	9.25E-05	9.27E-05	9.27E-05	9.72E-08	0.10%
96-Cm-244		5.15E-05	5.11E-05	5.132E-05	5.13E-05	1.13E-07	0.22%	5.14E-05	5.12E-05	5.13E-05	5.13E-05	5.09E-08	0.10%
96-Cm-245		6.47E-06	5.82E-06	6.029E-06	5.87E-06	2.66E-07	4.41%	6.45E-06	5.83E-06	6.02E-06	5.86E-06	2.62E-07	4.35%

5.4.2 Local Composition

Local composition (in the single cell examined) actually appears to settle below the 1% error level faster than the core-wide isotopics, but is slower in reaching finer tolerances. After only 5,000 x 100 particles tracked, the random seed variations only significantly affect ^{134}Cs and ^{236}U. These isotopes are not present in significant quantities, with ^{134}Cs accounting for slightly more than 0.1% by mass, and ^{236}U present only in trace amounts.

Table 31 provides a more detailed look at this cell, listing its composition and associated variance statistics. Note that there is no "reported" error, as MonteBurns does not carry errors forward in calculating composition for subsequent steps.

Table 30 - Isotopic Mass Density Summary for Cell 810

	5%
Avg.	0.66%
Median	0.27%
#	73
# < 1%	71
# < 0.5%	65
# < 0.1%	9
# < 0.05%	7

Table 31 - Local Variances in Composition of Cell 810 with Starting Random Number Seed (mass densities shown)

	Mean	Median	St. Dev.	Rel. St. Dev.
92236	0.00088	0.000879	5.40745E-06	0.61%
94236	1.52E-06	1.52E-06	2.22951E-08	1.47%
96242	0.003478	0.00348	1.05591E-05	0.30%
96243	0.000273	0.000273	8.22225E-07	0.30%
96246	7.28E-05	7.28E-05	4.11688E-07	0.57%
11023	0.28083	0.28083	3.27363E-06	0.00%
24052	0.212104	0.212105	1.25642E-05	0.01%
25055	0.009334	0.009333	1.32133E-06	0.01%
26056	1.425747	1.425783	7.06243E-05	0.00%
26057	0.005201	0.005196	4.68989E-05	0.90%
28058	0.008618	0.008618	1.1448E-06	0.01%
40090	0.491421	0.491423	1.77206E-05	0.00%
42098	0.079479	0.07948	3.81631E-05	0.05%
92235	0.001702	0.001703	6.11207E-06	0.36%
92238	2.980442	2.980504	0.001537105	0.05%
93237	0.015515	0.015536	9.93015E-05	0.64%
93239	0.002053	0.002054	1.1718E-05	0.57%
94238	0.020193	0.020192	3.12264E-05	0.15%
94239	0.34991	0.349983	0.000376121	0.11%
94240	0.168407	0.168434	0.000231256	0.14%
94241	0.028954	0.028956	4.07776E-05	0.14%
94242	0.034626	0.034626	3.00024E-05	0.09%
95241	0.015781	0.01579	4.70733E-05	0.30%
95242	0.001803	0.001803	2.7586E-06	0.15%
95243	0.008384	0.008381	1.46833E-05	0.18%
96244	0.004715	0.004716	1.3358E-05	0.28%
96245	0.000583	0.000583	2.46773E-06	0.42%
40092	0.008127	0.008125	2.30815E-05	0.28%
40093	0.010068	0.010067	2.80522E-05	0.28%
40094	0.010987	0.010985	3.05097E-05	0.28%
42095	0.00934	0.00934	2.59877E-05	0.28%
42097	0.013539	0.013537	3.66863E-05	0.27%
43099	0.014797	0.014794	3.71143E-05	0.25%
42100	0.017545	0.017541	4.6799E-05	0.27%
44101	0.01593	0.015931	4.13973E-05	0.26%
44102	0.02025	0.020248	5.82579E-05	0.29%
45103	0.015585	0.015583	3.89555E-05	0.25%
44104	0.017805	0.017801	4.68767E-05	0.26%
46105	0.012412	0.012408	2.95301E-05	0.24%
44106	0.00696	0.006957	2.21247E-05	0.32%
46106	0.008014	0.008013	2.68247E-05	0.33%
46107	0.007682	0.007683	1.83573E-05	0.24%
46108	0.007868	0.007868	2.38596E-05	0.30%
47109	0.00449	0.004488	1.12242E-05	0.25%
53127	0.00182	0.00182	4.92967E-06	0.27%
53129	0.004854	0.004853	1.28184E-05	0.26%
52130	0.008518	0.008516	2.34748E-05	0.28%
54131	0.01328	0.013277	3.49229E-05	0.26%
54132	0.019789	0.019785	5.47521E-05	0.28%
55133	0.022704	0.022703	5.75678E-05	0.25%
54134	0.026892	0.026888	7.30678E-05	0.27%
55134	0.001382	0.001479	0.000375777	27.19%
55135	0.026175	0.026173	6.99288E-05	0.27%
54136	0.025705	0.025701	6.95588E-05	0.27%
55137	0.023086	0.02308	6.26229E-05	0.27%
56138	0.023796	0.023793	6.46098E-05	0.27%
57139	0.022193	0.022189	6.01204E-05	0.27%
58140	0.020181	0.020177	5.4831E-05	0.27%
59141	0.019364	0.019359	5.08377E-05	0.26%
58142	0.019016	0.019012	5.19429E-05	0.27%
60143	0.016214	0.016211	4.18184E-05	0.26%
58144	0.007193	0.007189	2.55886E-05	0.36%
60144	0.008421	0.008419	2.48445E-05	0.30%
60145	0.0121	0.012101	3.31146E-05	0.27%
60146	0.011338	0.011333	3.27225E-05	0.29%
61147	0.005851	0.005851	1.55707E-05	0.27%
62147	0.001454	0.001454	4.17089E-06	0.29%
60148	0.00718	0.007177	1.98739E-05	0.28%
62149	0.004509	0.004508	1.22993E-05	0.27%
62151	0.002575	0.002577	8.64965E-06	0.34%
62152	0.003653	0.003652	1.43938E-05	0.39%
63153	0.001447	0.001447	4.36343E-06	0.30%
63154	0.000392	0.000392	2.20646E-06	0.56%

5.5 Run Times

This section is intended to provide a brief overview of performance observations as they apply to models used during the course of this study. However, this data is still significant, as it informs the evaluation of execution parameters on a time-vs.-quality basis.

5.5.1 Parallel Processing Efficiency

While there is a non-negligible efficiency penalty running MCNP across multiple computing nodes (e.g. running two parallel jobs in sequence as opposed to running two serial jobs simultaneously), the ability to run a depletion case in parallel significantly shortens the real time between starting a job and being able to analyze its output.

In comparing single-node to parallel processing times in table 33, lines 8, 17, and 18 provide examples of parallel execution times, and line 12 shows the same case run on a single node. In this case, the parallel jobs run no better than 42% efficiency—a result of the small batch size. Yet, lines 17 and 18 show that—with only 12 compute processes—a preliminary 2-step depletion can be executed in only 1 ½ hours; while line 1 shows that a much finer-step burn can be executed in less than three hours.

5.5.2 Code Version Differences

Significant performance differences have been observed when comparing MCNP5 to MCNPX. Typically, differences vary from 5 to 30%, depending on whether a job is run on a single processor or in parallel. An extreme case, lines 1 and 2 in table 33, shows a factor-of-three difference in runtime. This case, run in parallel with small batch sizes, shows some of the differences in how source particles are distributed and how message passing is executed. For single processor jobs, table 32 summarizes a comparison using the cases supporting figures 41 through 44. These cases were run in sequence, the matching pairs of cases running at the same time on a dual-processor node (i.e. both codes experienced very similar environments). On average, MCNP5 appears to be about 6% faster for these cases.

Table 32 - Single Processor Timing Comparision

	Elapsed	% Diff.
25 cycles, MCNP5	0:12:54	4.22%
25 cycles, MCNPX	0:12:22	
50 cycles, MCNP5	0:22:54	-20.10%
50 cycles, MCNPX	0:28:01	
100 cycles, MCNP5	0:44:14	-3.26%
100 cycles, MCNPX	0:45:42	
200 cycles, MCNP5	1:32:00	-4.74%
200 cycles, MCNPX	1:36:28	

Load balancing options vary between MCNP5 and MCNPX. Documentation for the former recommends that the *balance* keyword be used on the command line. This option varies the number of fission source particles sent to each sub-process every cycle based on performance statistics. This option would be most beneficial on a heterogeneous

computing cluster, but is significant even when used on a job run across identical machines. MCNPX has a similar option.

MCNPX by default runs parallel jobs in a mode where fission source particles are not recollected by the master node except when dumping data to the run tape. This mode is intended to reduce network traffic and reduce the idle CPU time between *kcode* cycles, yet—particularly with small batch sizes—there is still a large fraction of underutilized CPU time. MCNP5's CPU utilization seems to be much higher, even without load balancing enabled.

The difference in single-processor performance times is significant by itself, and is the primary reason MCNP5 is used preferentially in this study.

5.5.3 Random Number Generator and Stride Settings

Two additional parameters examined produced mixed results. The first, switching the random number generator option (MCNP5 only), was expected to produce some gain. Instead, as seen in lines 17 and 18 in table 33, there is virtually no difference. This may be in part a result of a reduced time spent generating random numbers in MCNP5.

Table 33 – MonteBurns Runtime Comparison

		Code	Neutrons/Batch	Duration
1	8 steps, 12 nodes	MCNP5	5000	2:53:55
2	8 steps, 12 nodes	MCNPX	5000	9:03:26
3		MCNPX	10000	14:39:28
4		MCNPX	20000	24:45:34
5	4 steps, 12 nodes	MCNPX	5000	5:04:23
6		MCNPX	10000	9:18:00
7		MCNPX	20000	12:44:11
8	2 steps, 12 nodes	MCNPX	5000	3:32:44
9	1 step, 1 node	MCNPX	5000	5:10:04
10		MCNPX	10000	10:19:55
11		MCNPX	20000	20:42:42
12	2 steps, 1 node	MCNPX	5000	7:09:41
13		MCNPX	10000	14:23:57
14		MCNPX	20000	29:51:18
15	8 steps, 12 slow (1.4GHz) nodes	MCNPX	50000	73:17:05
16	2 steps, 1 node, stride=3000	MCNPX	5000	6:15:53
17	2 steps, 12 nodes, gen=2	MCNP5	5000	1:29:18
18	2 steps, 12 nodes, gen=1 (default)	MCNP5	5000	1:24:42

Random number stride has virtually no effect on performance in MCNP5, but has a significant impact in MCNPX (lines 12 and 16), cutting the total execution time by nearly 15%. The impact of this setting is debatable; if it remains above the maximum stride used in the problem, it should have no effect on the results. However, some evidence exists to suggest that—even with a stride significantly smaller than the longest used in the

problem—the effect is still marginal. Consequently, it is advisable to set the random number stride much smaller than the default (152,000), as the maximum used in these calculations is ~10^4.

5.6 Miscellaneous Observations

- MonteBurns does not properly account for multiple listings of an isotope within a material. The materials generated by MonteBurns (which account for all but the initialization step) include only one of the values listed.
- Several opportunities exist to improve performance/capabilities of MonteBurns, and may include the following:
    - Restructuring file manipulation in the MonteBurns perl script. This likely has a minor impact on execution times, but may significantly decrease file system demand
    - Distributing depletion (ORIGEN or CINDER) calculations across multiple nodes (relatively minor impact on performance, since MCNP calculations still dominate in most cases)
    - Increasing the number of burn materials (MCNP can be built to accommodate more than the default of 100 tallies; it should not be overly difficult to modify the process to take advantage of this)
- Compute time, shown as *ctm*, is calculated differently in MCNP5 and MCNPX. Consequently, all timing information is based on wall clock time, taking precautions to ensure comparisons are run under controlled conditions (e.g. similar total cluster load, jobs run on same node/at same time).

5.7 Supplemental Process Information

Unless otherwise noted, all MonteBurns runs were executed using MCNP5 (RSICC release 1.40), with build date 8/28/2007, and ORIGEN2. All were run on a Rocks cluster, running kernel version 2.6.9-22.EL-x86_64. All nodes are AMD Opteron processors, at either 1.4GHz or 2.4GHz. Where MCNPX is referenced (primarily timing comparison), the executable is RSICC version 2.5.0, build date 6/24/2005.

Cross sections for all of the depletion analysis are accessed from the temperature-dependent, ENDF/B-VIIr0-derived *space07* library. All cross sections available in the library were included in the mbxs.inp file for MonteBurns, and the fractional importance threshold criteria (in MonteBurns input) was set at 0.001.

5.8 MCNPX/MCNP5 Limitations / Code QA Issues

5.8.1 Stack Size/MPI Limitations

One of the features significantly improving computation time with MCNP is the use of MPI (message passing interface) software for running in parallel across a homogeneous computing cluster. The use of MPI is limited by problem size—i.e. the amount of memory MCNP needs to run—as a function of both message size and stack size. The current structure of the parallelized code uses a master process to coordinate the other

processes, which actually track particles. This means that the master must have enough memory (both user data and stack space) to store all of the message data for each of the sub-processes. As a result, as problem size (and minimum stack size) grows, the number of processes that can be utilized decreases.

Several workarounds exist for increasing the tolerable problem size. Microsoft's IDE includes a utility called EDITBIN, which allows manipulation of the MCNP executable to set stack size. This allows marginal increases in problem size, subject to MPI limitations. A patch has also been developed to reduce memory requirements by excluding charged particles (other than electrons) in MCNPX. This results in a significant reduction in memory usage if charged particle tracking is not needed. This patch could be further extended to eliminate subroutines and static variables only needed for charged particles, and could be further improved by restructuring the code to allocate memory based on the problem mode.

5.8.2 32-bit vs. 64-bit Versions

The amount of memory that can be addressed by a process is limited by the address size, generally the same as the instruction length. For a 32-bit processor, this means that 2^{32} bytes (4GB) of memory can be addressed; while for a 64-bit processor, this grows to 2^{64} bytes (16 billion GB). However, this memory is partitioned into segments available for program data and the operating system kernel, establishing a 2GB process limit for a 32-bit processor using a standard Windows installation. A boot switch allows a 75/25 application/kernel split, increasing that limit to 3GB (but consequently limiting kernel space, which can be problematic in limiting the total number of processes that can run on a particular machine—this is particularly relevant in terminal-server environments). The limitation is effectively the same in Unix/Linux 32-bit environments, though, 3GB is available for user programs by default with 2.6 series kernels, and third-party patches are available to modify this split in custom kernel builds.

At this time, there is little experience with MCNP (either version) on 64-bit Windows systems. Linux 64-bit MCNP executables have been generated and used successfully using the Portland Group compiler.

5.8.3 Build Process

Both varieties of MCNP use *autoconf*/*make* scripting on Unix/Linux platforms, and use flags to set compiler directives and generate the compiled source on the fly. This does not leave a copy of the source code actually used in building the executable, as a separate preprocessor would, for verification that all directives were properly read and processed. For MCNP5, the process is improved somewhat for Windows systems, as projects are provided specifying all directives. While the as-compiled source is not provided by default, it can be generated from this self-contained set of compiler options. Further, the process of building MCNP5 in Windows is very straightforward with these projects.

5.8.4 Mixed-mode Compiling Challenges in Windows

MCNPX requires a very specific setup in terms of matching the Fortran compiler/version with the C compiler/version, with serviceable combinations only marginally documented. For example, the CVF compiler cannot be used with current versions of MS C++--the

recommendation is to use VC98 with CVF, and VC 2003 with the Intel Fortran Compiler. No support currently exists for the current (2005) edition of Microsoft's C compiler. The process relies on paths in a number of environment variables, and there is little documentation on specific requirements for each entry.

MCNP5 takes advantage of Visual Fortran packages, and handling C modules is transparent and automatically handled by the build process.

5.8.5 Compiler-Dependent Eigenvalue Observation

NOTE: Comments in this section are associated with MCNPX beta versions 2.5.e and 2.5.f, with IVF 9.1 and CVF 6.6c. No compelling information is available to suggest that these differences no longer exist; no cross-platform comparisons have been performed as part of this study.

With Intel's purchase of the Compaq Visual Fortran product, and the introduction of Intel Visual Fortran, a number of observations have been made comparing performance with the two different compilers. The IVF compiler is currently supported, and the CVF compiler is no longer supported by the MCNPX development team. With support for advanced instructions available on newer processors and perhaps improved optimization, an IVF-compiled executable generally runs a problem faster than its CVF counterpart. However, the results (particularly the eigenvalue) are not consistent. Eigenvalue biases of 200-300 pcm have been observed when the only difference is the executable used. It is possible that this problem has been addressed in subsequent versions of either MCNPX or IVF, though documentation of the problem and its remedy is not readily available. It would be prudent to make a similar comparison with the current code.

5.8.6 Dynamically-linked Libraries

In current form, parallel execution of MCNP requires the use of dynamically-linked libraries. Some of the known limitations associated with MPI preventing code execution have already been discussed, but the dependence on a third-party code for fundamental data integrity via a DLL can be problematic. As the MPI software must be present/loaded on each computational node, ensuring that a validated version of the software is available on every node is essential. There are mechanisms currently available to check DLL versions; however, this is a somewhat primitive check that does not prevent a flawed DLL with an accepted version number (essentially a text field for identification purposes) from being loaded. This type of version checking is not incorporated in MCNP.

5.8.7 Differences between MCNPX and MCNP5

This area needs some work to quantify the differences between MCNP versions, but the areas for comparison are likely as follows:

- Build Process – autoconf/make scripting for MCNPX is cumbersome on PC; MCNP5 provides CVF projects to allow for a 1-step build (MCNP5 still makes use of autoconf/make on *nix systems, but includes a menu-driven question-and-answer process that automatically executes the build). Essentially, the build processes can be similar on *nix systems, but MCNP5's build system is much better for the PC.

- Run time – MCNP5 has been observed to be significantly faster for cases in this study; this topic is discussed further in a dedicated section

- Features/differences – no extraordinarily important features relevant to reactor engineering uniquely exist in either code. MCNP5 reports Shannon entropy, which has some use in attempting to evaluate fission source convergence.

- Resource requirements – with the 2GB memory limit being an immediate concern (regardless of operating system), the amount of memory used for a particular problem is significant. Observation with cluster monitoring tools suggests that MCNP5 uses significantly less memory; data in the table below provides a comparison for a step-1 burn deck (associated with table 32) with tallies.

Table 34 - Memory Usage Comparison

	Data	VM	% Diff.
MCNP5	56048	71080	28.17%
MCNPX	73396	95408	

5.8.8 In-House MCNP Modifications/Tools

- Material mixing capability – adds the ability to specify a mixture of more than one material for a cell in an MCNP model.

- Code coverage analysis – software in-place to analyze which subroutines, functions, and lines of code are executed by particular test problems or by a test suite

- Delayed particle production for betas and photons – a patch that properly treats the delayed production of photons and beta particles

- Charged-particle elimination patch – a set of modifications that can reduce memory usage of certain routines by an order of magnitude by taking out memory allocations for 31 charged particle types (leaving behind neutrons, photons, and electrons); marginal performance improvement has also been observed